Restaurant wastewater treatment by electrochemical oxidation in continuous process

Songsak Klamklang

N° d'ordre :……

THESE

présentée

pour obtenir

LE TITRE DE DOCTEUR DE L'INSTITUT NATIONAL POLYTECHNIQUE DE TOULOUSE

École doctorale : Mécanique Energétique Génie Civil et Procédés……..

Spécialité : Génie des Procédés et Environnement ……..

Par M KLAMKLANG Songsak……

Titre de la thèse **Restaurant wastewater treatment by electrochemical oxidation in continuous process**

Soutenue le 13/11/2007. devant le jury composé de :

Mme	**Pattarapan PRASASSARAKICH**	Présidente
MM.	**Patrick DUVERNEUL** ……..	Directeur de thèse
	Somsak DAMRONGLERD	Codirecteur de thèse
	Jean Pierre BONINO ……..	Rapporteur
	Tawach CHATCHUPONG	Rapporteur
	Hugues VERGNES	Membre
	François SENOCQ	Invité
Mme	**Kejvalee PRUKSATHORN**	Invité
	Sangobtip PONGSTABODEE	Invitée

Institut National Polytechnique de Toulouse

Ecole doctorale : Transfert, Dynamique des Fluides, Energétique, Procédés

Université Chulalongkorn

Klamklang Songsak

- **Doctorat d'Université**
  Spécialité Génie des Procédés et de l'Environnement

Restaurant wastewater treatment by electrochemical oxidation in continuous process

Nom du directeur de thèse Professeur Patrick Duverneuil
Nom du co-directeur Professeur Somsak Damronglerd

Date de soutenance 13 novembre 2007

Composition du jury

M. J. P. Bonino

M. T. Chatchupong

Mlle. P. Prasassarakich

M. P. Duverneuil

M. S. Damronglerd

Mlle. K. Pruksathorn

M. H. Vergnes

M. F. Senocq

Mme. S. Pongstabodee

การบำบัดน้ำเสียจากภัตตาคารโดยออกซิเดชันเชิงไฟฟ้าเคมีในกระบวนการต่อเนื่อง

นายทรงศักดิ์ กล่ำคลัง

วิทยานิพนธ์นี้เป็นส่วนหนึ่งของการศึกษาตามหลักสูตรปริญญาวิทยาศาสตรดุษฎีบัณฑิต
สาขาวิชาเคมีเทคนิค ภาควิชาเคมีเทคนิค
คณะวิทยาศาสตร์ จุฬาลงกรณ์มหาวิทยาลัย
ปีการศึกษา 2549

ISBN 974-14-3476-6

RESTAURANT WASTEWATER TREATMENT BY ELECTROCHEMICAL OXIDATION IN CONTINUOUS PROCESS

Mr. Songsak Klamklang

A Dissertation Submitted in Partial Fulfillment of the Requirements
for the Degree of Doctor of Philosophy Program in Chemical Technology
Department of Chemical Technology
Faculty of Science
Chulalongkorn University
Academic year 2006

ISBN 974-14-3476-6

Thesis Title	RESTAURANT WASTEWATER TREATMENT BY ELECTROCHEMICAL OXIDATION IN CONTINUOUS PROCESS
By	Mr. Songsak Klamklang
Filed of study	Chemical Technology
Thesis Advisor	Professor Somsak Damronglerd, Dr. Ing.
Thesis Advisor	Professor Patrick Duverneuil, Dr. de l'INPT
Thesis Co-advisor	Associate Professor Kejvalee Pruksathorn, Dr. de l'INPT

Accepted by the Faculty of Science, Chulalongkorn University in Partial Fulfillment of the Requirements for the Doctoral Degree

……Dean of the Faculty of Science
(Professor Piamsak Menasveta, Ph.D.)

THESIS COMMITTEE

……...Chairman
(Professor Pattarapan Prasassarakich, Ph.D.)

……Thesis Advisor
(Professor Somsak Damronglerd, Dr. Ing.)

……Thesis Advisor
(Professor Patrick Duverneuil, Dr. de l'INPT)

……Thesis Co-advisor
(Associate Professor Kejvalee Pruksathorn, Dr. de l'INPT)

……Member
(Assistant Professor Hugues Vergnes, Dr. de l'INPT)

……Member
(Mr. François Senocq, Dr. de l'INPT))

……Member
(Mr. Thawach Chatchupong, Ph.D.)

……Member
(Mr. Jean Pierre Bonino, Dr. De l'INPT)

……Member
(Assistant Professor Sangobtip Pongstabodee, Ph.D.)

ทรงศักดิ์ กล่ำคลัง : การบำบัดน้ำเสียจากภัตตาคารโดยออกซิเดชันเชิงไฟฟ้าเคมีในกระบวนการต่อเนื่อง. (RESTAURANT WASTEWATER TREATMENT BY ELECTROCHEMICAL OXIDATION IN CONTINUOUS PROCESS) อ. ที่ปรึกษา: ศ. ดร. สมศักดิ์ ดำรงค์เลิศ, Prof. Patrick Duverneuil, Dr. de l'INPT อ. ที่ปรึกษาร่วม: รศ. ดร. เก็จวลี พฤกษาทร 199 หน้า. ISBN 974-14-3476-6.

การบำบัดน้ำเสียโดยการออกซิเดชันเชิงไฟฟ้าเคมีจำเป็นต้องใช้ขั้วไฟฟ้าที่มีประสิทธิภาพในการย่อยสลายสารมลพิษอินทรีย์ที่อยู่ในน้ำเสีย งานวิจัยนี้ศึกษาการเตรียมขั้วไฟฟ้า โดยเทคนิคการเคลือบผิวด้วยวิธี metal-organic chemical vapor deposition (MOCVD) การเคลือบผิวดังกล่าวแบ่งเป็น 2 ชั้น คือ การเคลือบผิวด้วยอีรีเดียมเพื่อป้องกันการสึกกร่อนของขั้วไฟฟ้าโดยใช้ (Methylcyclopentadienyl) (1,5-cyclooctadiene) iridium (I) เป็นสารตั้งต้น ที่ภาวะอุณหภูมิ 300 องศาเซลเซียส อัตราส่วนโดยโมลของ O_2/(MeCp)Ir(COD) เท่ากับ 125 ความดัน 12 ทอร์ และการเคลือบผิวด้วยดีบุกออกไซด์เป็นพื้นผิวสำหรับเกิดปฏิกิริยาการผลิตอนุมูลไฮดรอกซิลโดยใช้ tetraethyltin เป็นสารตั้งต้น ที่ภาวะอุณหภูมิ 380 องศาเซลเซียส อัตราส่วนโดยโมลของ O_2/TET เท่ากับ 1200 และความดัน 15 ทอร์ จากการจำลองกระบวนการเคลือบผิวด้วยอีรีเดียมโดยโปรแกรม FLUENT® พบว่า แบบจำลองมีความสอดคล้องกับผลการทดลอง

เมื่อนำขั้วไฟฟ้า SnO_2/Ir/Ti ที่เตรียมได้มาใช้ในการบำบัดน้ำเสียสังเคราะห์ที่เตรียมจากกรดออกซาลิค พบว่า สามารถลดปริมาณของคาร์บอนอินทรีย์ได้ร้อยละ 80 ภายในเวลา 2 ชั่วโมง โดยกลไกการย่อยสลายสารมลพิษอินทรีย์ในน้ำเสียแบ่งเป็น 2 แบบ คือ ปฏิกิริยาลำดับศูนย์และลำดับหนึ่ง เมื่อมีความเข้มข้นของสารมลพิษอินทรีย์ในน้ำเสียสูงและต่ำตามลำดับ ในการศึกษาการบำบัดน้ำเสียจากโรงอาหารของจุฬาลงกรณ์มหาวิทยาลัย พบว่า การเพิ่มความหนาแน่นกระแสไฟฟ้าที่ป้อนให้ขั้วไฟฟ้าจาก 5 เป็น 10 มิลลิแอมแปร์ต่อตารางเซนติเมตร ทำให้ประสิทธิภาพการกำจัดคาร์บอนอินทรีย์และค่าซีโอดีลดลง เนื่องจากการเพิ่มความหนาแน่นกระแสไฟฟ้าที่ป้อนให้ขั้วไฟฟ้าทำให้ศักย์ไฟฟ้าของเซลล์มีค่าสูงขึ้น ซึ่งทำให้เกิดปฏิกิริยาข้างเคียงมากขึ้น ส่วนการเพิ่มระยะเวลาที่น้ำเสียอยู่ในเครื่องปฏิกรณ์เพิ่มขึ้นจาก 2 เป็น 3 ชั่วโมง ทำให้ประสิทธิภาพการกำจัดคาร์บอนอินทรีย์และค่าซีโอดีเพิ่มขึ้นเล็กน้อย เนื่องจากอัตราการเกิดปฏิกิริยาในช่วง 2 ชั่วโมงแรกมีค่าสูง ความหนาของผิวเคลือบดีบุกออกไซด์ไม่มีผลต่อประสิทธิภาพการกำจัดคาร์บอนอินทรีย์และค่าซีโอดี เนื่องจากปฏิกิริยาการผลิตอนุมูลไฮดรอกซิลเกิดเพียงที่ผิวของขั้วไฟฟ้าเท่านั้น

ภาควิชา.....เคมีเทคนิค..... ลายมือชื่อนิสิต.....
สาขาวิชา.....เคมีเทคนิค..... ลายมือชื่ออาจารย์ที่ปรึกษา.....
ปีการศึกษา.....2549..... ลายมือชื่ออาจารย์ทีปรึกษา.…….....
ลายมือชื่ออาจารย์ทีปรึกษาร่วม.....

4473810523: MAJOR CHEMICAL TECHNOLOGY
KEY WORD: RESTAURANT WASTEWATER / ELECTROCHEMICAL OXIDATION / MOCVD / SnO_2 SPECIFIC ELECTRODE / WASTEWATER TREATMENT

SONGSAK KLAMKLANG: RESTAURANT WASTEWATER TREATMENT BY ELCTROCHEMICAL OXIDATION IN CONTINUOUS PROCESS. THESIS ADVISOR: PROF. SOMSAK DAMRONGLERD, Dr. Ing, PROF. PATRICK DUVERNEUIL, Dr. de l'INPT, THESIS CO-ADVISORS: ASSOC. PROF. KEJVALEE PRUKSATHORN, Dr. de l'INPT, 199 pp. ISBN 974-14-3476-6.

The specific electrode is necessary for destruction of organic pollutant in restaurant wastewater by electrochemical oxidation. In this research, the specific electrode was prepared by metal-organic chemical vapor deposition (MOCVD) in a hot-wall CVD reactor with the presence of O_2 under reduced pressure. The Ir protective layer was deposited by using (Methylcyclopentadienyl) (1,5-cyclooctadiene) iridium (I), (MeCp)Ir(COD), as precursor. Tetraethyltin (TET) was used as precursor for the deposition of SnO_2 active layer. The optimum condition for Ir film deposition was 300 ºC, 125 of O_2/(MeCp)Ir(COD) molar ratio and 12 torr of total pressure. While that of SnO_2 active layer was 380 ºC, 1200 of O_2/TET molar ratio and 15 torr of total pressure.

The simulation of Ir deposition using FLUENT® shows the good agreement with the experimental data. However, the case of 300 ºC and titanium substrate, the simulation results have deviated from the experimental data that maybe attributed by the different on surface chemistry of each substrate or the higher surface roughness of titanium substrate.

The prepared SnO_2/Ir/Ti electrodes were tested for anodic oxidation of organic pollutant in a simple three-electrode electrochemical reactor using oxalic acid as model solution. The electrochemical experiments indicate that more than 80% of organic pollutant was removed in 2 hr. In first 2 hr, the kinetic investigation gives a zero-order respect to TOC of model solution and the destruction of pollutant was limited by the reaction kinetic. Then, it was first-order respect to TOC of model solution that limited by the mass transfer of pollutant to the electrode.

Furthermore, the SnO_2/Ir/Ti electrodes were used in this restaurant wastewater treatment within Chulalongkorn University. The increase of current density leads to the decrease of TOC and COD removal efficiency as a results of the increases of cell voltage and side reaction. Increasing residence time from 2 to 3 hr had not greatly influenced on TOC and COD removal efficiency due to slower reaction after 2 hr. The SnO_2 film thickness had no effect on TOC and COD removal efficiency because the production of adsorbed hydroxyl radicals for pollutant destruction occurred only at the surface of electrode.

Department...Chemical Technology.....	Student's signature.....
Field of study...Chemical Technology.....	Advisor's signature.....
Academic Year …..2006.....	Advisor's signature.....
	Co-advisor's signature.....

4473810523: MAJOR CHEMICAL TECHNOLOGY
KEY WORD: RESTAURANT WASTEWATER / ELECTROCHEMICAL OXIDATION / MOCVD / SnO_2 SPECIFIC ELECTRODE / WASTEWATER TREATMENT

SONGSAK KLAMKLANG: RESTAURANT WASTEWATER TREATMENT BY ELCTROCHEMICAL OXIDATION IN CONTINUOUS PROCESS. THESIS ADVISOR: PROF. SOMSAK DAMRONGLERD, Dr. Ing, PROF. PATRICK DUVERNEUIL, Dr. de l'INPT, THESIS CO-ADVISORS: ASSOC. PROF. KEJVALEE PRUKSATHORN, Dr. de l'INPT, 199 pp. ISBN 974-14-3476-6.

Cette étude traite de l'élaboration et de la mise en œuvre d'électrodes spécifiques pour la destruction par oxydation électrochimiques des polluants organiques présents dans les eaux résiduaires de restaurants. Dans ce travail, les électrodes spécifiques sont préparées par dépôt chimique à partir d'une phase vapeur de précurseur organométallique (OMCVD). La sous-couche protectrice d'iridium ou d'oxyde d'iridium est déposée à partir d'iridium methylcyclopentadiene 1-5 cyclooctadiène, (MeCp)Ir(COD) ou d'acetylacétonate d'iridium, $Ir(acac)_3$. La couche catalytique d'oxyde d'étain est quant à elle déposée à partir de tétraéthyl étain (TET). La première partie de l'étude a consisté à déterminer les conditions opératoires optimales pour les différentes couches (iridium, oxyde d'iridium, oxyde d'étain). Un travail de modélisation a également été développé dans le cas du dépôt d'iridium afin d'identifier les paramètres clef du procédé et de faciliter un changement d'échelle du procédé.

Les électrodes composites (SnO_2/Ir/Ti) ont ensuite été testées lors de la dégradation de solution d'acide oxalique. Les résultats expérimentaux montrent que 80% de la pollution organique est éliminée en 2 heures. Une étude de la cinétique de cette réaction a permis de mettre en évidence que cette dégradation s'opère en deux étapes. La première étape, correspondant aux fortes concentrations de carbone organique total (COT) suit une loi d'ordre zéro alors que pour les faibles valeurs du COT, la cinétique suit une loi d'ordre un qui a été attribuée à une limitation par le transfert de matière.

Enfin, ces électrodes ont été mises en œuvre pour traiter les eaux résiduaires du restaurant universitaire de l'Université Chulalongkorn (Thaïlande). Il a été montré que l'augmentation de la densité de courant conduisait à une diminution de l'efficacité du procédé tant sur la demande chimique en oxygène (DCO) que sur le COT. Il est également apparu que l'augmentation du temps de traitement (de 2 heures à 3 heures) n'avait pas beaucoup d'effet sur l'efficacité du traitement. Il a été montré par ailleurs que l'épaisseur de la couche d'oxyde d'étain n'avait pas d'effet sur l'efficacité de la diminution du COT et de la DCO.

Department...Chemical Technology..... Student's signature.....

Field of study...Chemical Technology..... Advisor's signature.....

Academic Year …..2006..... Advisor's signature.....

Co-advisor's signature.....

Acknowledgements

I would like to express my sincere gratitude and appreciation to Professor Dr. Somsak Damronglerd, Professor Dr. Patrick Duverneuil and Associate Professor Dr. Kejvalee Pruksathorn, for providing me with the insights and guidance to recognize my mistakes and constant encouragement. I would also like to thank them for lending me adequate freedom and flexibility while working on my Ph.D. study.

I would like to thank Professor Dr. Pattarapan Prasassarakich for serving as chairman of the committee and also for some kindness helps during my Ph.D. study. Furthermore, I would like to thank Assistant Professor Dr. Hugues Vergnes and Dr. François Senocq for their keen observations regarding my work and for providing valuable suggests and for their care while I stayed at Toulouse, France. Dr. Jean Pierre Bonino, Dr. Thawach Chatchupong and Assistant Professor Dr. Sangobtip Pongstabodee have also been very supportive for my Ph.D. work. I would like to thank them for their guidance and for serving as members of my thesis committee.

I would like to acknowledge the Royal Golden Jubilee Ph.D. Program of the Thailand Research Fund and the Embassy of France in Thailand for the financial support to my Ph.D. work.

I wish to express my grateful appreciation to Department of Chemical Technology, Faculty of Science, Chulalongkorn University, Thailand. I also gratefully thank to Laboratoire de Génie Chimique and Centre Inter-universitaire de Recherche et d'Ingéniérie des Matériaux, Ecole Nationale Supérieure des Ingénieurs en Arts Chimiques et Technologiques, Institut National Polytechnique de Toulouse, France.

A very special thank has expressed to my father, my mother, my family and my friends for their encouragement and love.

Table of Contents

List of Tables

List of Figures

Chapter 1

General Introduction

1.1 Introduction

In a big city as Bangkok, there are a lot of restaurants, food shops and food centers, which everyday make large amounts of wastewater. The direct discharge of wastewater from these restaurants and food shops to the drainage system is a huge extra burden to the municipal wastewater collection and treatment works. The oil and grease contained in the wastewater aggregate and foul the sewer system and generate an unpleasant odor.

Basically, restaurant wastewater treatment facilities must be highly efficient in removing oil and grease, cause no food contamination and be compact size. Low capital and operating costs are important because profit margins of most restaurants are small. In addition, the technology has to be simple so that it can be operated easily either by a chef or a waiter [1].

Conventional biological processes are therefore ruled out due to the requirement of large space, long residence time and skilled technicians. Chemical coagulation/settlement is not practicable because of the low efficiency in removing light and finely dispersed oil particles and possible contamination of foods by chemicals. The G-bag approach, which uses a bag of absorbent to capture the pollutants and degrade the pollutants with the immobilized microorganisms on the absorbent, seems to be a good

alternative only if the system can be designed as simple and free from fouling [1].

Electrochemistry is a clean, versatile and powerful tool for the destruction of organic pollutants in water. Electrochemical oxidation of organic compounds in aqueous solution is an anodic process occurring in the potential region of water discharge to produce oxygen. Two different pathways are described in the literatures for the anode oxidation of undesired organic pollutants [2].

Electrochemical conversion transforms only the toxic non-biocompatible pollutants into biocompatible organics, so that biological treatment is still required after the electrochemical oxidation [3]. The ideal electrode material which can be used in the electrochemical conversion method must have high electrochemical activity for aromatic ring opening and low electrochemical activity for further oxidation of the aliphatic carboxylic acids which are in general biocompatible [3].

Electrochemical combustion method completely oxidizes the organic pollutants to CO_2 by physisorbed hydroxyl radicals. In this case, the electrode material must have high electrocatalytic activity towards the electrochemical oxidation of organics to CO_2 and H_2O [3].

Comparison of different anode materials, SnO_2 is one of the best candidates for removal of organic pollutants from wastewater by electrochemical oxidation [2]. There are varieties of methods suitable for preparing the SnO_2 layer for obtaining dimensionally stable anodes such as reactive sputtering, sol-gel dip coating, spray-pyrolysis or chemical vapor deposition [2].

Chemical vapor deposition (CVD) is very attractive for thin film coating. It has advantages for growing thin films such as good conformal coverage on patterned or rough surfaces because of high throwing power of gaseous reagents and a good ability for large-scale production. CVD is particularly well adapted to uniform deposition on complex-shaped base material with a relatively high growth rate [4]. Furthermore, using metal–organic chemical vapor deposition (MOCVD) permits decreasing significantly the deposition temperature and obtaining high purity of deposited layer.

In this research, metal-organic chemical vapor deposition was used as the technique for the preparation of electrocatalytic electrodes for electrochemical oxidation of organic pollutants presented in restaurant wastewater. The effects of substrate materials, SnO_2 active layer thickness and current density on pollutants removal efficiency of prepared electrodes were investigated.

1.2 Objectives

1. Design and fabricate the continuous electrochemical oxidation system for restaurant wastewater treatment
2. Determine the efficiency of pollutant reduction by electrochemical oxidation in continuous process
3. Prepare the economical evaluation for restaurant wastewater treatment by electrochemical oxidation in continuous process

1.3 The steps of work

- Literature surveys, that will continue throughout the research work.

- Part I Batch process

1. Prepare electrodes by metal-organic chemical vapor deposition and characterize the prepared electrodes by SEM and XRD.
    - In this part, the elaboration IrO_2 and Ir coating for using as protective layer were performed by using $Ir(Acac)_3$ and (MeCp)Ir(COD) as iridium source, repectively. Subsequently, the deposition of SnO_2 active layer was perform using TET as precursor. The deposition was perform in a hot-wall CVD reactor. Then, the coating will be characterization by SEM and XRD. The simulation of Ir deposition was archived using FLUENT® software.
2. Study and determine the optimum condition for removal of organic pollutants in batch electrochemical oxidation using the prepared electrodes;
    - The various type of elaborated electrodes as shown previously were utilized in destruction of organic pollutant using oxalic acid as model solution. The pollutant removal efficiency was determined on the effect of current density and SnO2 film thickness. The kinetic of pollutant destruction was also exmined in this part.

- Part II Continuous process

1. Fabricate the continuous electrochemical oxidation system.

2. Study and determine the organic pollutants removal efficiency from actual restaurant wastewater in the continuous process by using the optimum condition of batch experiment.

    - The influences of current density, residense time and SnO2 film thinkness were examined and treatment cost analysis was also determined in this part.

3. Result interpretation and discussions.
4. Conclude and write of dissertation manuscript

Chapter 2

Bibliography

2.1 Wastewater [5]

Water is a combination of two parts, hydrogen and oxygen as H_2O. However, pure water is only manufactured in a laboratory, water as we know, it is not pure hydrogen and oxygen. Even the distilled water we purchase in the store has measurable quantities of various substances in addition to hydrogen and oxygen. Rainwater, before it reaches the earth, contains many substances. These substances, since they are not found in pure water, may be considered as the impurities. When rain falls through the atmosphere, it gains nitrogen and other gases. As soon as the rain flows over land, it begins to dissolve from the earth and rocks such substances as calcium, magnesium, sodium, chloride, sulfate, iron, nitrogen, phosphorus, and many other materials. Organic matter is also dissolved by water from contact with decaying leaves, twigs, grass, or small insects and animals. Thus, a fresh flowing mountain stream may pick up many natural impurities, some possibly in harmful amounts, before it ever reaches civilization or is affected by the waste discharges of society. Many of these substances are needed in small amounts to support life and are useful to humans.

The waste discharge that first comes to mind in any discussion of stream pollution is the discharge of domestic wastewater, wastewater contains a large amount of organic waste. Industry also contributes

substantial amounts of organic waste. Some of these organic industrial wastes come from vegetable and fruit packing, dairy processing, meat packing, tanning and processing of poultry, oil, paper, and fiber (wood) and many more. All organic materials have one thing in common - they all contain carbon.

2.2 Restaurant wastewater [6]

Wastewater from restaurants and other commercial food service facilities differ significantly from residential wastewater. In addition to higher surge volumes during busy periods and generally higher temperature. The pollutants in restaurant wastewater are come from the cleaning of dishes, kitchen wares, meat and vegetable. Restaurant wastewater is typically higher in strength than residential wastewater. This due to the higher content in organic pollutants exactly oil and grease.

Oil and grease frequently cause problems of both wastewater collection and treatment systems. The problem occurs when oil and grease solidifies in sewage lines and will cover on the surface of treatment systems causing a decrease in the treatment system efficiency.

2.3 Wastewater treatment processes [7]

Wastewater treatment consists of applying known technology to improve or upgrade the quality of a wastewater. Usually wastewater

treatment will involve collecting the wastewater in a central, segregated location and subjecting the wastewater to various treatment processes. Most often, since large volumes of wastewater are involved, treatment processes are carried out on continuously flowing wastewaters or open systems rather than as batch or a series of periodic treatment processes in which treatment is carried out on parcels or batches of wastewaters. While most wastewater treatment processes are continuous flow, certain operations, such as vacuum filtration, involving as it does, storage of sludge, addition of chemicals, filtration and removal or disposal of the treated sludge, are routinely handled as periodic batch operations. Wastewater treatment can be organized or categorized by the nature of the treatment process operation being used such as physical, chemical or biological treatment.

2.3.1 Physical treatment [7]

Sedimentation

Sedimentation is employed for the removal of suspended solids from wastewaters. The process can be considered in the three basic classifications, depending on the nature of the solids present in the suspension, there are discrete, flocculent and zone settling. In the discrete settling, the particle maintains its individuality and does not change in size, shape or density during the settling process. Flocculent settling occurs the particles agglomerate during the settling period with a resulting change in size and settling rate. Zone settling involves a flocculated suspension which forms a lattice structure and settles as a mass, exhibiting a distinct interface during the settling process. Compaction of the settled sludge occurs in all sedimentation but will be considered separately under thickening.

Flotation

Flotation is used for the removal of suspended solids, oil and grease from the wastewaters and for the separation and concentration of sludge. The waste flow of a portion of clarified effluent is pressurized to 3.4-4.8 atm in the presence of sufficient air to approach saturation. When this pressurized air-liquid mixture released to atmospheric pressure in the floatation unit, minute air bubbles are released from the solution. The sludge flocs, suspended solids or oil globules are floated by these minute air bubbles, which attach themselves to and became in the floc particles. The air-solids mixture rises to the surface, where it is skimmed off. The clarified liquid is removed from the bottom of the flotation unit, at this time a portion of the effluent may be recycled back to the pressure chamber. When flocculent sludges are to be clarified, pressurized recycle will usually yield a superior effluent quality since the flocs are not subjected to shearing stress through the pumps and pressurizing system.

Coagulation

Coagulation is employed for the removal of waste materials in suspended or colloidal form. Colloids are presented by particles over a range of 0.1-1.0 nm. These particles do not settle out on standing and cannot be removed by conventional physical treatment processes.

Colloids present in wastewater can be either hydrophobic or hydrophilic. The hydrophobic colloids possess no affinity for the liquid medium and lack stability in the presence of electrolytes. They are readily susceptible to coagulation. Hydrophilic colloids, such as proteins, exhibit a

marked affinity for water. The absorbed water retards flocculation and frequently requires special treatment to achieve effective coagulation.

Electrical properties of the colloids create a repelling force and prevent agglomeration and settling. Stabilizing ions are strongly adsorbed to an inner fixed layer which provides a particle charge that varies with the valence and number of adsorbed ions. Ions of an opposite charge form a diffuse outer layer which is held near the surface by electrostatic forces. The stability of a colloid is due to the repulsive electrostatic forces and in the case of hydrophilic colloids to solvation in which an envelope of water retards coagulation.

Adsorption

Many wastewaters contain organics which are refractory and which are difficult or impossible to remove by conventional biological treatment processes, such as acrylonitrile-butadiene-styrene (ABS) and some of heterocyclic organics. These materials can frequently be removed by adsorption on an active-solid surface. The most commonly used adsorbent is activated carbon. The solid surface in contact with the solution tends to accumulation a surface layer of solute molecules because of the unbalance of the surface forces. The physical adsorption results from molecular condensation in the capillaries of the solid. In general, substances of high molecular weight are most easily adsorbed. There is a rapid formation of an equilibrium interfacial concentration, follow by the slow diffusion into the carbon particles. The overall rate of adsorption is controlled by the rate of diffusion of the solute molecules within the capillary pores of the carbon particles. The rate varies reciprocally with the square of the particle diameter

and increases with the increasing of solute concentration and increasing of temperature, but decreases with the increasing of molecular weight of the solute.

2.3.2 Biological treatment [7]

The biological processes in treatment plants are carried out by a very diversified group of organisms. It is only possible roughly to list which species are present as it proves that the fauna in a treatment plant is very dependent on the external conditions.

All organisms in the biological treatment plant must necessarily have their origins from the outside; that is, they come from the wastewaters, from the air, the soil or from the animals which live close to the plant. An essential part of individual organisms has grown in the plant itself.

The two main types of biological treatment plants are activated sludge and biofilters treatment plants.

Activated sludge treatment

The principle in activated sludge treatment plants is that a mass of activated sludge is kept moving in the water by stirring or aeration. Apart from the living biomass, the suspended solids contain inorganic as well as organic particles. Some of the organic particles can be degraded by subjecting them to hydrolysis whereas others are non-degraded.

The amount of suspended solids in the treatment plant is granulated through the recycle of the suspended solids and by removing the so called-

excess sludge. The handling and disposal of the excess-sludge is one of the environmentally difficult problems in water treatment processes.

Biofilters

Biofilters are characterized by bacteria being attached to a solid surface in the form of a biofilm. Biofilm is a dense layer of bacteria characterized by their ability to adhere to a solid medium and form a fixed film of polymers in which the bacteria are protected against sloughing off. Biofilters have a short hydraulic retention time and hence free bacteria in the water will be washed out.

The disadvantage of the biofilters is the low efficiency of the biomass. The reason is that the substances must be carried through the biofilm to be removed by the bacteria. This transport takes place by molecular diffusion which is a slow process. In practice it proves that the general rule is that the removal is limited by diffusion. These phenomena must be understood in order to understand the functioning of biofilters.

2.3.3 Chemical treatment [7]

Ozonation

Ozone is a gas at normal temperature and pressure. As with oxygen, the solubility of ozone in water depends on temperature and the partial pressure of ozone in the gas phase and has recently been thought to also be a function of pH. Ozone is unstable and the rate of decomposition increases with temperature and pH. The decomposition is catalyzed by the hydroxyl radical ($OH^{\bullet}$), the radical decomposition product of ozone, the organic solute

decomposition products and by variety of the other substances such as solid alkalis, transition metals, metal oxides and carbon. Under practical conditions, complete degradation of fairly unreactive compounds such as saturated hydrocarbons and halogenated aliphatic compounds does not occur with ozone alone, but current research has shown that ozone with addition of energy source such as sonification or ultraviolet readily decomposes these refractory compounds.

Ozonation of unsaturated aliphatic or aromatic compounds causes a reaction with water and oxygen to form acids, ketones and alcohols. At a pH greater than 9 in presence of redox salts such as Fe, Mn and Cu, aromatic may form some hydroxyaromatic structures (phenolic compound) with maybe toxic. Many of the byproducts of ozonation are readily biodegradable.

Organic removal is improved with the ultraviolet radiation. It is postulated that the ultraviolet activates the ozone molecule and may also activate the organics. Ozone-ultraviolet is effective for the oxidative destruction of pesticides to terminal end products of CO_2 and H_2O.

Hydrogen peroxide

Hydrogen peroxide in the presence of a catalyst such as iron, generated hydroxyl radical ($^{\bullet}OH$) which react with organics and reduced compounds in a similar to ozone [7].

$$Fe^{2+} + H_2O_2 \rightarrow Fe^{3+} + OH^- + {}^{\bullet}OH \qquad (2\text{-}1)$$

$$Fe^{3+} + H_2O_2 \rightarrow Fe^{2+} + {}^{\bullet}OOH + H^+ \qquad (2\text{-}2)$$

$$^{\bullet}OH + RH \rightarrow R^{\bullet} + H_2O \quad (2\text{-}3)$$

$$R^{\bullet} + H_2O_2 \rightarrow ROH + {}^{\bullet}OH \quad (2\text{-}4)$$

$$^{\bullet}OH + Fe^{2+} \rightarrow OH^{-} + Fe^{3+} \quad (2\text{-}5)$$

Chlorine

Chlorine may be used as a chemical oxidant. In reaction with inorganic materials terminal end products usually result such as NaCl and nitrogen gas were produced from the oxidation of cyanide by using NaOCl as chlorine source. While chlorinated hydrocarbons were produced from organic oxidations.

Wet air oxidation

Wet air oxidation has been successfully applied in a number of applications for organics reduction. Wet air oxidation is based on a liquid phase reaction between organic materials in wastewater and oxygen supplied by compressed air. The reaction takes place flamelessly in an enclosed vessel, which is pressurized and at high temperatures, typically 136 atm gauge and 288 ^{o}C. The system temperature is initiated by a startup boiler and maintained through autothermal combustion of organics once the reaction starts.

2.4 Electrochemical treatment [8]

Water treatment by electricity was used for several years, but electrochemical water or wastewater technologies did not find wide application by the limitation of relatively high capital investment and the expensive electricity supply. However, with the increasing standard of drinking water supply and the stringent environmental regulations regarding the wastewater discharge, electrochemical technologies have regained their importance worldwide during the past two decades. There are companies supplying facilities for metal recoveries, for treating drinking water or process water, treating various wastewaters resulting from tannery, electroplating, diary, textile processing, oil and oil-in-water emulsion, etc. Nowadays, electrochemical technologies have reached such a state that they are not only comparable with other technologies in terms of cost but also are more efficient and more compact. For some situations, electrochemical technologies may be the indispensable step in treating wastewaters containing refractory pollutants. In addition, electrochemical process is a clean process that does not generate by-product or other pollutants.

2.4.1 Electrocoagulation

Electrocoagulation involves the in situ generation of coagulants by dissolving electrically either aluminum or iron ions from aluminum or iron electrodes, repectively. The metal ions generation takes place at the anode, hydrogen gas is released from the cathode. The hydrogen gas would also help to float the flocculated particles out of the water. This process sometimes is called electroflocculation. It is schematically shown in Figure 2-1. The electrodes can be arranged in a mono-polar or bi-polar mode. The

materials can be aluminum or iron in plate form or packed form of scraps such as steel turnings, millings, etc. The chemical reactions taking place at the anode are given as follows.

For aluminum anode:

$$Al \rightarrow Al^{3+} + 3e^{-} \quad (2\text{-}6)$$

At alkaline conditions

$$Al^{3+} + 3OH^{-} \rightarrow Al(OH)_3 \quad (2\text{-}7)$$

At acidic conditions

$$Al^{3+} + 3H_2O \rightarrow Al(OH)_3 + 3H^{+} \quad (2\text{-}8)$$

For iron anode:

$$Fe \rightarrow Fe^{2+} + 2e^{-} \quad (2\text{-}9)$$

At alkaline conditions

$$Fe^{2+} + 2OH^{-} \rightarrow Fe(OH)_2 \quad (2\text{-}10)$$

At acidic conditions

$$4Fe^{2+} + O_2 + 2H_2O \rightarrow 4Fe^{3+} + 4OH^{-} \quad (2\text{-}11)$$

In addition, there is oxygen evolution reaction

$$2H_2O \rightarrow O_2 + 4H^{+} + 4e^{-} \quad (2\text{-}12)$$

The reaction at the cathode is

$$2H_2O + 2e^- \rightarrow H_2 + 2OH^- \qquad (2\text{-}13)$$

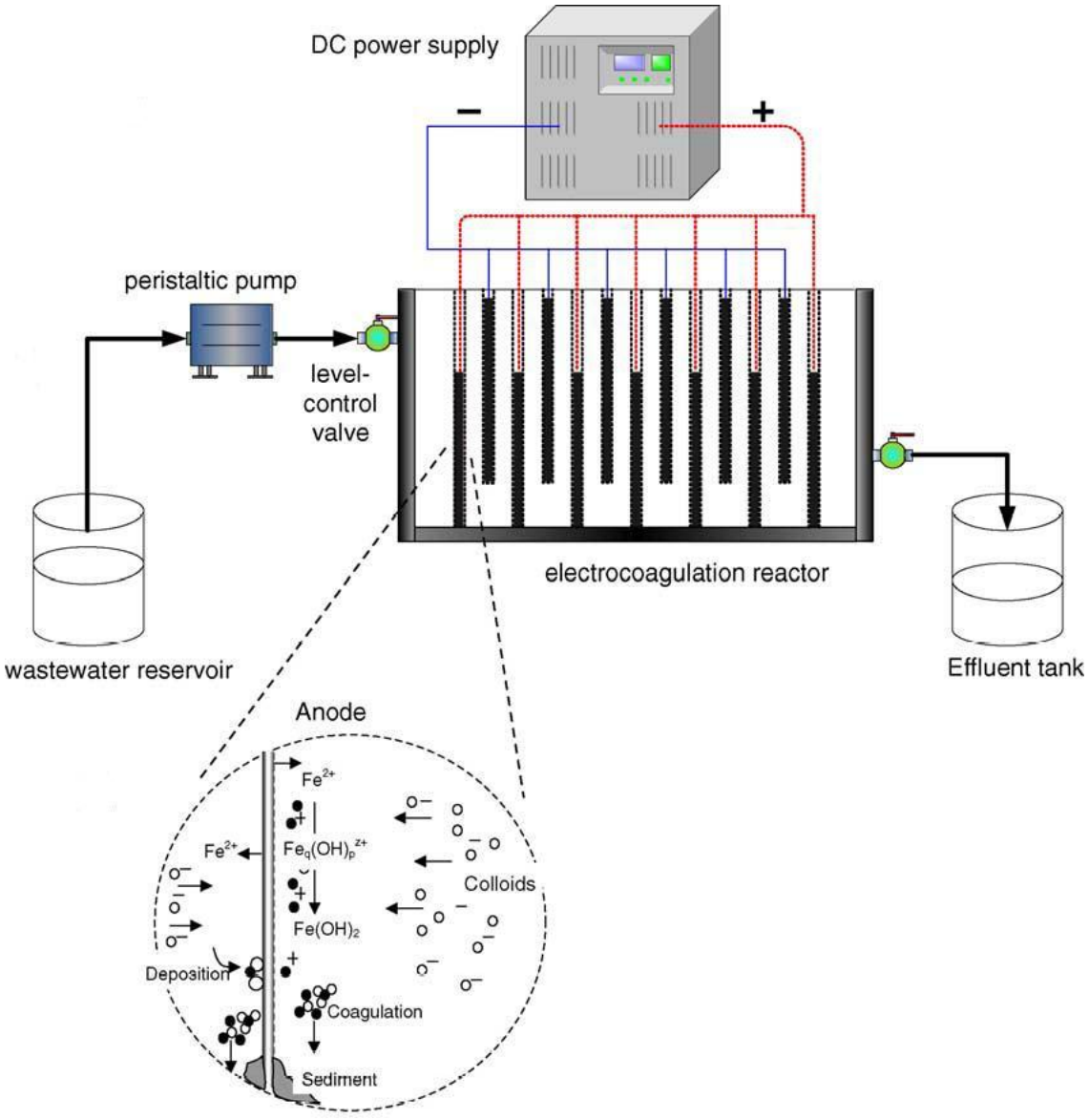

Figure 2-1 Scheme of electrocoagulation [9]

The Al^{3+} or Fe^{2+} ions are very efficient coagulants for particulates flocculating. The hydrolyzed aluminum ions can form large networks of Al–O–Al–OH that can chemically adsorb pollutants such as F^{-}. Aluminum is usually used for water treatment and iron for wastewater treatment [3]. The advantages of electrocoagulation include high particulate removal efficiency, compact treatment facility, relatively low cost and possibility of complete automation.

2.4.2 Electroflotation

Electroflotation is a simple process that floats pollutants to the surface of a water body by tiny bubbles of hydrogen and oxygen gases generated from water electrolysis. Therefore, the electrochemical reactions at the cathode and anode are hydrogen evolution and oxygen evolution reactions, respectively. The bubbles generated by electrochemistry are smaller the those generated by gases bubbling and help to remove the remove the aggregate generated by electrocoagulation. Figure 2-2 represents the process of electroflotation.

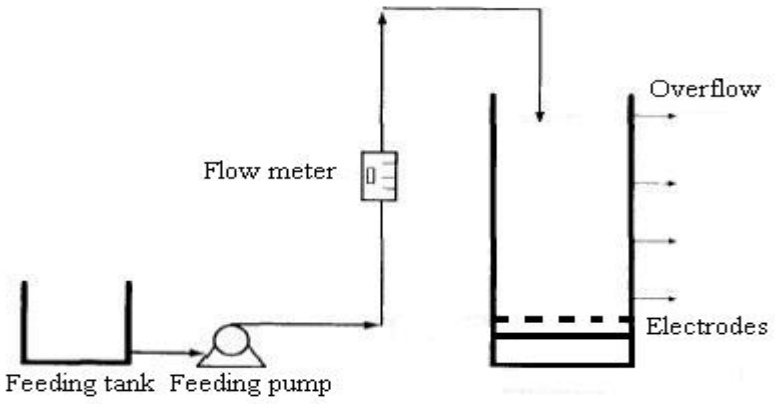

Figure 2-2 Electroflotation process [10]

2.4.3 Electrochemical oxidation

Study on electrochemical oxidation for wastewater treatment goes back to the 19th century, when electrochemical decomposition of cyanide was investigated [11]. Extensive investigation of this technology commenced since the late 1970s [8]. During the last two decades, research works have been focused on the efficiency in oxidizing various pollutants on different electrodes, improvement of the electrocatalytic activity and electrochemical stability of electrode materials, investigation of factors affecting the process performance, and exploration of the mechanisms and kinetics of pollutant degradation. Experimental investigations focus mostly on the behaviors of anodic materials, the effect of cathodic materials was not investigated extensively although Azzam et al. [12] have found a considerable influence of the counter electrode material in the anodic destruction of 4-chlorophenol.

2.5 Mechanisms of electrochemical oxidation [7]

In Figure 2-3, a generalized scheme of the electrochemical conversion and combustion of organics on metal oxide anode (MO_x) is presented. In the first step, H_2O in acid or OH^- in alkali solution is discharged at the anode to produce adsorbed hydroxyl radical according to the equation (2-14).

$$MO_X + H_2O \xrightarrow{k_1} MO_X(^{\bullet}OH) + H^+ + e^- \qquad (2\text{-}14)$$

In the second step, the adsorbed hydroxyl radicals may interact with the oxygen already present in the metal oxide anode with possible transition

of oxygen from the adsorbed hydroxyl radical to the lattice of the metal oxide anode forming the so-called higher oxide (MO_{X+1}) as represented in equation (2-15).

$$MO_X(^{\bullet}OH) \xrightarrow{k_2} MO_{X+1} + H^+ + e^- \qquad (2\text{-}15)$$

Thus, we can consider that at the anode surface, two states of active oxygen can be presented in physisorbed active oxygen (adsorbed hydroxyl radicals, $^{\bullet}OH$) and chemisorbed active oxygen (oxygen in the oxide lattice, MO_{x+1}).

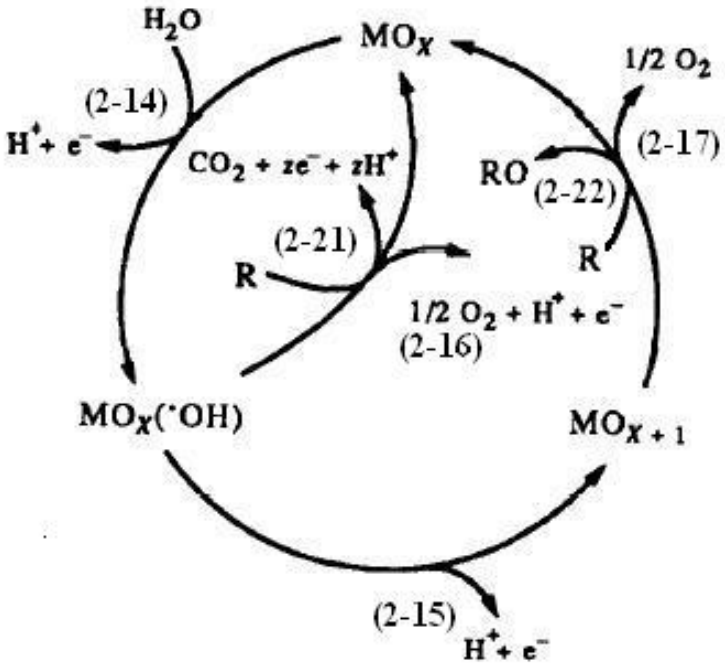

Figure 2-3 Generalized scheme of the electrochemical conversion and combustion of organics with simultaneous oxygen evolution: (2-14) H_2O discharge and (2-15) transition of O from $^{\bullet}OH$ to the lattice of the oxide anode [7].

In the absence of any oxidizable organics, the physisorbed and chemisorbed active oxygen produce dioxygen according to the equation (2-16) and (2-17).

$$MO_X(^{\bullet}OH) \xrightarrow{k_o} \frac{1}{2}O_2 + H^+ + e^- + MO_X \quad (2\text{-}16)$$

$$MO_{X+1} \xrightarrow{k_d} MO_X + \frac{1}{2}O_2 \quad (2\text{-}17)$$

Direct evidence for the last route of oxygen evolution at platinum oxide (PtO_x) is provided by the work of Rosenthal [13] who used ^{18}O as a tracer to show that portion of the evolved gas comes from oxygen already present in the oxide film. This view was put forward several times with other electrodes (RuO_2, IrO_2, $NiCo_2O_4$ and NiOOH) [14].

Such a result may be explained in terms of the equations (MO = oxide anode).

$$2M^{18}O + 2H_2{}^{16}O \rightarrow 2M^{18}O(^{16\bullet}OH) + 2H^+ + 2e^- \quad (2\text{-}18)$$

$$2M^{18}O(^{16\bullet}OH) \rightarrow 2M^{18/16}O_2 + 2H^+ + 2e^- \quad (2\text{-}19)$$

$$2M^{18/16}O_2 \rightarrow M^{18}O + M^{16}O + {}^{18/16}O_2 \quad (2\text{-}20)$$

In the presence of oxidizable organics, it is speculated that the physisorbed active oxygen ($^{\bullet}$OH) should cause predominantly the complete combustion of organics according to equation (2-21), and chemisorbed

active oxygen (MO_{x+1}) participate in the formation of selective oxidation products as represented in equation (2-22).

Complete combustion:

$$R + MO_X(^{\bullet}OH) \xrightarrow{k_c} CO_2 + zH^+ + ze^- + MO_X \quad (2\text{-}21)$$

Selective oxidation:

$$R + MO_{X+1} \xrightarrow{k_S} RO + MO_X \quad (2\text{-}22)$$

2.5.1 Electrochemical conversion

For the electrochemical conversion or selective oxidation of organics, the concentration of adsorbed hydroxyl radicals on the anode surface must be almost zero. To satisfy this condition, the rate of transition of oxygen into the oxide lattice in equation (2-15), must be much more faster than the rate of hydroxyl radicals formation in equation (2-14).

when

Rate of hydroxyl radicals formation = $k_1[MO_X]$

Rate of transition of oxygen in the oxide lattice = $k_2[\ ]$

$$k_2[\ ] \gg k_1[MO_X] \quad (2\text{-}23)$$

where

k_1 = Electrochemical rate constant for H_2O discharge

k_2 = Electrochemical rate constant for transition of oxygen into oxide lattice

$[MO_X]$= Concentration of active sites on the oxide anode

$[\ ]$ = Concentration of oxygen vacancies in the oxide lattice.

Thus, efficient anodes for selective oxidation or electrochemical conversion of organics must have low concentration of active sites on the anode surface and must have a high concentration of oxygen vacancies in the oxide lattice.

Oxides forming is called higher oxide (MO_{x+1}) at potentials above the thermodynamic potential for O_2 evolution can be considered as oxides having a high concentration of oxygen vacancies and can favor selective oxidation of organics.

The current efficiency depends on the relative rate of the selective oxidation of organics, equation (2-22) to rate of oxygen evolution by decomposition of the higher oxide according to equation (2-17)

When

Rate of selective oxidation of organics = $z_s k_s [O][R]_t$

Rate of O_2 evolution by decomposition of MO_{x+1} = $k_d[O]$

Where

z_s = Stoichiometry factor for selective oxidation;

k_s = Electrochemical rate constant for the selective oxidation of organics in equation (2-22)

k_d = Electrochemical rate constant for O_2 evolution in equation (2-17)

$[O]$ = Steady state concentration of active oxygen in the oxide lattice

$[R]_t$ = Concentration of organics at a given time, t

The instantaneous current efficiency (ICE) can be given by the relation in equation (2-24)

$$ICE = \frac{z_s k_s [R]_t}{z_s k_s [R]_t + k_d} \qquad (2\text{-}24)$$

This relation shows that the instantaneous current efficiency for the selective oxidation is independent of the anode potential ,but depends on the reactivity of organics. High ICE can be obtained with reactive organics and with anodes having low rate for the decomposition of their higher oxide.

2.5.2 Electrochemical combustion

For the combustion of organics, high concentration of hydroxyl radicals on the anode surface must be present. This is the case when the rate of hydroxyl radicals formation according to equation (2-14), is much faster than the rate of oxygen transition into oxide lattice as represented in equation (2-15). The following relation must be satisfied.

$$k_1[MO_X] \quad » \quad k_2[\ ] \qquad (2\text{-}25)$$

Thus efficient oxide anodes for combustion of organics must have a large number of active sites for the adsorption of hydroxyl radicals and must have a very low concentration of oxygen vacancies in the oxide lattice.

Oxides in which the oxidation state of the cation is the highest possible and/or which contains an excess oxygen in the oxide lattice can be considered as oxides at the surface of which the hydroxyl radicals are accumulated and favor the combustion of organics.

The current efficiency for the combustion of organics depends on the relative rate of combustion of organics, represented in equation (2-21), to the rate of oxygen by discharge of the adsorbed hydroxyl radicals according to equation (2-16).

when

Rate of combustion of organics = $z_c k_c [\cdot OH][R]_t$

Rate of O_2 evolution by discharge of ·OH = $k_0[\cdot OH]$

where

z_c = Stoichiometry factor for complete combustion of organics

k_c = Electrochemical rate constant for the combustion of organics

k_0 = Electrochemical rate constant for O_2 evolution

$[\cdot OH]$ = Steady-state concentration of adsorbed hydroxyl radicals at the oxide anode

$[R]_t$ = Concentration of organics at a given time

The instantaneous current efficiency for electrochemical combustion can be given by the relation.

$$ICE = \frac{z_c k_c [R]_t}{z_c k_c [R]_t + k_0} \qquad (2\text{-}26)$$

This relation shows that the instantaneous current efficiency for the combustion of organics depends on the nature of organics, its concentration, the anode material and on the anode potential. High instantaneous current

efficiency for the combustion of organics can be obtained with anodes having low electrochemical activity for O_2 evolution by discharge of hydroxyl radicals according to equation (2-16).

In the mechanism, it is very probable that dioxygen participates also in the combustion of organics according to the following reaction scheme:

Formation of organic radicals by a hydrogen abstraction mechanism:

$$R\text{-}H + \cdot OH \rightarrow R\cdot + H_2O \qquad (2\text{-}27)$$

Reaction of the organic radicals with dioxygen formed at the anode:

$$R\cdot + O_2 \rightarrow ROO\cdot \qquad (2\text{-}28)$$

Further abstraction of a hydrogen atom with the formation of an organic hydroperoxide (ROOH) and another organic radical:

$$ROO\cdot + R'H \rightarrow ROOH + R'\cdot \qquad (2\text{-}29)$$

Since the organic hydroperoxides formed are relatively unstable, decomposition of such intermediates often leads to molecular breakdown and formation of subsequent intermediates with lower carbon numbers. These scission reactions continue rapidly until the formation of carbon dioxide and water.

2.5.3 Electrochemical oxidation performance

There are several researchers' work on the parameters that affect on the electrochemical oxidation process efficiency. In this section, we literate on some important parameters for electrochemical treatment by electrochemical oxidation.

Support materials

Vercesi et al. [15] worked on searching for a good dimensionally stable electrode (DSA) that long service life for O_2-evolution based on the effects of support materials. Titanium, tantalum, zirconium, niobium and some of their alloys were used as support materials on the performance of IrO_2-Ta_2O_5 coated electrodes. The thermal behavior and oxygen affinity sequence of the metals, in relation to the electrode preparation procedure, were determined thermogravimetrically. The electrochemical corrosion of base metals was represented in Figure 2-4, the tantalum-based materials presented the highest stability with the minimum corrosion rate. The chemical and electrochemical stability of the base metals was found to be directly related to the service life of the electrode, measured in 30% H_2SO_4 at 80°C and 750 mA/cm^2. Tantalum-based electrodes represented the highest service life, 1700 h and 120 h for titanium-based electrodes.

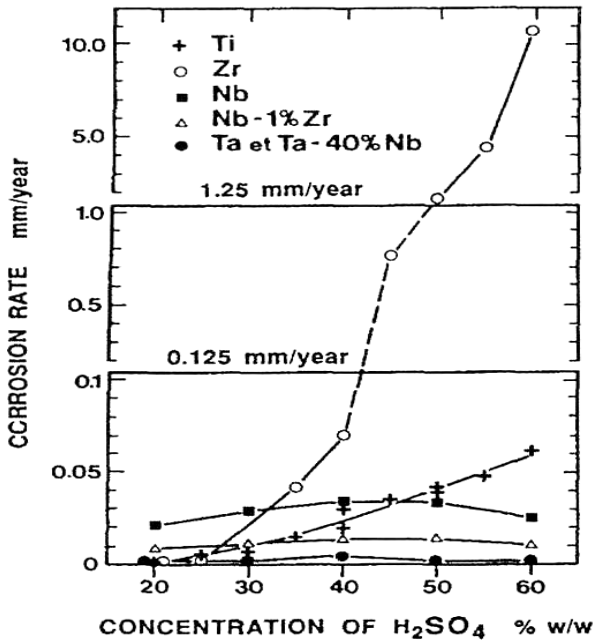

Figure 2-4 Electrochemical corrosion rate of base metals as a function of H_2SO_4 concentration at anode potential of 2 V/SCE

Coating materials

The active coating materials of electrodes are very important for pollutants degradation in electrochemical oxidation process. It could point the project to be benefit or insolvent. The coating enables the electrical charge transport between the base metal and the electrode/electrolyte interface. It must have high chemical and electrochemical stability and able to catalyse the desired electrochemical reaction.

There are some works focusing on the active coating materials for electrochemical degradation of organic pollutants in wastewater. Comninellis and Vercesi [16] found that the Ta_2O_5-doped IrO_2 represented

the highest service life. However, Comninellis [3] proposed in 1994 that the mechanism of electrochemical oxidation of organic pollutant on IrO_2 electrode was the electrochemical selective oxidation while that on SnO_2 electrode was the electrochemical combustion. On SnO_2 electrode, the organic pollutants were oxidized to CO_2 and water. Figure 2-5 represents the comparison of current efficiency of some various coating materials. The SnO_2 electrode presents the highest current efficiency. Because of its highest oxidation state which contains excess oxygen in the oxide lattice as possible. At SnO_2 surface, the hydroxyl radicals are accumulated and favor the combustion of organics while the other oxides having a high concentration of oxygen vacancies and can favor selective oxidation of organics more than combustion.

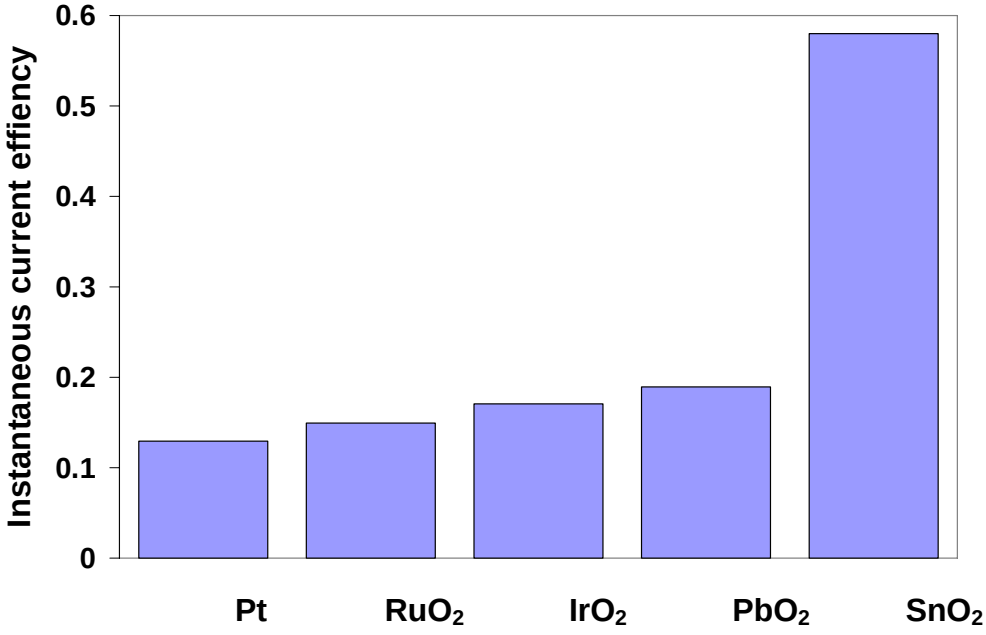

Figure 2-5 Instantaneous current efficiency of various coating materials [3, 16-17]

Not only SnO_2 electrode has the good attractive to be used as electrode for wastewater treatment in electrochemical oxidation, the diamond thin films have been widely used in electrochemical studies due to the unique properties like chemical stability, large potential range and mechanical resistance. Their applications embrace the electroanalysis, electrosynthesis, fuel cell and the organic pollutant degradation in wastewater [18]. Some studies showed that conducting diamond electrodes could be grown by energy-assisted (plasma or hot-filament) chemical vapor deposition on several substrates, such as silicon, titanium, niobium, tantalum, molybdenum, glassy carbon. Although all these substrates are currently used, they still have some drawbacks. In fact, a silicon substrate is very brittle, Nb, Ta, W are too expensive and the stability of the diamond layer deposited on the Ti substrate is still not satisfactory, because cracks may appear and cause the detachment of the diamond film during long-term electrolysis [19]. The organic compound electrochemical oxidation efficiency strongly depends on the used anode material and diamond is very interesting due to its superior properties [18]. In recent years, there are some publications on the application of diamond electrode for wastewater treatment [18-22]. However, the application of diamond electrode for organic pollutant degradation still limited due to the cost of diamond electrode is too expensive.

pH

Normally, the efficiency of the oxidation of organics tends to be superior in alkaline solution. That also holds for the anodic treatment using standard electrode materials. The wastewater accessible to treatment process has any pH and pH adjustment before treatment to the more favorable value

above 7 will be too expensive. Moreover, Stuki et. al. [23] proved that on SnO_2 electrodes, the degradation of benzoic acid was pH independent. Cañizares et. al [24] proposed that the pH does not influence in the global oxidation rate. Even if initial oxidation rate was higher in alkaline media. However, after the galvanostatic developed, the oxidation rate in acidic media surpasses those in the alkaline media. Because the accumulation of oxalic acid in alkaline media was higher than that in acidic media, due to its lower oxidazability at alkaline conditions.

Current density

The effect of current density was studied many times, Comninellis and Nerini [17] in 1995 found that the degradation of phenol was independent from the current density. Figure 2-6 shows that the phenol elimination depends only on the specific electrical charge. Almost complete phenol elimination can be archived after the passage of an electrical charge of 17-20 Ah/dm^3.

The higher current densities increase the initial reaction rate (dCOD/dt) but decrease lightly the initial efficiencies of the process (dCOD/dQ). Nevertheless, both treatments end nearly at the same charge passed. This behavior is a characteristic of electrochemical systems in which both direct and mediated oxidation reactions play an important role. But the low current density experiment achieves initially a higher mineralization rate. This fact can be easily explained that the amount of oxalic acid, that is an end of chain product and difficult to destroy, accumulated in the high current density experiment is greater than those obtained in the low current density experiments [24].

Although, the current density might not affect on the kinetic of surface electrochemical oxidation of organic pollutant, it also enhances the production of bulk chemicals, which may contribute to the degradation process through parallel reaction schemes.

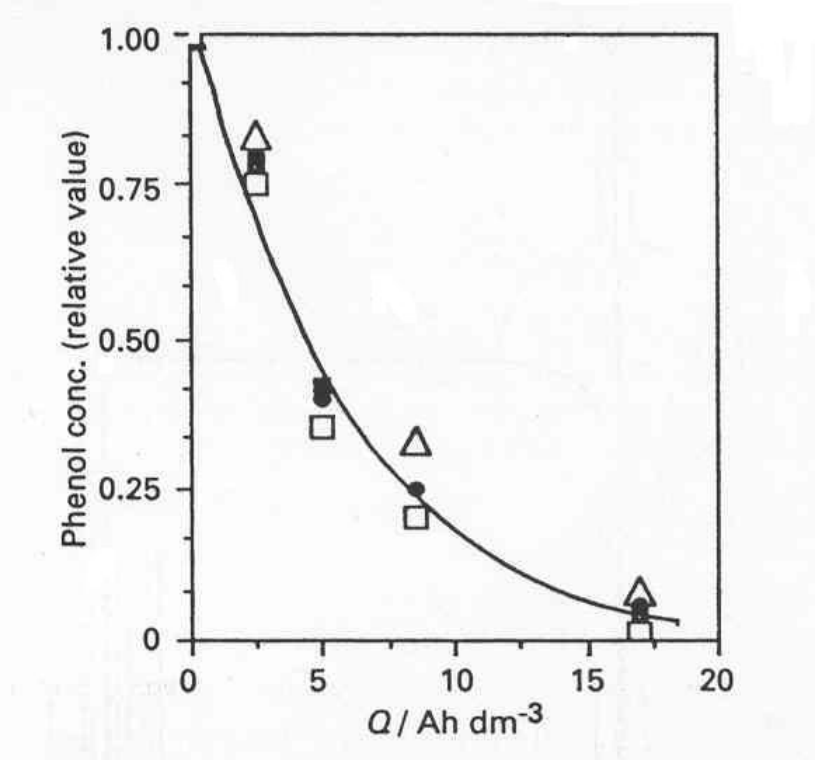

Figure 2-6 Influence of the current density on the degradation rate of phenol, (Δ) 0.10 A/cm^2, (●) 0.18 A/cm^2, (□) 0.20 A/cm^2 and (■) 0.30 A/cm^2 [17]

Temperature

An increase in the temperature leads to more efficient processes by global oxidation. While direct oxidation processes remain almost unaffected by temperature, this fact may be explained in terms of the presence of inorganic electrogenerated reagents. The oxidation carried out by these redox reagents is a chemical reaction. Consequently, its rate normally increases with temperature. But the oxidation process can be carried out either at the electrode surface and by electrogenerated reagents-mainly hypochlorite and peroxodisulphates. However, the new organic intermediates are not formed with the increase of temperature, indicating that the process mechanisms do not vary with temperature [24].

2.6 Electrocatalytic electrodes [25]

Electrochemical degradation of organic pollutants, presence in the wastewater needs specific electrodes. Typical substrates that used as electrocatalytic electrodes must have low voltage drop through the substrates and substrate-solvent interface. Many metallic electrodes could answer these criteria and many alloys can also be used as good composite electrodes covered with an active layer and a long service life of electrodes.

The complexity of electrode behaviors and our lack of detailed insights make it impossible to select the optimum electrode for a given process on a theoretical basis. Instead, an empirical approach must be used. The initial selection is based on process experience, and this is then tested and refined during an extensive development program. Indeed, it is very

difficult to predict the success of an electrode material or to define its lifetime without extended studies under realistic process conditions. Accelerated testing is rarely satisfactory except to indicate catastrophic failure.

There are some general guidelines to assist the choice of an electrode material;

Physical stability

The electrode material must have adequate mechanical strength, must not be prone to erosion by the electrolyte, reactants, or products, and must be resistant to cracking.

Chemical stability

The electrode material must be resistant to corrosion, unwanted oxide or hydride formation, and the deposition of inhibiting organic films under all conditions (e.g., potential and temperature) experienced by the electrode.

Suitable physical form

It must be possible to fabricate the material into the form demanded by the reactor design, to facilitate sound electrical connections, and to permit easy installation and replacement at a variety of scales. The shape and design of the electrode may take into account the separation of products, including the disengagement of gases or solids.

Rate and product selectivity

The electrode material must support the desired reaction and, in some cases, significant electrocatalytic properties are essential. The electrode material must promote the desired chemical change while inhibiting all competing chemical changes.

Electrical conductivity

This must be reasonably high throughout the electrode system including the current feeder, electrode connections, and the entire electrode surface exposed to the electrolyte. Only in this fashion it is possible to obtain a uniform current and potential distribution as well as to avoid voltage losses leading to energy inefficiencies.

Cost/lifetime

A reasonable and reproducible performance including a lifetime probably extending over several years must be achieved for an acceptable initial investment.

It is important to note that the choice of working and counter electrodes cannot be made independently since the chemistry at each has consequences to the solution composition throughout the cell. Indeed, the selection of electrode material and its form must be an integrated decision within the prospective of the cell and process design. In some cases such as the manufacture of pharmaceutical products, the electrodes and their compounds must have a low toxicity.

2.7 Influence of electrode material on process performance [25]

This section is literated the ways in which the choice of electrode material influences the design of electrochemical reactors and process performance.

Energy Consumption

The specific energy consumption should be minimized in order to minimize the power costs. In general, the total power requirement has contributions for both electrolysis and movement of either the solution or the electrode. The design of electrodes and cell has an important role in reducing each of these components. Thus, a very open flow-through porous electrode will have a low pressure drop associated with it, giving rise to modest pumping costs and facilitating reactor sealing. A high surface area electrode which itself a turbulence promoter in bed electrode, will give rise to a moderately high mass transfer coefficient and active area without the need for high flow rates through the cell; the pumping cost will again be moderately low.

The direct electrolytic power could be minimized by

- Obtaining a current efficiency approaching 1.0
- Minimizing the cell voltage.

It is therefore important to select the electrode material and operating conditions so as to maintain a high current efficiency. This also assists the operation of the process by reducing the amount of product purification that is necessary and/or byproducts that must be handled.

The cell voltage is a function of the reversible cell voltage, the over-potentials at the two electrodes, and ohmic drops in the electrolyte, the electrodes, busbars etc., and any separator in the cell. Again, the maintenance of a low cell voltage demands attention to the design of both electrodes and cell. Where possible, the following features should be included:

- The counter electrode reaction should be chosen so as to minimize the reversible cell voltage. This requires the availability of a suitably stable electrode material.
- The over-potentials at both electrodes should be minimized by the use of electrocatalysts.
- The electrodes, current feeders, and connectors should be made from highly conducting materials to lower ohmic drops.
- The electrodes should facilitate low *IR* drop in the electrolyte by, for example, allowing efficient gas disengagement and passage out of the interelectrode gap. Meshes as well as louvred and lantern blade electrodes can be used.
- Electrode and cell design should allow a small interelectrode or electrode membrane gap. In the limit, the electrode may touch the membrane as in zero-gap or solid polymer electrolyte cells.
- A separator should be avoided by suitable selection of the counter electrode chemistry or, if essential, a thin conductive membrane should be used.

Current efficiency

Current efficiency is the fraction of the total charge passed that is used in the formation of the desired product. This can be a strong function of electrode material, e.g., because of differences in the rate of hydrogen evolution as a competing reaction. Competing reactions can also lead to the corrosion and/or erosion of the electrode material as well changes to the electrode (e.g., by formation of a hydroxide or oxide or the deposition of another metal onto the surface).

Material Yield

This is the fraction of the starting material that is converted into the desired product. This is also dependent on electrode material in many cases. Values less than one indicate byproducts and hence perhaps the need to introduce additional purification steps that inevitably increases the complexity of the overall process and costs.

Space-Time Yield

One of the most valuable statements of reactor performance is the space-time yield or weight of product per unit time per unit volume of reactor. It is determined by the current density, the current efficiency, and the area of electrode per unit volume of cell, all dependent on the electrode material and its form. Commonly, the cell is operated in conditions where the electrode reaction is mass-transport controlled (especially when a high fractional conversion is desirable or when the concentration of reactant is limited by solubility or process considerations. Then, the current density is determined by the concentration of reactant and the mass transport condition.

The latter is therefore frequently enhanced by the use of high flow rates, turbulence promoters, and/or electrode movement.

The current is proportional to the active electrode area in the cell. A compact cell design requires a high area per unit cell volume. This suggests the use of a three-dimensional electrode but such electrodes make it difficult to maintain a uniform fluid flow and electrode potential, i.e., to control the reaction environment. Hence, the use of porous, flow-through electrodes often involves a trade-off between enhanced electrode area and material yield and/or current efficiency.

Ease of product isolation

Many industrial electrosyntheses benefit from clever process design to reduce the number of steps in the product isolation and purification. This can be critical to the process economics.

Other Factors

Of course, other factors are important in the design of electrodes and cells. These include cost, safety, ease of maintenance, and convenience to use. It is also essential that the performance of the electrodes is maintained throughout the projected operating life of the cell, maybe several years. Examples of problems that frequently arise include (a) deposition onto cathode surfaces of hydrogen evolution catalysts due to trace transitional metal ions in the electrolyte and (b) poisoning of PbO_2 anodes by organic molecules leading to enhanced corrosion as well as oxygen evolution.

2.8 SnO_2 type dimensionally stable anodes (DSA)

The discovery of the dimensionally stable anodes (DSA) has brought significant improvements in the chlor-alkali industry and in many other applications such as water electrolysis, metal electrowinning, selective synthesis and destructive oxidation of organic contaminants [26]. The DSA electrodes consist of pure or mixed metal oxide coatings deposited on a base metal using an appropriate precursor.

The pure SnO_2 is an n-type semiconductor with a direct band gap of roughly 3.5 eV and can be used as an electrode material with reasonable conductivity only at high temperatures. The doped SnO_2 has been used as transparent electrode material in photoelectrochemistry. The electrochemical properties of polycrystalline as well as single crystalline, SnO_2 were investigated by several researchers [27].

The combination of high chemical and electrochemical stability as a consequence of the rather large band gap, high conductivity of doped SnO_2 and the high oxygen evolution overpotential, makes SnO_2 as an attractive electrode material for the anodic oxidation of organics in aqueous solutions [27]. The crystalline structure of SnO_2 is presented in Figure 2-7 [28].

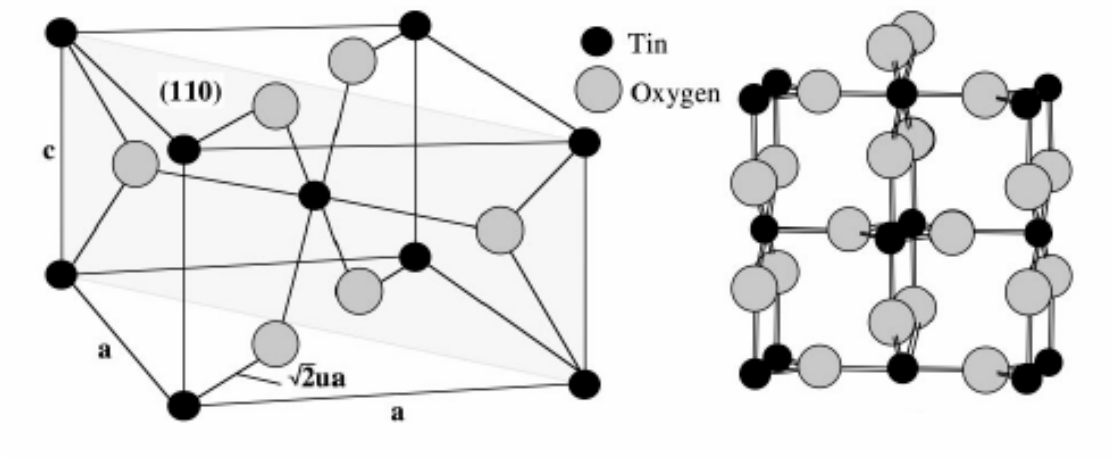

Figure 2-7 Crystalline structure of SnO_2 [28]

2.8.1 Preparation of SnO_2 type dimensionally stable anodes

There are a variety of methods available for coating the catalyst support for obtain the dimensionally stable anodes;

Sputtering [29]

The principle of sputtering is relatively simple. A source, also called the target, is bombarded in a high vacuum with gas ions that have been accelerated by a high voltage, producing a glow discharge or plasma. Atoms from the target are ejected by momentum transfer and move across the vacuum chamber to be deposited on the substrate to be coated.

Very low initial pressure is required to remove impurities from the system. The development of a magnetically enhanced cathode or magnetron has considerably expanded the potential of sputtering. The magnetron sends

the electron into spiral paths to increase collision frequency and enhance ionization.

Reactive sputtering occurs when the species are sputtered in a reactive atmosphere such as nitrogen or methane. The process is now used extensively for the deposition of nitrides and carbides. Sputtering can produce a wide variety of coatings with excellent adhesion and good composition control without the high temperature requirements as CVD. Its major disadvantages are its low deposition rate and its line-of-sight characteristic. The latter can be overcome to some extent by operating at higher pressure, but at some sacrifice in deposition rate.

Ruske et. al. [30] studied the coating of SnO_2 on silicon wafer by DC and MF reactive sputtering in Ar/O_2 atmosphere with while the system was represented in Figure 2-8. The higher film densities and hardness were observed for MF sputtering coating. The morphology of samples coated by MF sputtering were strongly depend on deposition pressure, it was changed from close-packed fibrous grains to columnar structure when deposition pressures increased from 0.3 to 1.0 Pa. The crytal orientation of DC sputtering films changed from 110 to 101 with the increasing of 0.3 to 0.6 Pa. It also changed from 110 to 211 for MF coated films with the increasing of deposition pressure from 0.3 to 1.0 Pa. The internal stress is higher for MF coated film. However, it could be reduced by increasing of deposition pressure.

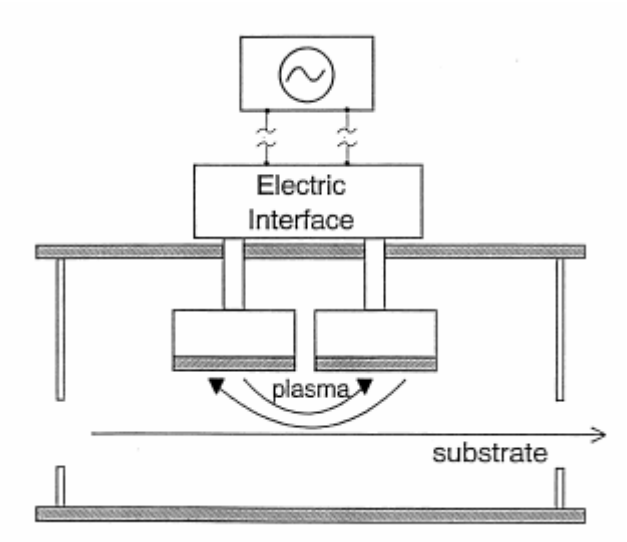

Figure 2-8 Schematic overview of a medium frequency (MF) powered twin magnetron reactive sputtering system [30]

Sol-gel dip coating [29]

Sol-gel processing or, more broadly speaking, the processing of ceramics and glasses from chemical precursors, is an emerging technology with a great potential especially in coatings and fiber production. At present, the development of sol-gel is still predominantly in the laboratory, yet it as spurred a great deal of interest in high-technology industries such as semiconductors, optoelectronics, optics, and structural ceramics. Sol-gel is already used in a sizable range of applications particularly in thin films. These applications include the spin-on-glass (SOG) process which is used in semiconductor fabrication and the coating of architectural glass to control optical properties.

The sol-gel process uses a liquid reactive precursor material that is converted into the final product by chemical and thermal means. This

precursor is prepared to form a colloidal suspension or solution (sol) which goes through a gelling stage (gel) followed by drying and consolidation. The process requires only moderate temperatures, in many cases less than half the conventional glass or ceramics processing temperatures. It also permits very close control of the composition and structure of the deposit on the molecular level and mates possible the production of near-net shapes. These are very important advantages.

A number of processing problems still need to be solved. The need for better control of shrinkage and cracking is critical. The cracking of coating was presented in Figure 2-9 [31]. Moreover, the cost of precursor materials is still high, although it is likely to come down as applications are developed and consumption increases.

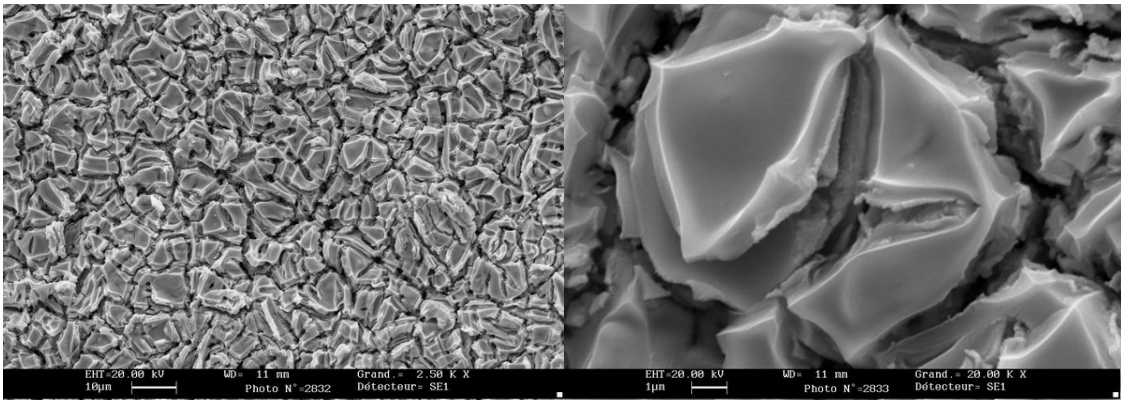

a) **b)**

Figure 2-9 Cracking of IrO_2 layer by sol-gel dip coating technique a) 2,500X and b) 20,000X [31]

Liu et. al. [32] prepared the IrO_2/SnO_2 mixed oxide electrodes by sol-gel technique. The prepared electrodes were performed by brushed precursor solution on titanium substrates and annealed at various temperatures. It was found that the crystalline IrO_2 and SnO_2 were formed at 300 °C or higher. However, the best annealing temperature was 400 °C. Nevertheless, the substrate is not protected from the shrinkage and cracking of coating layer and could be quickly destroy.

Spray pyrolysis [33]

In the spray deposition process, a precursor solution is pulverized by means of a neutral gas, so that it arrives at the substrate in the form of very fine droplets. The constituents react to form a chemical compound onto the substrate. The chemical reactants are selected such that the products other than the desired compound are volatile at the temperature of deposition.

Figure 2-10 represents a typical spraying system [33]. It mainly consists of spray nozzle, precursor solution, substrate heater, temperature controller and air compressor or gas propellant. To measure flow of precursor solution and air, liquid and gas flow meters are used. Vertical and slanted spray deposition arrangements with stationary or linearly moving spray nozzle are frequently used in this technique. To achieve uniform deposition the moving arrangements (either nozzle or substrates or both) have been used. Sometimes the spray assembly is mounted on a moving table and is rastered across the substrates using stepping motors.

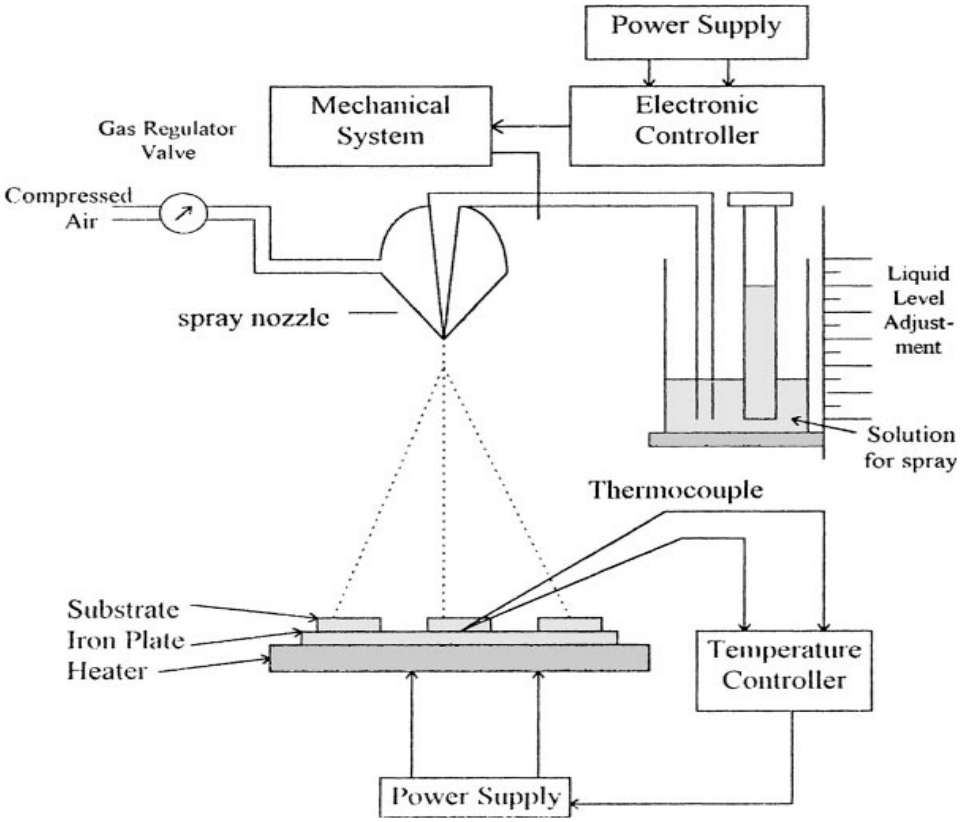

Figure 2-10 Schematic set-up for spray pyrolysis technique [33]

The properties of the film depend upon the anion to cation ratio, spray rate, substrate temperature, ambient atmosphere, carrier gas, droplet size and also the cooling rate after deposition. The film thickness depends upon the distance between the spray nozzle and substrate, substrate temperature, the concentration of the precursor solution and the quantity of the precursor solution sprayed.

The film formation depends on the process of droplet landing, reaction and solvent evaporation, which are related to droplet size and momentum. An ideal deposition condition is when the droplet approaches the substrate

just as the solvent is completely removed. Lampkin [34] showed that, depending on droplet velocity and flow direction, a droplet will flatten, skip along the surface or hover motionless.

Kötz et. al. [27] prepared the Sb, F and Cl doped SnO_2 electrodes on titanium substrate by using of $SnCl_4x5H_2O$ as precursor and $SbCl_3$, NH_4F and residue Cl were used as doping agent at temperature around 500 °C. The best composition of spray solution was found to be 10 g of $SnCl_4x5H_2O$ and 0.1 g of $SbCl_3$ in 100 ml of ethanol. The results represented that lowest resistance films are fluorine doped SnO_2 film at temperature between 400-500 °C. At reference current density 0.1 mA/cm^2 in 0.1 N H_2SO_4 the oxygen evolution potential increased from 1.50 to 1.65 and to 1.95 V/SCE for Pt, PbO_2 and prepared SnO_2 electrode, respectively. Furthermore, it was found that the reaction mechanism of phenol anodic oxidation on SnO_2 electrode was different from that on Pt/Ti electrode. The quinine intermediates was not formed in the reaction. That means that either the quinines are much more rapid oxidized on SnO_2 than on platinum or the ring-opening of phenol was occurred as the first step of the reaction.

2.9 Chemical vapor deposition [35]

Chemical vapor deposition (CVD) is the process of chemically reacting a volatile compound of a material with other gases to be deposited, to produce a nonvolatile solid that deposits atomistically on a suitably placed substrate. It differs from physical vapor deposition (PVD), which relies on material transfer from condensed-phase evaporant or sputter target sources.

Because CVD processes do not require vacuum or unusual levels of electric power, they were practiced commercially prior to PVD. A century ago, CVD methods were used to deposit a protective tungsten coating on carbon filaments in an attempt to extend the life of incandescent lamps. Today, high-temperature CVD processes for producing thin films and coatings have found increasing applications in such diverse technologies as the fabrication of solid-state electronic devices, the manufacture of ball bearings and cutting tools, and the production of rocket engine and nuclear reactor components. In particular, the need for high-quality epitaxial films with single crystal in both silicon and compound-semiconductor technology, coupled with the necessity to deposit associated insulating and passivating films, has served as a powerful driver spurring the development of CVD processing methods.

Among the reasons for the growing adoption of CVD methods is the ability to produce a large variety of films and coatings of metals, semiconductors and inorganic as well as organic compounds in either a crystalline or vitreous form, possessing desirable properties. Furthermore, the ability to controllably create films of widely varying stoichiometry makes CVD unique among deposition techniques. Other advantages include the affordable cost of the equipment and operating expenses, the suitability for both batch and semi-continuous operation, and the compatibility with other processing steps. Because of this, many variants of CVD processing have been researched and developed, including atmospheric pressure (APCVD), low-pressure (LPCVD), plasma-enhanced (PECVD), and laser-enhanced (LECVD) chemical vapor deposition. Hybrid processes combining features of both physical and chemical vapor deposition have also emerged.

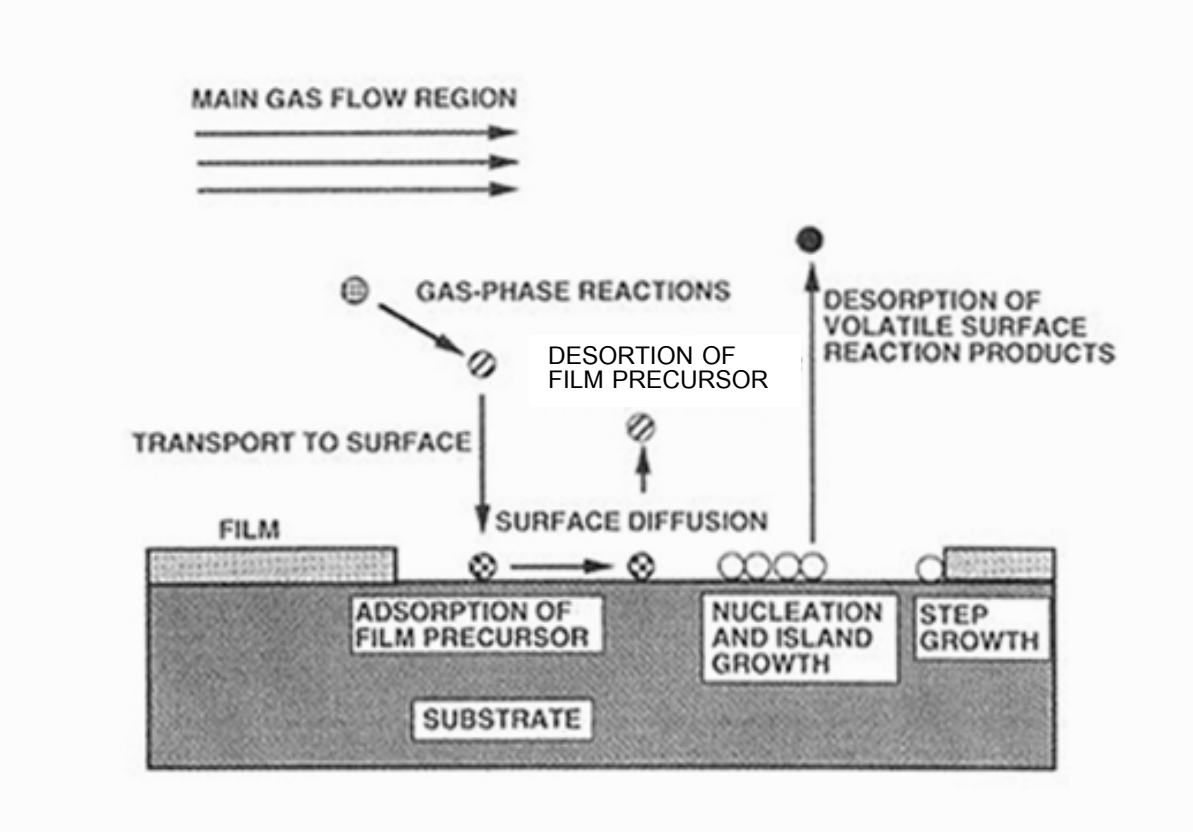

Figure 2-11 Sequence of gas transport and reaction processes contributing to CVD film growth [35]

The fundamental sequential steps that occur in every CVD process are sketched in Figure 2-11. and include:

1. Convective and diffusive transport of reactants from the gas inlets to the reaction zone
2. Chemical reactions in the gas phase to produce new reactive species and by-products
3. Transport of the initial reactants and their products to the substrate surface

4. Adsorption (chemical and physical) and diffusion of these species on the substrate surface
5. Heterogeneous reactions catalyzed by the surface leading to film formation
6. Desorption of the volatile by-products of surface reactions
7. Convective and diffusive transport of the reaction by-products away from the reaction zone

Figure 2-12 provides a perspective that integrates many of these steps, here subdivided into coordinates related to basic chemistry and physics, gas transport phenomena and to the reactors that must efficiently deposit films.

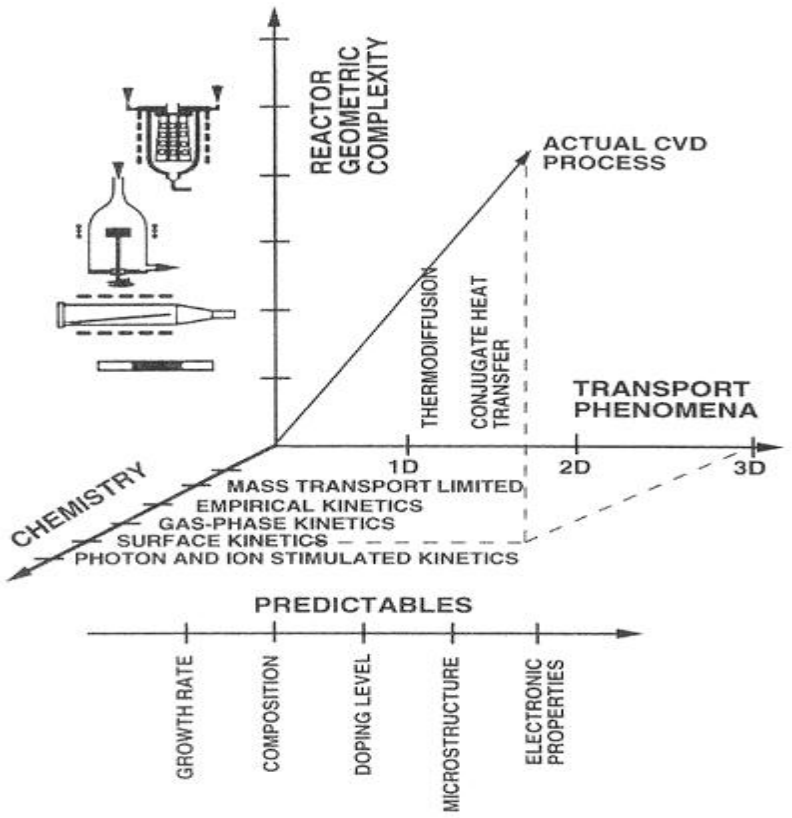

Figure 2-12 Schematic diagram of chemical, transport and geometrical complexities involved in modeling CVD process [35]

2.9.1 Thermodynamics of chemical vapor deposition [35]

Reaction feasibility

Thermodynamics addresses a number of important issues with respect to CVD. Once it is shown that a reaction is possible, thermodynamic calculation can frequently provide information on the partial pressures of the involved gaseous species and the direction of transport in the case of reversible reactions. Importantly, it provides an upper limit of what to expect under specified conditions. However, address questions related to the speed of the reaction and resulting film growth rates. Actually, processes which are thermodynamically possible frequently proceed at such low rates because of both vapor transport kinetics and vapor-solid reaction limitations that they are unfeasible in practice. Furthermore, the use of thermodynamics implies that chemical equilibrium has been attained. Although this may occur in a closed system, it is generally not the case in an open or flow reactor where gaseous reactants and products are continuously introduced and removed. In general, CVD may be viewed as an empirical science with thermodynamic guidelines.

Condition of equilibrium

Thermodynamics can provide us with much more than a prediction of whether a reaction will proceed or not. Under certain circumstances, it can yield quantitative information on the operating intensive variables which characterize the equilibrium. The problem is to evaluate the partial pressures or concentrations of the involved species within the reactor given the reactant compositions and operating temperature. In practice, the calculation

is frequently more complicated than initially envisioned because in situ mass spectroscopic analysis of operating reactors has surprisingly revealed the presence of unexpected species which must be accounted.

2.9.2 Thermal chemical vapor deposition processes [35]

This topic builds on the fundamentals of gas flow and reactions in CVD processes by describing their practical exploitation in producing films and coatings of interest. Most CVD processes can be conveniently subdivided into two categories. Thermal CVD processes employ heat energy to activate the required gas and gas-solid phase reactions. In contrast, the plasma-enhanced CVD processes derive benefit from plasma activation of the involved chemical species. However, even with similar input gases used to deposit the same nominal materials, films produced by thermal and plasma CVD processes can differ widely with respect to film structure, composition, and properties.

The great variety of materials deposited by thermal CVD methods has inspired the design and construction of an equally large number of processes and systems. Thermal processes have been broadly differentiated by such descriptors as low and high temperature, atmospheric and low pressure, cold and hot wall, and closed and open system. Within a specific category of process, the variations in design and operating variables frequently make it difficult to compare performance of individual systems or reactors, even when depositing the same material. Regardless of process type, however, the associated equipment must have the following capabilities:

1. Deliver and meter the reactant and diluent gaseous into the reactor

2. Supply heat to the substrates so that reaction and deposition can proceed efficiently
3. Remove the by-product and depleted gases

2.9.3 Metal-organic chemical vapor deposition (MOCVD)

Metal-organic chemical vapor deposition is sometime called organometallic vapor phase epitaxy (OMVPE) or metal-organic vapor phase epitaxy (MOVPE) [36]. It was originally developed in the late 1960s to grow epitaxial compound semiconductor films [37]. Metal-organic chemical vapor deposition is a specialized area of chemical vapor deposition which used metal-organic compounds as precursors usually in combination with hydrides or other reactants [29]. The early results demonstrated that deposition of critical semiconductor materials could be obtained at lower temperature than conventional thermal CVD in a continuous flow process and that epitaxial growth could be successfully achieved. The quality of the equipment and the diversity and purity of the precursor chemicals have steadily improved since then and the process is being refined constantly [38].

A wide variety of materials can be deposited by MOCVD, either as single crystal, polycrystalline or amorphous films [39]. The most important application is deposition of the group III-V semiconductor compounds [29].

Metal-organic chemical vapor deposition possess has the high potential for large-area deposition, good composition control and film uniformity, high film-deposition rates and densities, and conformal step coverage. The success of MOCVD strongly hinges on the availability of suitable precursors [35].

The great advantage of metal-organics is their generally high volatility at moderately low temperatures. Since all constituents are in the vapor phase, precise electronic control of gas flow rates and partial pressures is possible without dealing with troublesome liquid or solid sources in the reactor. That, combined with pyrolysis reactions which are relatively insensitive to temperature, allows for efficient and reproducible deposition. Carbon contamination of films is a disadvantage of MOCVD [35], but it was solved by the addition of co-reagent in the gas phase to eliminate the carbon impurity [4].

The commercial scale-up of metal-organic chemical vapor deposition requires the following:

1. Batch precursor amounts must rise from a few grams to a few kilograms
2. Production yields must rise and quality be consistent
3. The environmental impact must be minimal
4. Safety must be assured

2.9.4 Metal-organic chemical vapor deposition of tin oxide (SnO_2)

Several researchers have studied about the preparation of SnO_2 thin films by metal-organic chemical vapor deposition and some parameter effects on coating performance and film properties were studied [40-43].

Some organo-tin can be used as precursors for preparation of SnO_2 in MOCVD process. Table 2-1 presents some data about various organo-tin precursors.

Table 2-1 Properties of various organo-tin

Precursor name	Molecular formula	Melting point (°C)	Boiling point (°C)
Dibutyl tin diacetate[1]	$(C_4H_9)_2Sn(CH_3COO)_2$	12	>200
Tetrabutyl tin	$Sn(C_4H_9)_4$	-97	127-145[2]
Tetraethyl tin	$Sn(C_2H_5)_4$	-112	181[3]
Tetramethyl tin	$Sn(CH_3)_4$	-53	74-75[3]

Remark: [1]From http://www.chemtrack.org/MSDS.asp

[2]At 10 mm Hg

[3]At 760 mm Hg

Kaminori and Mizuhashi [42] studied MOCVD of SnO_2 by various organo-tin, dibutyl tin diacetate (DTD), tetrabutyl tin (TBT), tetraethyl tin (TET) and tetramethyl tin (TMT) were used in their work. The depositions were performed in a cold-wall CVD reactor with rotating substrate holder. They found that, the best tin precursor is TET because of its molecular size is most appropriate for forming regularly arranged Sn-O bonds leading to the prepared SnO_2 film with good crystallinity.

Amjoud et. al. [40] prepared the thin SnO_2 films by using tetraethyl tin as precursor with deposition temperature between 320-470 °C. Results from energy dispersive spectroscopy, show that deposited film at 320 °C contained some excess of Sn. It seems to be the uncompleted oxidation of the precursor.

At temperatures between 320-360 °C the films represented a columnar growth. When the temperature was increased to 360-440 °C, the films were well formed and faceted grains. The grains size was increased with the increasing of deposition temperature; it reached 1 μm when the deposition temperature was 470 °C.

Amjoud et al. [43] studied the effect of tetraethyl tin molar fraction in vapor phase in the range between $2x10^{-4}$-$1x10^{-3}$. The grain size decreased with the increasing of tetraethyl tin molar fraction in vapor phase, because it was affected by the higher nucleation rate of coating. Consequently, the SnO_2 films will be smoother and dense at high tetraethyl tin composition. Moreover, when the mean grain size and film roughness decreased, the film porosity will be decreased, that will decrease the electrical resistivity of the films.

Reaction mechanism of SnO_2 deposition by MOCVD

The reaction mechanism of SnO_2 deposition by MOCVD with using TET as precursor could be separated in homogeneous gas phase reaction and heterogeneous reaction. The mechanism was presented by Bertrand, N. [44].

The reaction mechanism was initiated by a pyrolysis of the TET that takes place at 380 °C and led to a rupture of a connection C-Sn. This homolytic rupture of a connection leads to the formation of two free radicals from both side of the TET molecule as presented in equation (2-30).

$$(CH_3\text{-}CH_2)_4Sn \rightarrow (CH_3\text{-}CH_2)_3Sn^{\bullet} + CH_3\text{-}CH_2^{\bullet} \qquad (2\text{-}30)$$

Then, the triethyltin radicals ($(CH_3\text{-}CH_2)_3Sn^{\bullet}$) will be oxidized. There are two oxidation path ways of triethyltin radicals.

Mechanism 1: The triethyltin radicals are reacted with oxygen gas to produce $(CH_3\text{-}CH_2)_2Sn{=}O$ and $CH_3\text{-}CH_2O^{\bullet}$ radicals represents in equation (2-31).

$$(CH_3\text{-}CH_2)_3Sn^{\bullet} + O_2 \rightleftarrows (CH_3\text{-}CH_2)_2Sn{=}O + (CH_3\text{-}CH_2)\text{-}O^{\bullet} \qquad (2\text{-}31)$$

Mechanism 2: The triethyltin radicals are reacted with oxygen gas to produce $(CH_3\text{-}CH_2)Sn^{\bullet}(OH)_2$ radicals and C_4H_8 as shown in equation (2-32).

$$(CH_3\text{-}CH_2)_3Sn^{\bullet} + O_2 \rightleftarrows (CH_3\text{-}CH_2)Sn^{\bullet}(OH)_2 + C_4H_8 \qquad (2\text{-}32)$$

The $(CH_3\text{-}CH_2)_2Sn{=}O$ species, formed during the oxidation of the $(CH_3\text{-}CH_2)_3Sn^{\bullet}$ radical according to path 1, is a very active species due to its double bond in Sn=O connection. This species strongly reacts with the $CH_3\text{-}CH_2^{\bullet}$ radical to produce $(CH_3\text{-}CH_2)_2Sn^{\bullet}OH$, as shown in equation (2-33).

$$(CH_3\text{-}CH_2)_2Sn{=}O + CH_3\text{-}CH_2^{\bullet} \rightleftarrows (CH_3\text{-}CH_2)_2Sn^{\bullet}OH + C_2H_4 \qquad (2\text{-}33)$$

Mechanism 3: $(CH_3\text{-}CH_2)_2Sn^{\bullet}OH$ could be oxidized in the CVD reactor to produced $(CH_3\text{-}CH_2)SnOOH$. Then $(CH_3\text{-}CH_2)SnOOH$ is reacted with $CH_3\text{-}CH_2^{\bullet}$ to produce $(CH_3\text{-}CH_2)Sn^{\bullet}(OH)_2$ and C_2H_4 presented in equation (2-34) and (2-35).

$$(CH_3\text{-}CH_2)_2Sn^{\bullet}OH + O_2 \rightleftarrows (CH_3\text{-}CH_2)SnOOH + CH_3\text{-}CH_2\text{-}O^{\bullet} \quad (2\text{-}34)$$

$$(CH_3\text{-}CH_2)SnOOH + CH_3\text{-}CH_2^{\bullet} \rightleftarrows (CH_3\text{-}CH_2)Sn^{\bullet}(OH)_2 + C_2H_4 \quad (2\text{-}35)$$

Mechanism 4: However, $(CH_3\text{-}CH_2)_2Sn^{\bullet}OH$ could be reacted with O_2 to produce SnO as in equation (2-36)

$$(CH_3\text{-}CH_2)_2Sn^{\bullet}OH + O_2 \rightleftarrows SnO + C_4H_8 + {}^{\bullet}OH + H_2O \quad (2\text{-}36)$$

The $(CH_3\text{-}CH_2)Sn^{\bullet}(OH)_2$ from both equation (2-32) and (2-35) is oxidized to produce SnO_2 as presented in equation (2-37).

$$(CH_3\text{-}CH_2)Sn^{\bullet}(OH)_2 + O_2 \rightarrow SnO_2 + C_2H_4 + {}^{\bullet}OH + H_2O \quad (2\text{-}37)$$

In addition, the TET also reacted with $^{\bullet}OH$, produced form equation (2-36) and (2-37), to produce $(CH_3\text{-}CH_2)_3Sn(OH)$ as present in equation (2-38).

$$(CH_3\text{-}CH_2)_4Sn + {}^{\bullet}OH \rightarrow (CH_3\text{-}CH_2)_3Sn(OH) + CH_3\text{-}CH_2^{\bullet} \quad (2\text{-}38)$$

The $(CH_3\text{-}CH_2)_3Sn(OH)$ decompose to produce $(CH_3\text{-}CH_2)_2Sn^{\bullet}OH$ as presented in equation (2-39).

$$(CH_3\text{-}CH_2)_3Sn(OH) \rightarrow (CH_3\text{-}CH_2)_2Sn^{\bullet}OH + CH_3\text{-}CH_2^{\bullet} \quad (2\text{-}39)$$

There are some possible reactions in the SnO_2 listed previously. However, with the thermodynamic point of view, there are 2 reaction path ways that possible occur during the deposition of SnO_2 film could be summary.

Path way 1:

$$(CH_3\text{-}CH_2)_4Sn \rightarrow (CH_3\text{-}CH_2)_3Sn^{\bullet} + CH_3\text{-}CH_2^{\bullet} \quad (2\text{-}30)$$

$$(CH_3\text{-}CH_2)_3Sn^{\bullet} + O_2 \rightleftarrows (CH_3\text{-}CH_2)_2Sn{=}O + (CH_3\text{-}CH_2)\text{-}O^{\bullet} \quad (2\text{-}31)$$

$$(CH_3\text{-}CH_2)_2Sn{=}O + CH_3\text{-}CH_2^{\bullet} \rightleftarrows (CH_3\text{-}CH_2)_2Sn^{\bullet}OH + C_2H_4 \quad (2\text{-}33)$$

$$(CH_3\text{-}CH_2)_4Sn + {}^{\bullet}OH \rightarrow (CH_3\text{-}CH_2)_3Sn(OH) + CH_3\text{-}CH_2^{\bullet} \quad (2\text{-}38)$$

$$(CH_3\text{-}CH_2)_3Sn(OH) \rightarrow (CH_3\text{-}CH_2)_2Sn^{\bullet}OH + CH_3\text{-}CH_2^{\bullet} \quad (2\text{-}39)$$

Path way 2:

$$(CH_3\text{-}CH_2)_4Sn \rightarrow (CH_3\text{-}CH_2)_3Sn^{\bullet} + CH_3\text{-}CH_2^{\bullet} \quad (2\text{-}30)$$

$$(CH_3\text{-}CH_2)_3Sn^{\bullet} + O_2 \rightleftarrows (CH_3\text{-}CH_2)Sn^{\bullet}(OH)_2 + C_4H_8 \quad (2\text{-}32)$$

$$(CH_3\text{-}CH_2)Sn^{\bullet}(OH)_2 + O_2 \rightarrow SnO_2 + C_2H_4 + {}^{\bullet}OH + H_2O \quad (2\text{-}37)$$

$$(CH_3\text{-}CH_2)_4Sn + {}^{\bullet}OH \rightarrow (CH_3\text{-}CH_2)_3Sn(OH) + CH_3\text{-}CH_2^{\bullet} \quad (2\text{-}38)$$

$$(CH_3\text{-}CH_2)_3Sn(OH) \rightarrow (CH_3\text{-}CH_2)_2Sn^{\bullet}OH + CH_3\text{-}CH_2^{\bullet} \quad (2\text{-}39)$$

$$(CH_3\text{-}CH_2)_2Sn^{\bullet}OH + O_2 \rightleftarrows SnO + C_4H_8 + {}^{\bullet}OH + H_2O \quad (2\text{-}36)$$

In heterogeneous reaction, the SnO in gas phase is reacted with O_2 and deposited on the substrate as presented in equation (2-40) and (2-41).

$$SnO_{(g)} + O_2 \rightarrow SnO_{2(s)} + 1/2\ O_2 \quad (2\text{-}40)$$

$$SnO_{2(g)} \rightarrow SnO_{2(s)} \quad (2\text{-}41)$$

2.9.5 Metal-organic chemical vapor deposition of iridium (Ir) and iridium oxide (IrO_2)

Iridium (Ir) and Iridium oxide (IrO_2) films have attracted much attention due to their excellent properties. Iridium is a noble metal with a small unit cell dimension, high melting point (2727 K) and good chemical stability. Due to its properties, iridium is a good diffusion barrier for oxygen. Iridium has a great interest as protective layer due to its good resistance against corrosion and oxidation at high temperature [4]. Iridium oxide films have excellent properties, especially their electrocatalyic properties and good stability in strong acidic solution for chlorine and oxygen evolution [33].

Several methods have been developed for preparing Ir and IrO_2 films such as metal-organic chemical vapor deposition. There are some influences on the deposition of Ir and IrO_2 films, such as choice of precursors, deposition temperature and co-reactive gaseous, etc.

Because of the potential of Ir and IrO_2 films for application, many types of Ir source precursors were investigated for Ir and IrO_2 films coating by CVD. Initially, Ir(III) halides were used as precursor for Ir and IrO_2 CVD [4, 45]. Due to its low volatility and high decomposition temperature typically more than 800 ºC [4], iridium halides were not good alternative. In addition, corrosive and harmful atmosphere is generated during the decomposition of iridium halides.

Due to some drawbacks of iridium halides precursor, organometallic iridium compounds are preferred for Ir film CVD. The iridium *tris*-acetylacetonate ($Ir(acac)_3$) and iridium *tris*-alkyl ($Ir(C_3H_5)_3$) complexes, are two chemical species commonly used as CVD precursors. For commercial available, $Ir(acac)_3$ is a better choice due to its excellent air stability. However, the high melting point and low volatility of $Ir(acac)_3$ has limited its development as the industrial standard [45].

In addition, other iridium sources reagents consist of Ir(I) metal complexes such as (MeCp)Ir(COD) [4, 46-50], Ir(COD)(acac) [51], $[Ir(COD)(\mu\text{-}OAc)]_2$ [52], Ir(COD)(hfac) [53] and Ir(COD)(amak) [47] appear to be more useful for Ir and IrO_2 deposition due to their enhanced volatility and vapor phase transport properties which are uncomplicated by monomer-dimer equilibria. The physical properties of some Ir precursors are presented in Table 2-2.

Table 2-2 Physical properties of iridium CVD precursors

Compound	Melting point (ºC)	Deposition temperature (ºC)	Sublimation condition
$Ir(acac)_3$	269-271	300-400	180-200 ºC
$Ir(C_3H_5)_3$	Decompose at 65	100	50 ºC/ 15 Torr
(MeCp)Ir(COD)	38-40	270-350	95 ºC/ 0.05 Torr
Ir(COD)(hfac)	120	250-400	60 ºC/ 0.05 Torr
Ir(COD)(amak)	127	350	50 ºC/ 0.2 Torr
$[Ir(COD)(\mu\text{-}OAc)]_2$	135	250	125 ºC/ 0.07 Torr

Maury and Senocq [4] studied the deposition of Ir film by MOCVD in hot-wall CVD reactor by using (MeCp)Ir(COD) as liquid Ir source. The influences of H_2 and O_2 addition, deposition temperature and residence time were obtained. In H_2 atmosphere, deposition of Ir film is very sensitive on the residence time and the decomposition temperature. Deposition started from 300 ºC at residence time 0.05 sec. But, when increased deposition temperature to 400 ºC, the Ir film abruptly deposited only a few centimeters from the entrance of the reactor due to the high reactivity of the feed gas mixture, which made difficultly control of film growth rate and uniform deposition along the reactor. With the presence of O_2, the Ir films was dense when the thickness was less than 100 nm, similar to surface morphology in presence with H_2. However, the microstructure trended to be columnar when film thickness is more than 1 micron. The coatings deposited using a high excess of oxygen, O_2/(MeCp)Ir(COD) of 1000 lead to the mixture of Ir and

IrO_2. However, the co-deposition of Ir and IrO_2 was not observed at O_2/(MeCp)Ir(COD) molar ratio less than 135. In addition, the film thickness gradient was observed with the increasing of O_2 partial pressure. For high temperature and residence time, the growth rate is maximum at the entrance of the reactor, but rapidly decreases downstream. Better thickness uniformity can be obtained by optimization of O_2 feed rate, deposition temperature and residence time that detrimental to the conversion rate of the precursor, subsequently, to achieve the mean growth rate along the reactor.

Chen [50] deposited IrO_2 on Si substrate in vertical cold-wall CVD reactor by using of (MeCp)Ir(COD) as iridium source. The oxygen was used as both carrier and reactive gas. The supplying rate of oxygen is 100 sccm and oxygen pressure was 1, 10 and 30 torr. The deposition temperature ranged between 250 and 500 °C. At 1 torr, high Ir purity film was obtained at temperature below 400 °C. At 450 and 500 °C, the rutile IrO_2 was detected. However, the diffraction signal due to the IrO_2 phase at 500 °C was diminished. At 10 torr, the Ir signal obtained at temperature ≤ 300 °C and the optimized temperature for growth of IrO_2 is between 400 and 450 °C. At 30 torr, the highly 101 orientation IrO_2 nanorods were deposited at temperature between 300-350 °C.

2.10 Computational fluid dynamics (CFD) [54]

Computational fluid dynamics (CFD) was originally developed from the pioneering accomplishments of enthusiasts [55-56], who in their endeavors to procure insight into fluid motion instigated the development of

powerful numerical techniques that have advanced the numerical description of all types of fluid flow [57]. CFD is now maturing into a powerful and pervasive tool in many industries, with each solution representing a rich tapestry of mathematical physics, numerical methods, user interfaces and state-of-the art visualization techniques [58]. So great has the impetus been to propel CFD that it is now used as much as the traditional didactic methods of experimentation and analytical modeling to solve fluid flow problems. This recent adoption of CFD has been both inevitable and progressive, as the high costs and time consumption associated with experimentation has often precluded the desire to produce efficient in-depth results. Moreover, the assumptions, generalizations and approximations associated with analytical models have swayed their reduction in the development of flow solutions. By considering these limitations coupled with recent achievements in the development of numerical solutions for the Navier–Stokes equations and the amelioration of computing power and efficiency, it is easy to understand why confidence has both increased and advanced the application of CFD as a viable alternative in industry and science.

The technical achievements observed in the last two decades include vast improvements in numerical algorithms and CFD modeling techniques [58]. This means that features like unstructured and adaptive meshing, moving boundaries and multiple frames of reference now cooperate with physical models to confront complex phenomena involving Newtonian and non-Newtonian fluid flow.

2.10.1 Fundamentals of computational fluid dynamics

Governing equations

The governing equations of fluid flow and heat transfer can be considered as mathematical formulations of the conservation laws of fluid mechanics and are referred to as the Navier–Stokes equations. When applied to a fluid continuum, these conservation laws relate the rate of change of a desired fluid property to external forces and can be considered as:

1. The law of conservation of mass or continuity, which states that the mass flows entering a fluid element must balance exactly with those leaving.
2. The law of conservation of momentum or Newton's second law of motion, which states that the sum of the external forces acting on a fluid particle is equal to its rate of change of linear momentum.
3. The law of conservation of energy or the first law of thermodynamics, which states that the rate of change of energy of a fluid particle is equal to the heat addition and the work done on the particle.

By enforcing these conservation laws over discrete spatial volumes in a fluid domain, it is possible to achieve a systematic account of the changes in mass, momentum and energy as the flow crosses the volume boundaries. The resulting equations can be written as:

Continuity equation:

$$\frac{\partial \rho}{\partial t} + \frac{\partial}{\partial x_i}\left(\rho u_j\right) = 0 \qquad (2\text{-}42)$$

Momentum equation:

$$\frac{\partial}{\partial t}(\rho u_i) + \frac{\partial}{\partial x_j}(\rho u_i u_j) = \frac{\partial}{\partial x_j}\left[- p\delta_{ij} + \mu\left(\frac{\partial u_i}{\partial x_j} + \frac{\partial u_j}{\partial x_i}\right)\right] + \rho g_i \qquad (2\text{-}43)$$

Energy equation:

$$\frac{\partial}{\partial t}(\rho C_a T) + \frac{\partial}{\partial x_j}(\rho u_j C_a T) - \frac{\partial}{\partial x_j}\left(\lambda \frac{\partial T}{\partial x_j}\right) = s_T \qquad (2\text{-}44)$$

There are two ways to model the density variations that occur due to buoyancy. The first is to assume that the density differentials in the flow are only required in the momentum equations and are represented by:

$$\rho = \rho_{ref}\left[1 - \beta\left(T - T_{ref}\right)\right] \qquad (2\text{-}45)$$

This method is known as the Buossinesq approximation [59]. However, at high temperature differentials, the approximation is no longer valid and another method must be applied [60]. One way is to treat the fluid as an ideal gas and express the density by means of the following equation:

$$\rho = \frac{p_{ref} W_a}{RT} \qquad (2\text{-}46)$$

This method can be considered as a weakly compressible formulation, which means that the density of the fluid is dependent on temperature and composition but not pressure. This assumption has also been used successfully in some engineering applications. However, solutions were found to be more difficult to converge using this method [61].

Numerical analysis

A fundamental consideration for CFD code developers is the choice of suitable techniques to discretise the modeled fluid continuum. Of the many existing techniques, the most important include finite difference, finite elements and finite volumes. Although all these produce the same solution at high grid resolutions, the range of suitable problems is different for each. This means that the employed numerical technique is determined by the conceived range of code applications [54].

Finite difference techniques are limited use in many engineering flows due to difficulties in their handling of complex geometries. This has led to increased use of finite elements and finite volumes, which employ suitable meshing structures to deal appropriately with arbitrary geometry. Finite elements can be shown to have optimality properties for some types of equations [60]. However, only a limited number of commercial finite element packages exist, which is undoubtedly a reflection of the difficulties involved in the programming and understanding of this technique [54].

Fortunately, such difficulties are obviated through implementation of finite volumes methods. When the governing equations are expressed through finite volumes, they form a physically intuitive method of achieving a systematic account of the changes in mass, momentum and energy as fluid crosses the boundaries of discrete spatial volumes within the computational domain [62]. The ease in the understanding, programming and versatility of finite volumes has meant that they are now the most commonly used techniques by CFD code developers.

Solving the flow problem

In order to solve for a flow field a CFD code must take the mathematical statements inputted by the user, structure them into a suitable arrangement and solve them for the specified boundary conditions. Iterative methods are commonly used by CFD codes to solve a whole set of discretised equations so that they may be applied to a single dependent variable. The segregated solver SIMPLE (Semi-Implicit Method for Pressure-Linked Equations), devised by Patankar and Spalding in 1972 [63], or its descendents are conventionally employed by many commercial packages [54]. SIMPLE determines the pressure field indirectly by closing the discretised momentum equations with the continuity equations in a sequential manner. Consequently, as the number of cells increases, the elliptic nature of the pressure field becomes more profound and the convergence rate decreases substantially [64]. This has led to the development of multigrid techniques that compute velocity and pressure corrections in a simultaneous fashion, thereby enhancing convergence rates. Unfortunately, the improvement in solver efficiency afforded by multigrid is foiled by memory requirements that increase in tandem with the number of cells, thus making it difficult, in some cases, to achieve grid independency with current computing capabilities [54]. Nevertheless, many CFD packages, even those based on unstructured grids now successfully employ multigrid as the default solver option. Detailed techniques used by multigrid are described in the literature [64].

Interpreting the solution

Visualization is often necessary to represent the resulting field solution. Contour, vector and line plots enhance the accurate interpretation of results and have been used successfully in many studies to aid in system design [65]. In addition, field data are often easily exported to external modeling programs so that they can be processed further.

2.10.2 Commercial CFD software package

Over the last two decades, there has been enormous development of commercial CFD codes to enhance their marriage with the sophisticated modeling requirements of many research fields, thereby accentuating their versatility and attractiveness. These challenges have led to unprecedented competition between commercial CFD developers and have expedited non-uniform development, causing the range of afforded functionalities to vary from code to code. Thus, among the many codes that exist today not all provide the features required in engineering. Such requirements include the provision of powerful pre-processor, solver and post-processor environments, the power to import grid geometry, boundary conditions and initial conditions from an external text file, and the capability to model non-Newtonian fluids, two-phase flows, flow dependent properties, phase change and flow through porous media [66]. Therefore, intuitive functional considerations of a code should be taken into account before selection. The commercial software packages featured incorporate at least a minimum number of all these functionalities, employ graphical user interfaces, and support Windows, UNIX and Linux platforms. State-of-the-art features of the most commonly used general-purpose codes available are elucidated

with their associated cost in Table 2-3 [54]. Details on three of the most routinely used commercial codes are elaborated below.

Table 2-3 Common commercial CFD software [54]

Company	Software package	Features
ANSYS Inc.	ANSYS CFX®	Menter-Langtry turb, Coupled Lagrangian and particle tracker Coupled multiphase and interphase models
CHAM Ltd.,	PHOENICS®	LEVL and MFM turb, PARSOL, IMMERSOL CHEMKIN, MTSM
FLUENT Inc.	FLUENT®	Dynamic mesh, chemical mixing and reaction models, wall film models
	FIDAP®	Complex rheology and electrohydrodynamic modeling
	POLYFLOW®	Integral and differential viscoelastic flow modeling

CFX®

CFX® was recently taken over by ANSYS Inc. in 2003 and is now branded as ANSYS CFX®. Within the framework of ANSYS CFX® numerous different types of software packages exist that can be used to solve various types of flow problems. There are also a large number of up-to-date fully functional physical models, which include multiphase flow, porous media, heat transfer, combustion and radiation models. Advanced turbulence models are also a feature of ANSYS CFX® and it contains a predictive laminar to turbulent flow transition model (Menter–Langtry γ–θ model). ANSYS CFX® also affords an easy-to-use fully parametrical CAD tool with a bi-directional link compatible with most CAD software [54].

PHOENICS®

PHOENICS® is a multipurpose CFD package that has numerous modeling capabilities, including Newtonian and non-Newtonian fluid modeling, flow through porous media with direction-dependent resistances, and conjugate heat transfer. There is also an extensive suite of embedded turbulence models including the unique wall distance turbulence model (LVEL), which circumvents the inaccuracies associated with wall-function computations of most turbulence models by using the knowledge of wall distances, and local velocities to compute the near-wall flow. PHOENICS® is a structured grid code and it necessitates the use of body fitted coordinates to model complex geometry. This can substantially increase the pre-processing and solution times of a simulation.

FLUENT®

FLUENT Inc. offers three software packages within the CFD framework that are suitable for modeling needs. The three packages are FLUENT® (general purpose with multiphysics capabilities), FIDAP® (modelling complex physics) and POLYFLOW® (polymer modeling). FLUENT® Inc. is presently one of the leading suppliers of CFD software in the world. The most interesting features of the FLUENT® software include models for heat exchangers, discrete phase models for multiphase flows, numerous high quality reaction models and the phase change model which tracks the melting and freezing in the bulk fluid. FIDAP® is a finite element based software that offers unique abilities for modeling non-Newtonian flows and free surface flows. It also contains sophisticated radiation, dispersion and heat transfer models. POLYFLOW® is a general-purpose finite element CFD tool for the analysis of polymer processing such as glass forming, thermoforming and fiber spinning.

2.10.3 Simulation by using FLUENT® [68]

FLUENT® is a state-of-the-art computer program for modeling fluid flow and heat transfer in complex geometries. FLUENT® provides complete mesh flexibility, solving flow problems with unstructured meshes that can be generated about complex geometries with relative ease. Supported mesh types include 2D triangular/quadrilateral, 3D tetrahedral/hexahedral/ pyramid/wedge, and mixed (hybrid) meshes. FLUENT® also allows you to refine or coarsen grid based on the flow solution.

This solution-adaptive grid capability is particularly useful for accurately predicting flow fields in regions with large gradients, such as free shear layers and boundary layers. In comparison to solutions on structured or block structured grids, this feature significantly reduces the time required to generate a good grid. Solution-adaptive refinement makes it easier to perform grid refinement studies and reduces the computational effort required to achieve a desired level of accuracy, since mesh refinement is limited to those regions where greater mesh resolution is needed.

FLUENT® is written in the C computer language and makes full use of the flexibility and power offered by the language. Consequently, true dynamic memory allocation, efficient data structures, and flexible solver control are all made possible. In addition, FLUENT® uses a PC/server architecture, which allows it to run as separate simultaneous processes on desktop workstations and powerful compute servers, for efficient execution, interactive control, and complete flexibility of machine or operating system type.

All functions required to compute a solution and display the results are accessible in FLUENT® through an interactive, menu-driven interface. The user interface is written in a language called Scheme, a dialect of LISP. The advanced user can customize and enhance the interface by writing menu macros and functions.

2.10.4 Simulation of CVD Process Using FLUENT® [68]

FLUENT® CFD software provides the important physics required for CVD reactor modeling, including gas phase/surface reaction chemistry,

multicomponent and Soret diffusion, natural convection, non-grey radiation with participating media, and the ability to include fully compressible flow regions. FLUENT® CFD software also combines physically accurate transport models with proposed gas-phase and surface chemistry mechanisms and predicts uniformity of film thickness and composition variation during selective growth that applying for MOCVD simulation.

2.11 Conclusions

The literature review presents that SnO_2 electrocatalytic electrode is practical for destruction of organic pollutant in wastewater. However, it needs the protection from protective layer. IrO_2 and Ir have some attractive properties for using as protective layer. The literatures also show that metal-organic chemical vapor deposition is a powerful tool for elaboration of both active and protective layers.

Chapter 3

Materials and Methods

This chapter presents the experimental set-up for this work. It will be started with the materials and chemicals had been used in this study. Then, the electrodes preparation techniques will be introduced, it composes of substrate pretreatment, metal-organic chemical vapor deposition of Ir, IrO_2 and SnO_2 over various substrates and also the simulation of Ir deposition using FLUENT® software. The set up using for electrochemical oxidation of model solution and restaurant effluent from Chulalongkorn University Student Canteen are presented. Finally, the material characterization methods are also introduced in this chapter.

3.1 Chemicals

(Methylcyclopentadienyl) (1,5-cyclooctadiene) iridium (I), 99 %w/w was supplied by Strem Chemicals, Inc., Iridium (III) acetylacetonate, 98 %w/w, Tetraethyltin 97 %w/w were supplied by Aldrich Chemical Co., Inc. and oxalic acid 98%w/w was supplied by BDH Chemicals Inc. The other chemicals used in this research work are analytical grade.

The effluent from Chulalongkorn University Student Canteen was used in this study. The effluent was collected from the wastewater collection system of Chulalongkorn University after passed the grease trap.

3.2 Substrate pretreatment

To improve the surface roughness of substrates and the adhesion of deposited films, the substrates need to be cleaned by the appropriating solvent and/or etched by specific acid. In this part, the several treatment techniques for some substrates are presented.

3.2.1 Stainless steel 316L

To remove some impurities stainless steel SUS 316L sheets (25.4 mm x 16.2 mm x 10 mm) were polished by sand paper No. 0. Degreased in acetone with sonication for 15 minute, rinsed with deionized water and dried by compressed air.

3.2.2 Borosilicate glass

The borosilicate glass sheets (25.4 mm x 16.2 mm x 10 mm) were carefully degreased in acetone with sonication for 15 minute, rinsed with deionized water and dried by compressed air

3.2.3 Silicon wafer

The Si wafers (8 mm x 10 mm) were degreased in hot acetone, rinsed with deionized water and dried by compressed air.

3.2.4 Titanium

Ti sheets (8 mm x 30 mm) were etched in hot 35% HCl for 1 hr, rinsed by deionized water and dried by compressed air. The pretreatment of Ti substrate was followed Duverneuil et al. [41].

3.2.5 Tantalum

Ta substrates (8 mm x 30 mm) were etched in 40% HF from 1 min to 24 hr, rinsed by deionized water and dried by compressed air.

3.2.6 Tantalum carbide over tantalum

TaC/Ta sheets were brushed by stainless steel rotating brush and etched in 40% HF for 1 hr to remove free carbon on the surface.

3.3 Deposition of TiO_2 by spray coating

The deposition of TiO_2 coated electrode was the following [69].

1. 1 g of TiO_2 was suspended in 100 ml of methanol, the suspension was homogenized by sonication
2. The cleaned SUS 316L was heated to 80 ºC
3. The precursor solution in (1) was sprayed to heated substrate using simple atomizer
4. The procedure was repeated until a uniform coating of TiO_2 was visible on the substrates.
5. The coated substrates were annealed in air at 700 ºC. After 1 h the substrates were removed from the furnace and allowed to cool at room temperature

3.4 Deposition of SnO_2 using spray pyrolysis

The most common procedure to apply a thin layer of SnO_2 is a spraying of tin precursor solution onto a hot substrate surface. To

improve the conductivity of SnO_2 film, it can be doped with other metal ions such as Sb^{3+}. The procedure of SnO_2 coating by spray pyrolysis was the following [27].

1. Dissolve10 g $SnCl_4 \cdot 5H_2O$ and 0.1 g $SbCl_3$ in 100 ml of methanol
2. The cleaned borosilicate glass sheet was heated to 500 ºC.
3. The precursor solution in (1) was sprayed on the hot borosilicate glass surface by using a simple atomizer with around 30 cm distance from the substrate
4. The procedure was repeated until a uniform coating of Sb_2O_5 doped SnO_2 was visible on the substrates

3.5 Metal-organic chemical vapor deposition

From some attractive advantages for the growth of thin film, MOCVD was adapted to the deposition for electrode preparation in this research work. The metal-organic chemical vapor deposition of IrO_2, Ir and SnO_2 films were studied with the CVD apparatus presented in Figure 3-1.

The deposition was studied in horizontal hot-wall CVD reactor with 1.2 cm diameter and 15 cm isothermal zone. The organometallic precursors were contained in a thermostated bubbler at desired temperature. Helium was used as the carrier and oxygen was as co-reactive gas. The gas flow rate was monitored and controlled by mass-flow controller and the total pressure was automatically controlled by using an absolute pressure gauge coupled to the throttle valve system.

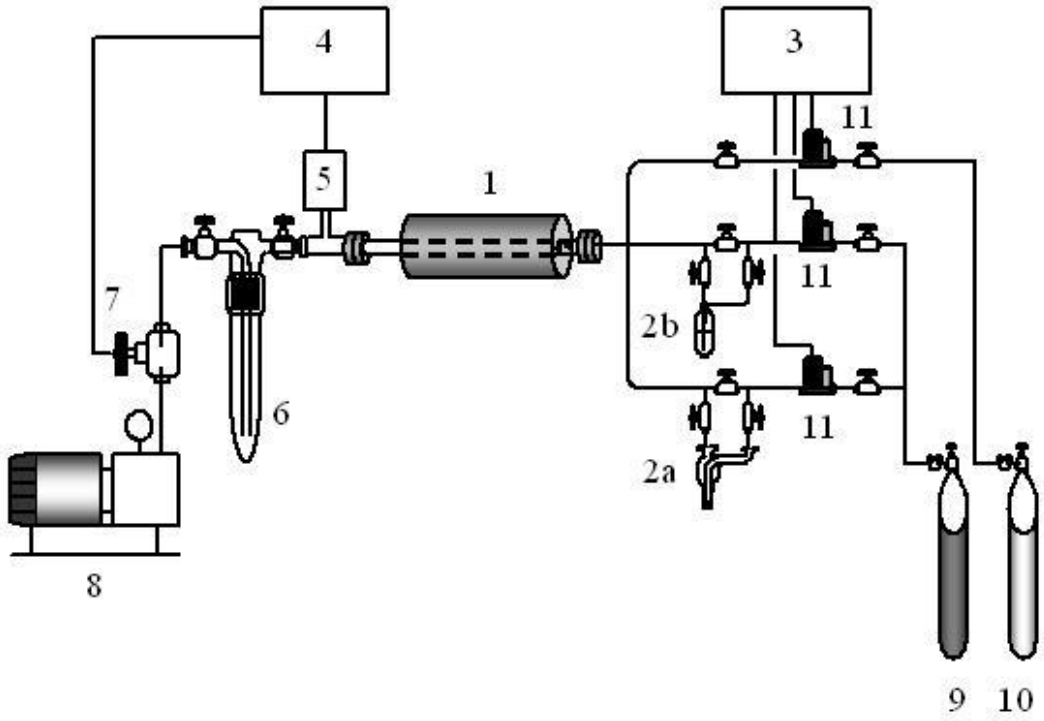

Figure 3-1 MOCVD apparatus; 1) Hot-wall CVD reactor, 2a) 1st bubbler for $Ir(acac)_3$ or (MeCp)Ir(COD), 2b) 2nd bubbler for TET, 3) Gas flow controller, 4) Pressure controller, 5) Pressure regulator, 6) Cold trap, 7) Throttle valve, 8) Vacuum pump, 9) He tank, 10) O_2 tank and 11) Mass-flow controller

3.5.1 Choice of precursor

There are several iridium source precursors were used in deposition of Ir and IrO_2 by metal-organic chemical vapor deposition [45-53]. Due to its excellent air stability, $Ir(acac)_3$ was used as precursor for IrO_2 deposition. However, its high melting point, low volatility of $Ir(acac)_3$ and difficulty control of mass transport has limited $Ir(acac)_3$ in this work.

For better volatility and vapor phase transport properties, the other iridium source, (MeCp)Ir(COD) was used in this study.

There is some organo-tin which can be used as precursors for preparation of SnO_2 in MOCVD process [42]. However, the best tin precursor is tetraethyl tin because its molecular size is most appropriate for forming of regularly arranged Sn-O bonds leading to the prepared SnO_2 film with good crystallinity [42]. Due to its good properties, tetraethyl tin was used as tin source precursor in this work.

3.5.2 Choice of substrate

The various types of substrates were used in this study. Due to its low cost and easy for processing, the silicon wafer was as substrate for the calibration of MOCVD. Titanium was used as substrate for Ir and IrO_2 deposition by MOCVD. Titanium, iridium coated titanium, tantalum and tantalum carbide over tantalum were used as substrates for SnO_2 deposition.

3.5.3 Substrate placement

To study the growth rate profile of coatings in the reactor, Si wafer substrate was used in the calibration of the reactor. The cleaned Si wafer (8 x 10 cm) was placed in each 2.5 cm from the entrance of the reactor. In case of IrO_2 deposition, Si wafer at 5.0-7.5 cm were substituted by Ti substrate. For Ir and SnO_2 deposition, the Si wafer was substituted by actual substrate at 10.0-12.5 cm and 17.5-20.0 cm, respectively. The placement of Si wafer and actual substrates is presented in Figure 3-2.

For better control of deposition on both side of the real substrate, it was set up on the substrate holder during the deposition.

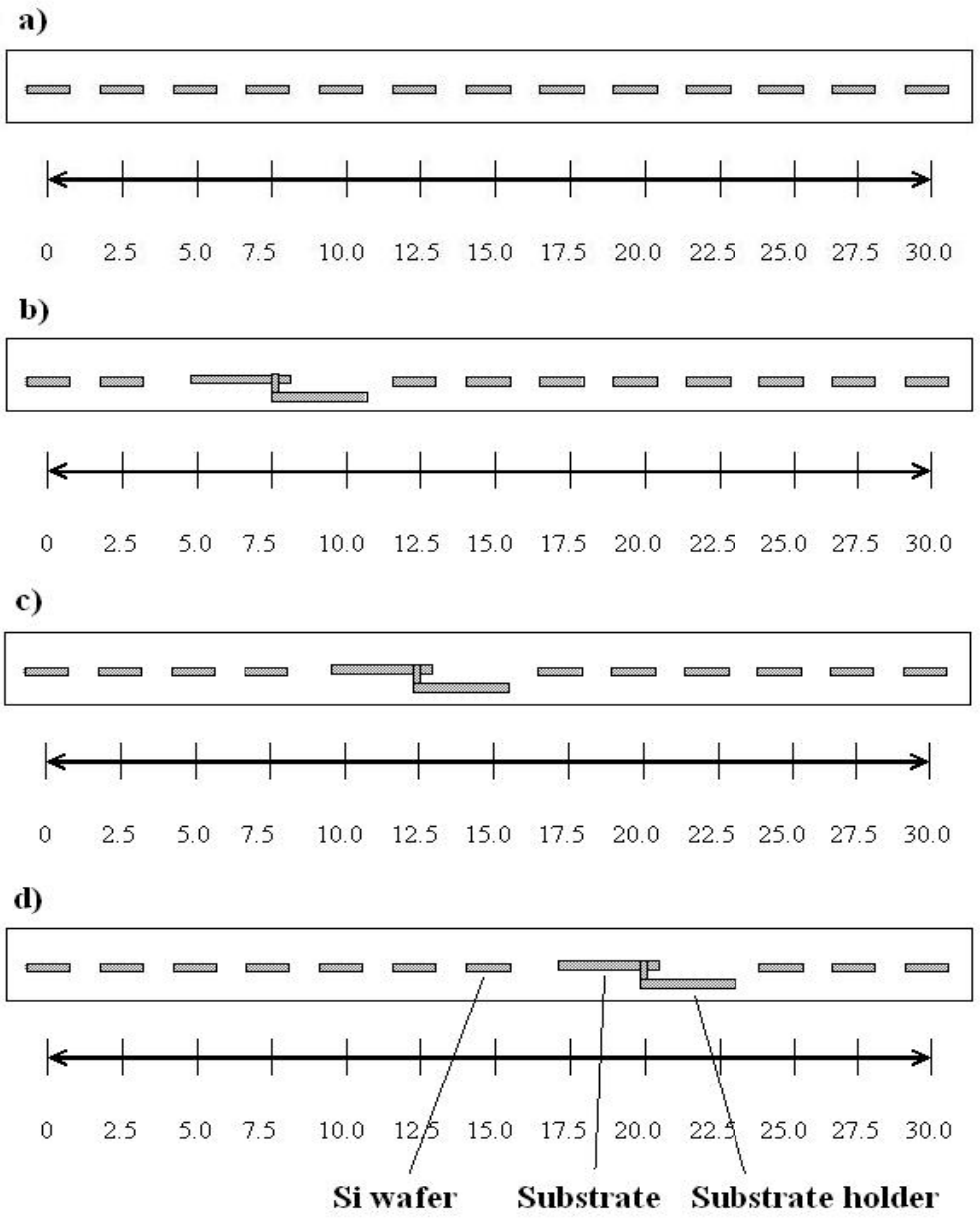

Figure 3-2 Schematic diagram of silicon wafer and actual substrates placement in MOCVD reactor; a) Reactor calibration, b) IrO_2 deposition, c) Ir deposition and d) SnO_2 deposition

3.5.4 Deposition condition

The deposition conditions for IrO_2, Ir and SnO_2 are presented in Table 3-1, 3-2 and 3-3.

Table 3-1 Operating conditions of IrO_2 deposition using $Ir(acac)_3$ as precursor

Electrode no.	Operating condition									
	Temperature of reactor (^oC)	Temperature of bubbler (^oC)	Temperature of helium (^oC)	Temperature of oxygen (^oC)	Temperature of feed line (^oC)	Flow rate of helium (sccm)	Flow rate of oxygen (sccm)	Total Flow (sccm)	Total pressure (Torr)	Duration (min)
1	400	150	160	160	120	100	80	180	25	180
2	400	150	160	160	120	100	160	260	25	192
3	400	160	160	160	120	100	160	260	25	120
4	350	160	160	160	140	100	160	260	25	120
5	350	160	160	160	140	100	160	260	25	60
6	400	150	160	160	140	100	160	260	25	60
7	350	150	150	160	140	100	160	260	25	60
8	400	150	150	160	140	100	250	350	25	61
9	400	140	140	140	140	100	250	350	25	120
10	400	150	150	150	140	100	300	400	25	120
11	400	150	150	150	140	100	375	475	25	120
12	400	140	140	140	140	100	375	475	25	180
13	400	140	140	140	140	100	375	475	25	181
35	400	140	140	140	140	100	375	475	25	300
36	400	140	140	140	140	100	375	475	15	180
37	400	150	150	150	150	100	375	475	15	330

Table 3-2 Operating conditions of Ir deposition using ((MeCp)Ir(COD) as precursor

Electrode no.	Operating condition										
	Temp. of reactor (^{o}C)	Temp. of precursor (^{o}C)	Temp. of helium/ carrier (^{o}C)	Temp. of helium/ dilutant (^{o}C)	Temp. of oxygen (^{o}C)	Flow rate. of helium/ carrier (sccm)	Flow rate of helium/ dilutant (sccm)	Flow rate of oxygen (sccm)	Total Flow (sccm)	Total pressure (Torr)	Duration (min)
38	300	100	100	18	100	10	315	25	350	40	120
39	350	85	85	18	85	10	315	25	350	12	120
40	325	85	85	18	85	10	315	25	350	12	120
41	300	85	85	18	85	10	355	25	390	12	120
42	300	85	85	18	85	25	350	5	380	12	120
43	300	85	85	18	85	25	350	5	380	12	270
45	350	85	85	18	85	25	350	10	385	12	300
46	400	85	85	18	85	25	770	5	800	20	120
47	300	85	85	18	85	25	350	5	380	12	135
48	300	85	85	18	85	25	350	5	380	12	480
49	300	85	85	18	85	25	350	5	380	12	270
50	300	85	85	18	85	25	350	5	380	12	135
53	300	85	85	18	85	25	350	5	380	12	90
54	300	85	85	18	85	25	350	5	380	12	360
56	300	85	85	18	85	25	350	5	380	12	270
58	300	85	85	18	85	25	350	5	380	12	270

Table 3-3 Operating conditions of SnO_2 deposition using tetraethyl tin as precursor

Electrode no.	Operating condition									
	Temperature of reactor (^oC)	Temperature of bubbler (^oC)	Temperature of helium (^oC)	Temperature of oxygen (^oC)	Temperature of feed line (^oC)	Flow rate of helium (sccm)	Flow rate of oxygen (sccm)	Total Flow (sccm)	Total pressure (Torr)	Duration (min)
14	380	10	N/A	N/A	N/A	20	280	300	100	120
15	380	20	N/A	N/A	N/A	20	280	300	100	120
16	380	20	N/A	N/A	N/A	20	280	300	25	120
17	380	10	N/A	N/A	N/A	20	280	300	25	120
18	380	2	N/A	N/A	N/A	20	280	300	15	120
19	380	2	N/A	N/A	N/A	20	280	300	15	480
20	380	2	N/A	N/A	N/A	20	280	300	15	480
21	380	2	N/A	N/A	N/A	20	280	300	15	480
22	380	2	21.0	21.0	21.0	20	280	300	15	480
23	380	2	21.4	21.4	21.4	20	280	300	15	480
24	380	2	21.5	21.5	21.5	20	280	300	15	480
25	380	-	21.5	21.5	21.5	20	280	300	15	480
26	380	-	19.5	19.5	19.5	20	280	300	15	480
27	380	2	21	21	21	20	280	300	15	480
28	380	2	23	23	23	20	280	300	15	480
29	380	2	N/A	N/A	N/A	20	280	300	15	480
30	380	2	22	22	22	20	280	300	15	480
31	380	2	24-26	24-26	24-26	20	280	300	15	480

Table 3-3 Operating conditions of SnO_2 deposition using tetraethyl tin as precursor (cont.)

Electrode no.	Operating condition									
	Temperature of reactor (^oC)	Temperature of bubbler (^oC)	Temperature of helium (^oC)	Temperature of oxygen (^oC)	Temperature of feed line (^oC)	Flow rate of helium (sccm)	Flow rate of oxygen (sccm)	Total Flow (sccm)	Total pressure (Torr)	Duration (min)
32	380	2	24-26	24-26	24-26	20	280	300	15	480
33	380	2	25	25	25	20	280	300	15	480
34	380	2	21	21	21	20	280	300	15	480
44	380	2	23	23	23	20	280	300	15	450
51	380	2	19	19	19	20	280	300	15	480
52	380	2	N/A	N/A	N/A	20	280	300	15	480
55	380	2	19	19	19	20	280	300	15	480
57	380	2	N/A	N/A	N/A	20	280	300	15	720
59	380	2	18	18	18	20	280	300	16	240

3.5.5 Deposition characterization

The surface morphology and microstructure of the coatings were characterized by X-ray diffraction (XRD, Cu Kα), scanning electron microscope (SEM) and profilometer for roughness measurement. The relative average deposited films growth rate was determined by weight measurement.

3.6 Simulation of Ir deposition using FLUENT®

3.6.1 Simulation domain and boundary conditions

As geometry reduction of the simulation domain could not be easily made, it was decided to work with the real domain in 3-dimension simulation. It consisted of a tube of 1.1 cm of inside diameter and 30 cm in long of heating zone in which the silicon pieces of wafer (or silicon control substrate), electrode (or substrate) and electrode holder (or substrate holder) are placed as shown in Figure **3-3 and 3-4**. The domain was meshed using a mix of regular and hybrid meshes.

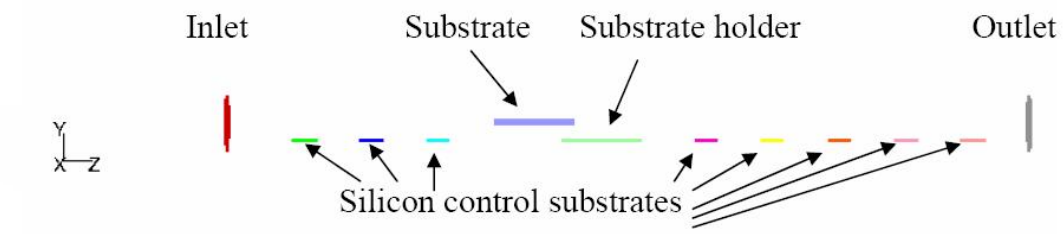

Figure 3-3 Side view of the simulation domain

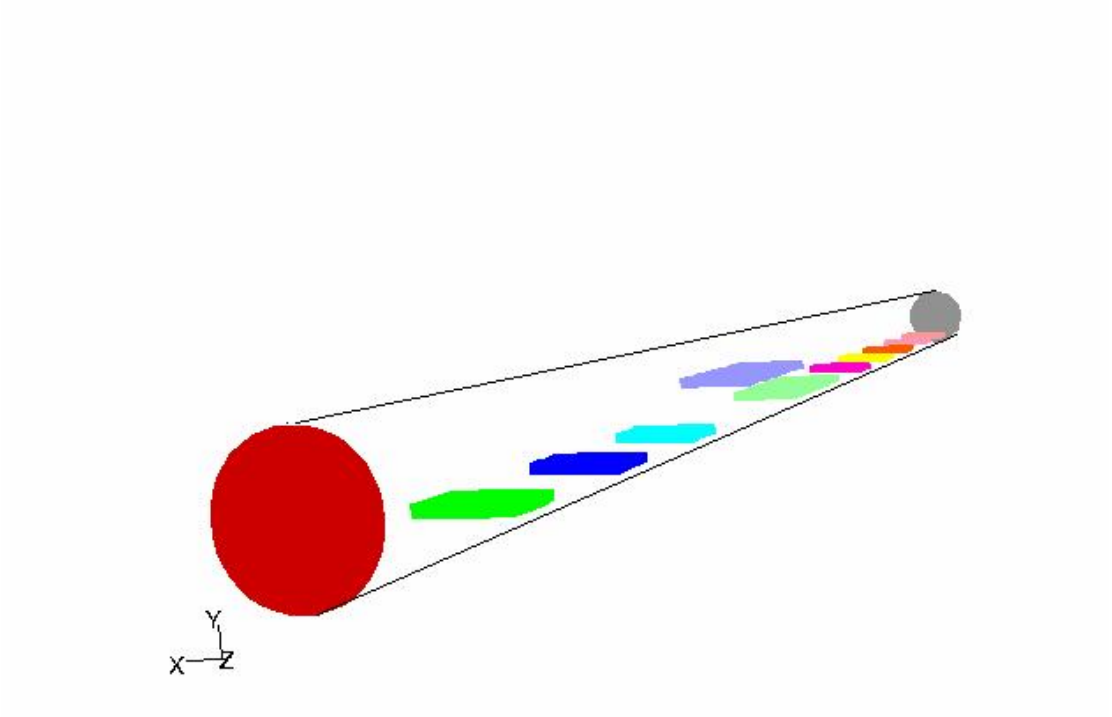

Figure 3-4 Isometric view of the simulation domain

The boundary conditions linked with the simulation domain are given.

Inlet

Mass flow inlet boundary conditions were used as compressible flows to prescribe a mass flow rate at an inlet. It was not necessary to use mass flow inlets as incompressible flows because when density is constant, velocity inlet boundary conditions will fix the mass flow.

Momentum; mass flow inlet determined by flow rate and composition used for the considered experiments, velocity normal to the surface.

Thermal condition; temperature was corresponding to the measured experimental value.

Species; mass fraction was corresponding to operating conditions using simulation.

Substrate, substrate holder, silicon control substrate and reactor wall

Momentum; stationary wall and no slip condition.

Thermal conditions; temperature fixed using experimental thermal profile.

Species; flow was corresponding to the kinetics reaction.

Outlet

Outflow conditions for momentum, thermal and species; outflow boundary conditions were used to simulate the flow exited where the details of the flow velocity and pressure were unknown prior to solution of the flow problem. They are appropriate where the exit flow was close to a fully developed condition, as the outflow boundary condition assumed a zero normal gradient for all flow variables except pressure. They were inappropriate for compressible flow calculations.

As thermal boundary conditions, it has been decide to fix these values to the values measured experimentally.

3.6.2 Main assumptions for the simulation

As the pressure drop through the reactor was very low, less than 1 torr, it was assumed that gases could be considered as incompressible ideal gases.

The mass diffusivity has been calculated using kinetic-theory and Lennard-Jones parameters. Values for Lennard-Jones parameters were taken from the data table of the FLUENT® software for referenced species.

Viscosity and thermal capacity have been computed using mixing law using FLUENT® software.

It has been assumed that the flow was laminar. Energy equation was solved for determine the thermal profile in the gas mixtures. As the temperature was not quite high, radiation effect was taken into account and only convective and diffusive energy transport were considered.

Figures 3-5, 3-6 and 3-7 represents the different planes that were taken into account for the presentation of the results of the simulation. It will be used a horizontal plane ($y = 0$) corresponding to the bottom of substrate. We will use also a vertical plane ($x = 0$) corresponding to the only symmetry plane of the system. The plane for $z = 0.129$ m corresponded to the vertical plane for the end of the substrate.

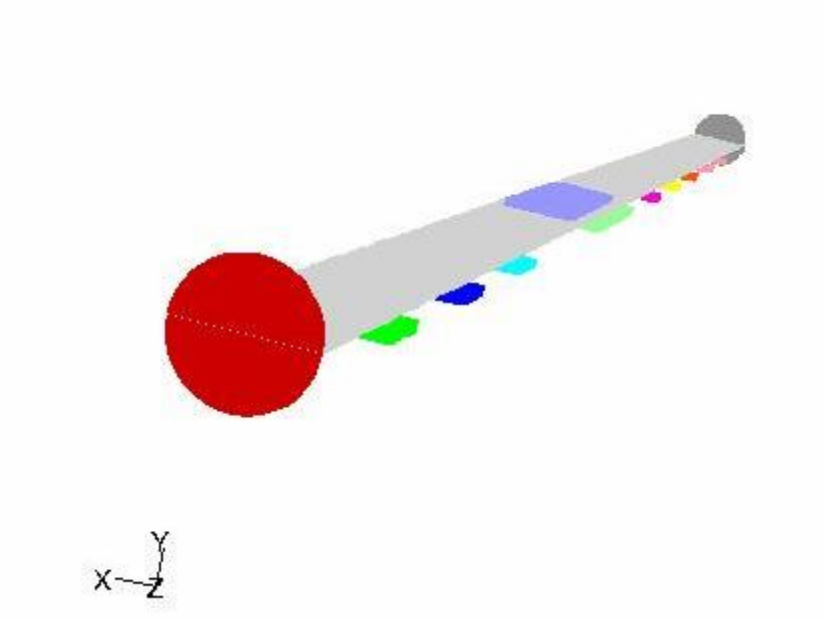

Figure 3-5 Visualization of horizontal plane at y = 0

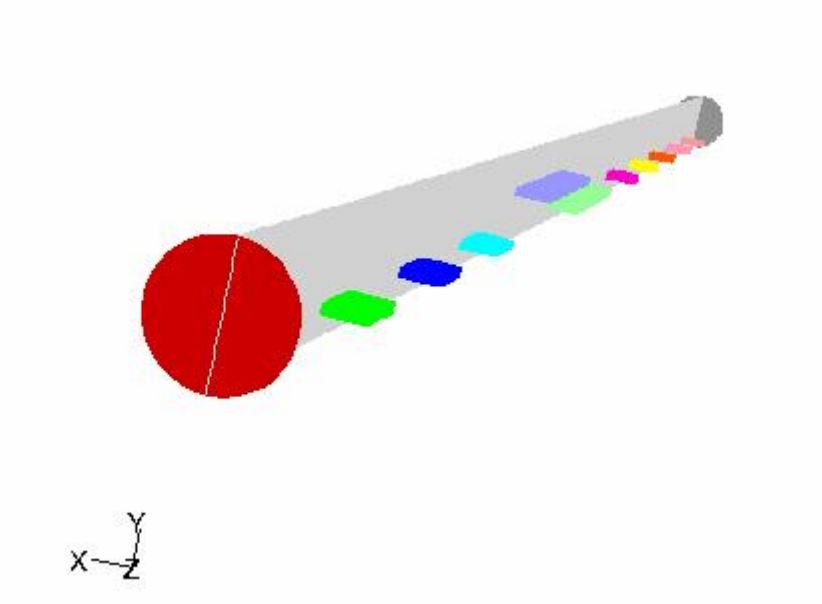

Figure 3-6 Visualization of vertical plane at x = 0

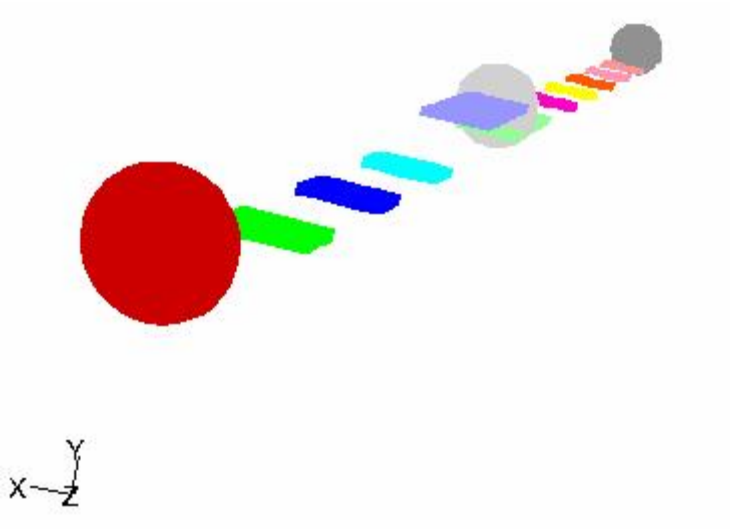

Figure 3-7 Visualization of vertical plane at z = 0.129 m

3.7 Electrochemical Characterization

The electrochemical oxidation of organic pollutants was conducted in the two parts of experiments. Firstly, the experiments were operated in batch condition. Then, the experiments were operated in continuous condition. The electrochemical oxidation was studied with the mode of constant applied current.

3.7.1 Batch electrochemical oxidation

The electrochemical characterization was performed in a three-electrode electrochemical reactor with 18 ml capacity. The prepared electrodes were used as anode, the 316L stainless steel was used as cathode and the saturated calomel was used as reference electrode. The apparatus is presented in Figure 3-8. The characteristic of model solution and operating conditions were presented in Tables 3-4 and 3-5, respectively.

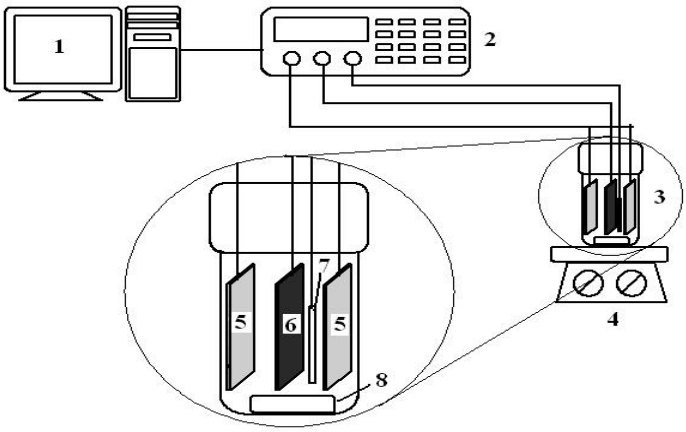

Figure 3-8 Schema of batch electrochemical oxidation apparatus; 1) PC with control software, 2) Potentiostat, 3) Electrochemical reactor set, 4) Magnetic stirrer, 5) SUS 316L cathodes, 6) Anode, 7) Reference electrode and 8) Magnetic bar

Table 3-4 Characteristics of model solution

Parameter	Amount
Oxalic acid (mg/L)	756
Sulfuric acid (mg/L)	14.7
Total organic carbon (mg/L)	160

Table 3-5 Operating conditions for batch electrochemical oxidation of model solution

Parameter	Operating condition
Current density	5-10 mA/cm^2
SnO_2 film thickness	1.8-3.6 micron
Residence time	0-6 hr
Stirring	300 rpm

3.7.2 Continuous electrochemical oxidation

The continuous electrochemical oxidation was also performed in a three-electrode electrochemical reactor with 18 ml capacity. The prepared electrodes were used as anode, the 316L stainless steel was used as cathode. The feed solution was fed to the reactor by peristaltic pump and the effluent was collected at sample trap. The apparatus is presented in Figure 3-9. The operating conditions were represented in Table 3-6.

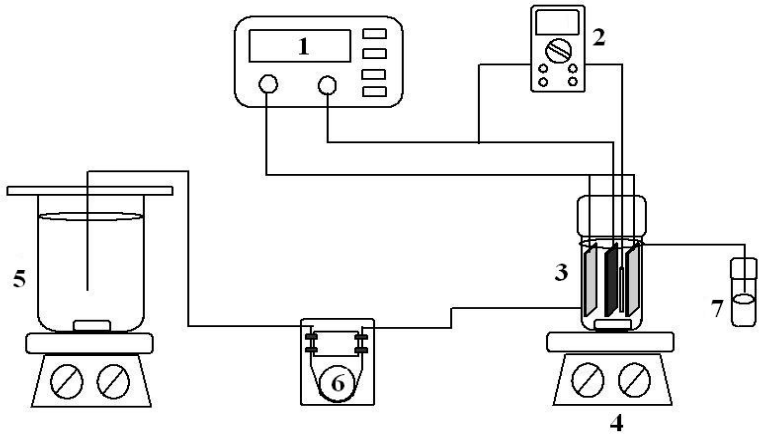

Figure 3-9 Schematic diagram of continuous electrochemical oxidation apparatus; 1) Power supply, 2) Volt meter, 3) Electrochemical reactor set, 4) Magnetic stirrer, 5) Feed reservoir, 6) Peristaltic pump , 7) Sample trap

Table 3-6 Operating conditions for continuous electrochemical oxidation

Parameter	**Operating condition**
Current density	5-10 mA/cm^2
SnO_2 film thickness	1.8-3.6 micron
Residence time	2-3 hr
Elapse time	24 hr
Stirring	300 rpm

3.7.3 Pollutant removal efficiency

The pollutant removal efficiency was investigated by using oxalic acid and effluent from Chulalongkorn University Student Canteen as model solution. The total organic carbon (TOC) was determined by Shimadzu TOC-5050A analyzer. The instrument is presented in Figure 3-10. The chemical oxygen demand (COD) was determined by closed reflux-titration method. Both total organic carbon and chemical oxygen demand were followed standard methods for the examination of water and wastewater [72].

Figure 3-10 Shimadzu TOC-5050A TOC analyzer

3.7.4 Characteristics of restaurant wastewater

Although, the wastewater from Chulalongkorn University Student Canteen had been treated by the physical treatment process as grease trap, but it still had high organic strength. Table 3-7 presents the characterization of effluent from Chulalongkorn University Student Canteen. It shows that the effluent has high BOD, COD and oil and grease, which cause the big problem for public wastewater collection and treatment system.

Table 3-7 Characterization of wastewater from Chulalongkorn University Student Canteen

Parameter	Value
pH	4.62
BOD (mg/L)	1,050
COD (mg/L)	2,000
TOC (mg/L)	896
Oil and Grease (mg/L)	2,270

3.8 Conclusions

In the elaboration of protective layer, it was studied on the deposition of IrO_2 with the effect of O_2/$Ir(Acac)_3$. While the coating of Ir was studied on the effect of O_2/(MeCp)Ir(COD) and deposition temperature. The effects of O_2/TET and total pressure were also studied on deposition of SnO_2 active layer. The elaborated electrodes were

utilized in the destruction of organic pollutant in both model solution and actual restaurant wastewater. In addition, the FLUENT® software was used for simulation of Ir deposition.

Chapter 4

Electrodes Elaboration

In this chapter, the results dealing the elaboration of electrodes are presented. Firstly, with the underlayer coating of IrO_2 and Ir. Then, it will be focused the deposition of SnO_2 electrocatalytic layer. Finally, the simulation of Ir deposition using FLUENT® software is presented.

4.1 Treatment of substrates

To improve the surface roughness of substrates for better adhesion of deposited films, the substrates need to be etched by the appropriating acid. In case of Ta substrate, the 40% HF was used as etching reagent. After etching, the average surface roughness of Ta substrates was increased. The Ta surface roughness progressed slowly comparing with Ti substrates etched by hot-HCl for 1 hr. Figures 4-1 and 4-2 represent the surface profile of 24 hr etched Ta in HF and 1 hr etched Ti substrate in hot-HCl. Although, Ta substrate was etched by stronger acid as HF, but the Ta surface roughness was still smaller than Ti surface because the chemical stability of Ta is much higher than that of Ti substrate. The average surface roughness measured by using profilometer of 1 hr hot-HCl etched Ti was 414 nm, while the average surface roughness of Ta substrates increase slightly with etching time, it was less than 300 nm after etched in HF for 24 hr as presented in Figure 4-3. The increasing surface area was confirmed by the observation with SEM in Figure 4-4. The surface of Ta and Ti substrate has not the same faces. It was large terrasse for Ta substrate while it was spongy with open area.

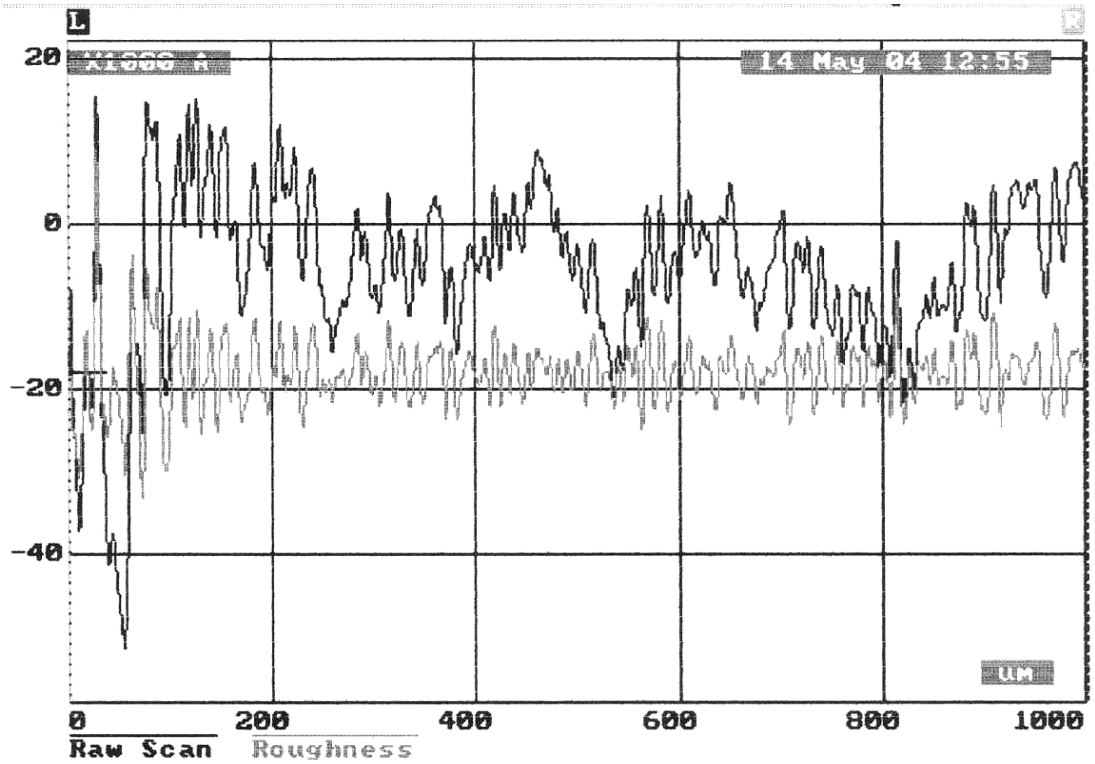

Figure 4-1 Roughness profile of 24 hr HF etched Ta substrate

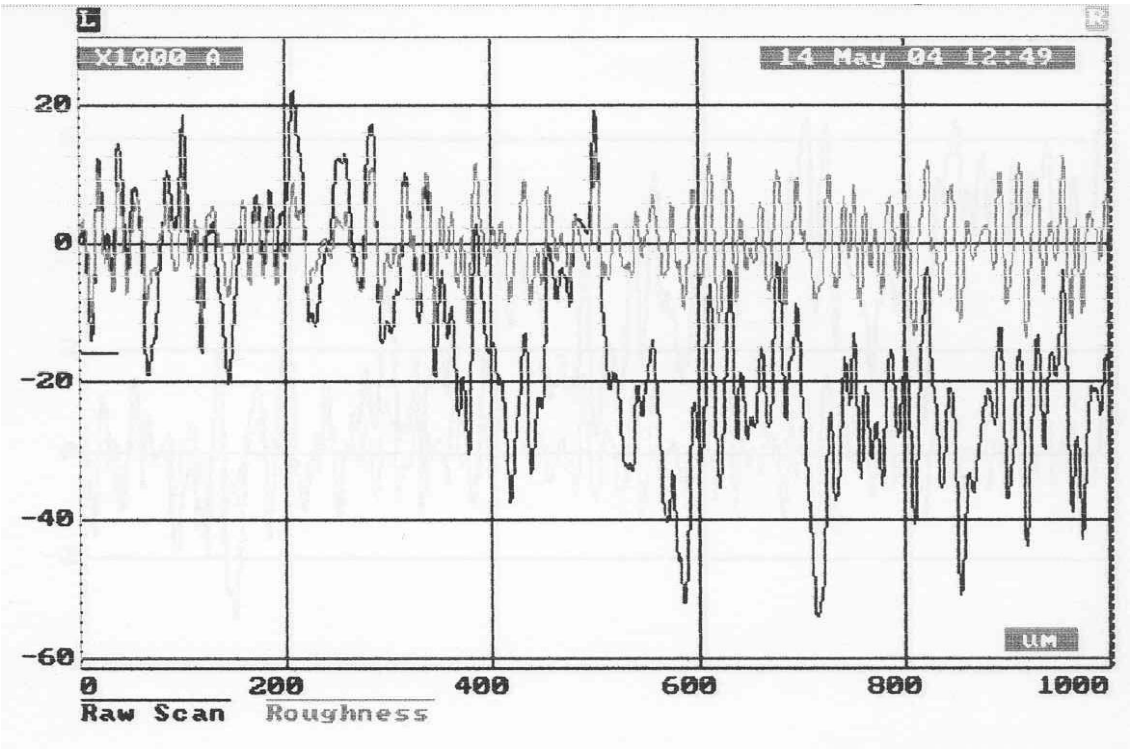

Figure 4-2 Roughness profile of 1 hr hot-HCl etched Ti substrate

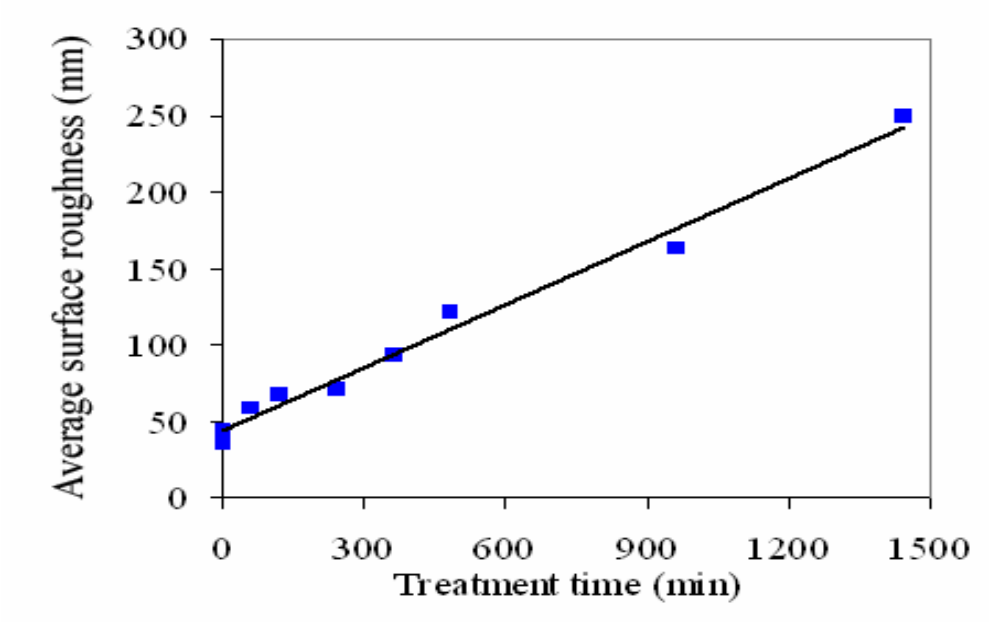

Figure 4-3 The average surface roughness of Ta substrates with various etching time by HF

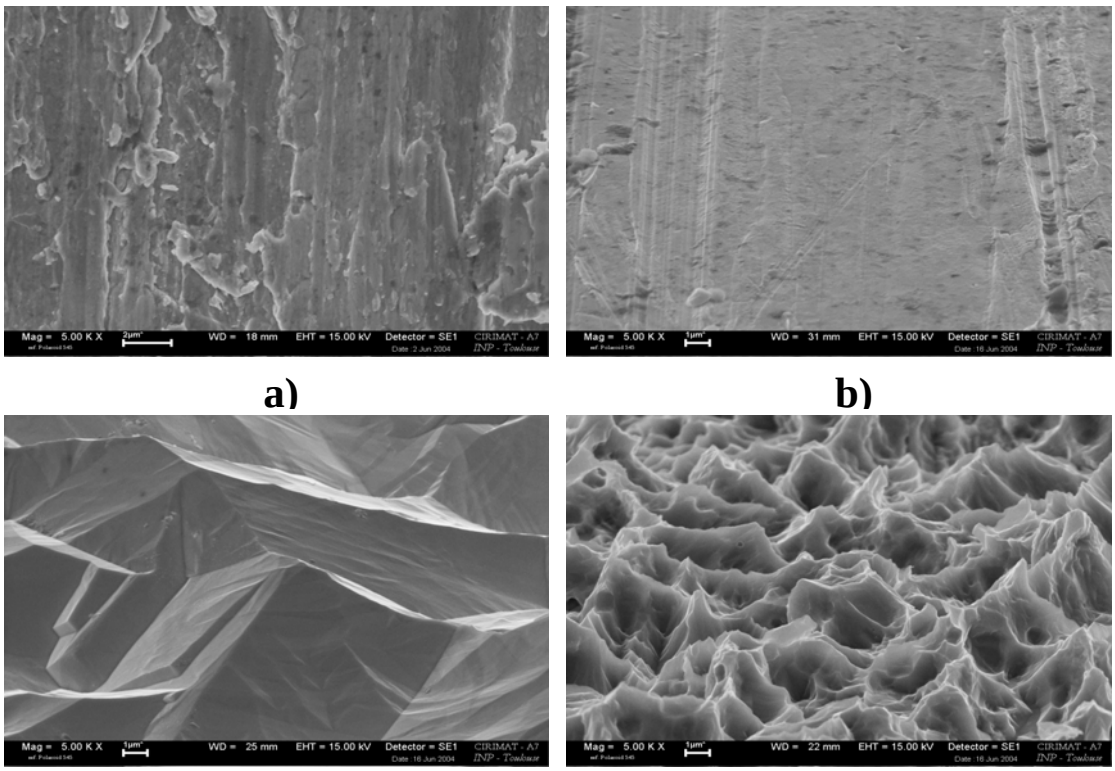

Figure 4-4 Scanning electron micrographs of some substrates a) Ta without etching, b) Ta with 1 hr etching, c) Ta with 24 hr etching and d) Ti with 1 hr etching

4.2 Protective underlayers elaboration

4.2.1 Deposition of IrO_2 by MOCVD

The deposition of IrO_2 film with presence of O_2 was investigated at 400 ºC and 25 Torr. The $O_2/Ir(acac)_3$ molar ratios were 11,000 (No. 9) and 17,000 (No. 12) on Si wafer and Ti substrate.

The effect of $O_2/Ir(acac)_3$ molar ratio on IrO_2 film growth rate is presented in Figure 4-5. The IrO_2 film growth rate increased to the maximum growth rate at 2.5 cm from the entrance of reactor, but it decreased immediately downstream. When the $O_2/Ir(acac)_3$ molar ratio was 17,000, the maximum growth rate was 1.9 nm/min and reduced to 0.9 nm/min at 7.5 cm from the entrance. However, the IrO_2 growth rate was undetected after passing into the reactor more than 12.5 cm. Although $O_2/Ir(acac)_3$ ratio was decreased to 11,000, the maximum IrO_2 growth rate was 2.9 nm/min still at 2.5 cm position and was reduced to 1.9 nm/nim at 7.5 cm from the entrance of the reactor.

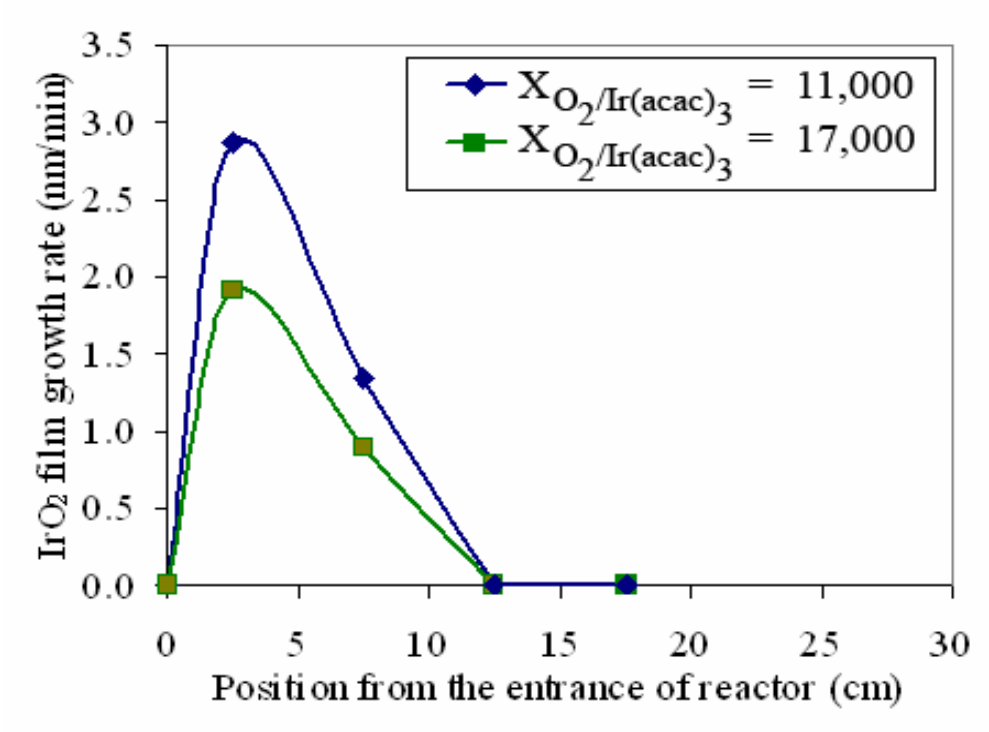

Figure 4-5 Effect of $O_2/Ir(acac)_3$ molar ratio on IrO_2 film growth rate at 400 ºC and 25 Torr

The comparison of IrO_2 growth rate when $O_2/Ir(acac)_3$ molar ratio was decreased from 17,000 and 11,000. It was found that the higher Ir source ratio is the higher IrO_2 film growth rate obtains due to its higher Ir precursor concentration in feed vapor. However, decreasing $O_2/Ir(acac)_3$ molar ratio could not improve the deposition in more homogeneous and uniform deposition; the IrO_2 thickness profile was still similar. It was caused by the $Ir(acac)_3$ consumed and deposited immediately after entering to the reactor only a few centimeters. The $Ir(acac)_3$ reacted with mixed oxygen at lower temperature than desired deposition temperature. It was confirmed by the deposition of Ir film at the 1.0-1.5 cm from the entrance of reactor that lower temperature was observed in some experiments. However, the IrO_2 film growth rate was significantly affected by $O_2/Ir(acac)_3$ molar ratio.

The $O_2/Ir(acac)_3$ molar ratio not only affected on IrO_2 film growth rate, but it also affected on the microstructure of IrO_2 film. The X-ray diffraction of IrO_2 film deposited at 2 cm from the entrance of reactor was presented in Figure 4-6. It was found that when decreased the $O_2/Ir(acac)_3$ molar ratio from 17,000 to 11,000, the peak of (101) orientation was decreased, but the peak of (110) orientation was outstanding, while the other peaks were not quite changed.

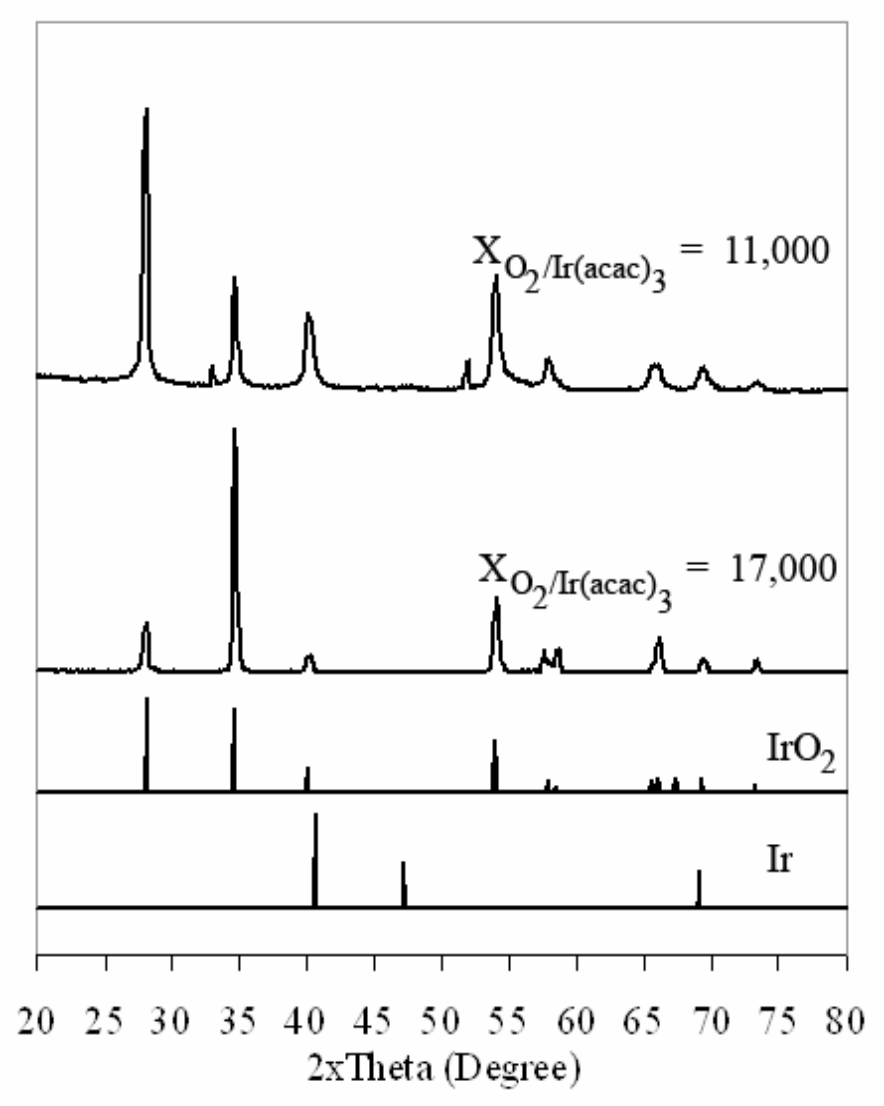

Figure 4-6 X-Ray diffraction of IrO_2 coated Si wafer

The effect of $O_2/Ir(acac)_3$ ratio was confirmed by SEM images in Figure 4-7, the columnar growth of IrO_2 with (101) orientation was observed when $O_2/Ir(acac)_3$ molar ratio was 17,000, while the dense IrO_2 film with (110) orientation was observed at molar ratio of 11,000.

Although, the IrO_2 film had homogeneous microstructure and good coverage on Si wafer, when Si wafer was substituted by actual Ti substrate, the gradient deposition of IrO_2 film was observed. It was occurred due to the low volatility and difficult to control mass transfer of $Ir(acac)_3$.

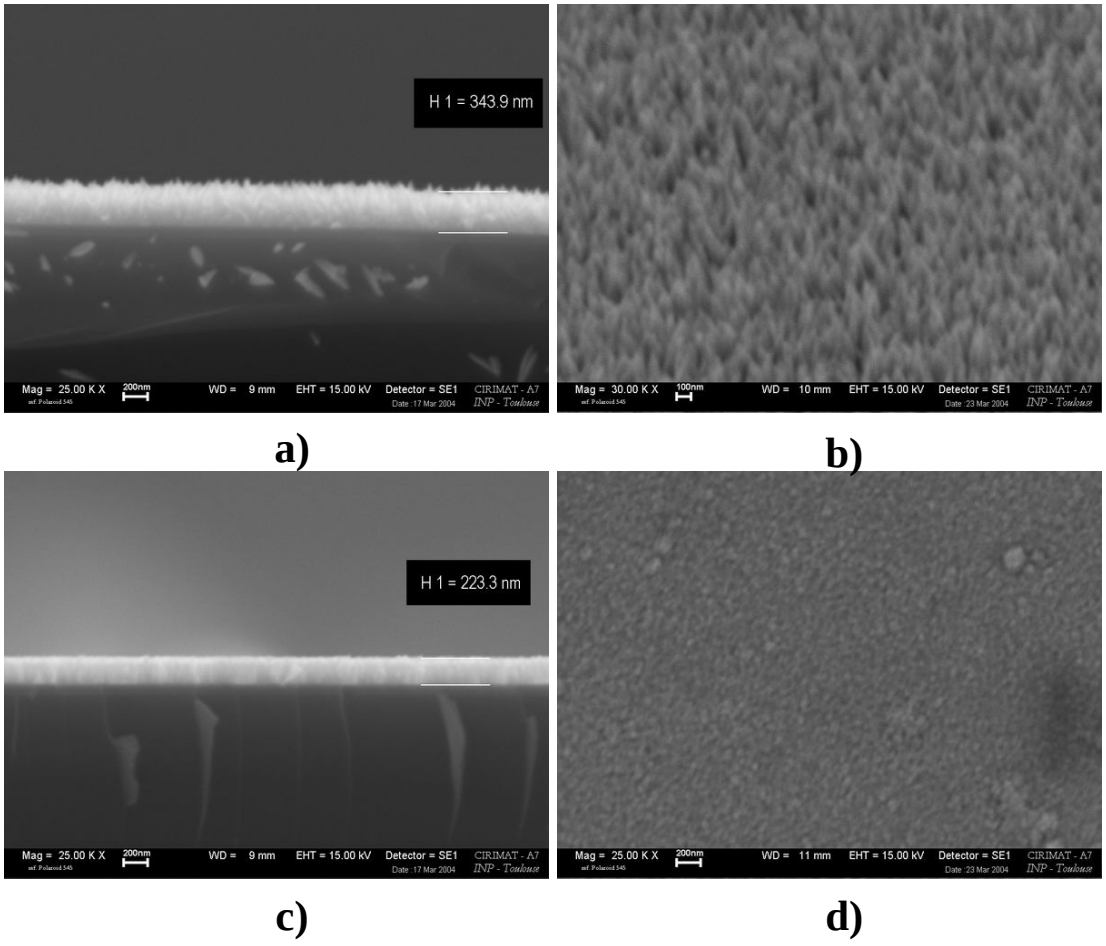

Figure 4-7 Cross-sectional and surface microstructure of IrO_2 film over Si wafer; a-b) $O_2/Ir(acac)_3$ molar ratio of 17,000 and c-d) $O_2/Ir(acac)_3$ molar ratio of 11,000

4.2.2 Deposition of Ir by MOCVD

Deposition of Ir film by using (MeCp)Ir(COD) as precursor with MOCVD could be operated at various condition as reported in some literatures [4, 48]. In this work, the deposition of Ir film with the presence of O_2 was investigated. It was found that the deposition of Ir film was strongly affected by deposition temperature and oxygen content in feed vapor mixture.

The effect of deposition temperature on the Ir film deposition is represented in Figure 4-8. At high O_2/(MeCp)Ir(COD) molar ratio in feed gas mixture (1500), the increasing deposition temperature from 300 (No. 41) to 325 (No. 40) and 350 (No. 39) ºC has significantly affected on the deposition area of Ir film. The deposition area of Ir film was decreased from 13 to 11 and 9.75 cm from the entrance of the reactor, respectively. It agrees with some results in Figure 4-9, the growth rate of Ir film was very high at a few centimeters nearby the entrance of the reactor. However, the Ir film growth rate rapidly decreased downstream. It may be affected by at high deposition temperature, the precursor had higher internal energy. Consequently, the precursor reacted with co-reactive gas and consumed immediately in a few centimeter from the entrance. However, the deposition temperature could be reduced to lower than 300 °C, due to the (MeCp)Ir(COD) will not be decomposed that was found by Chen [50].

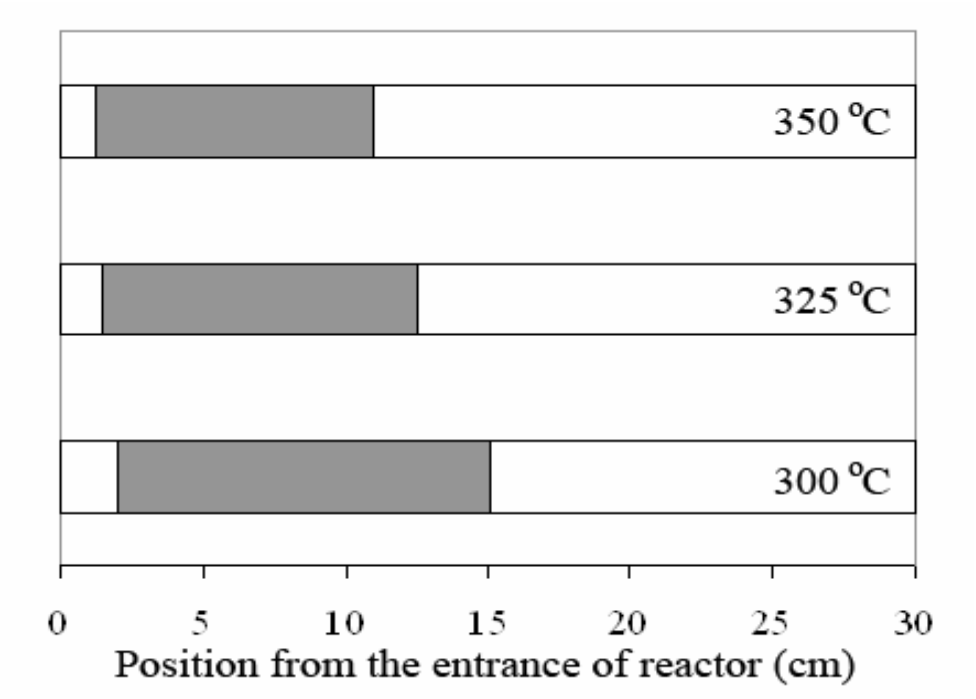

Figure 4-8 Effect of deposition temperature on deposition area of Ir film at 12 Torr and O_2/(MeCp)Ir(COD) molar ratio of 1500, ( ) deposition area

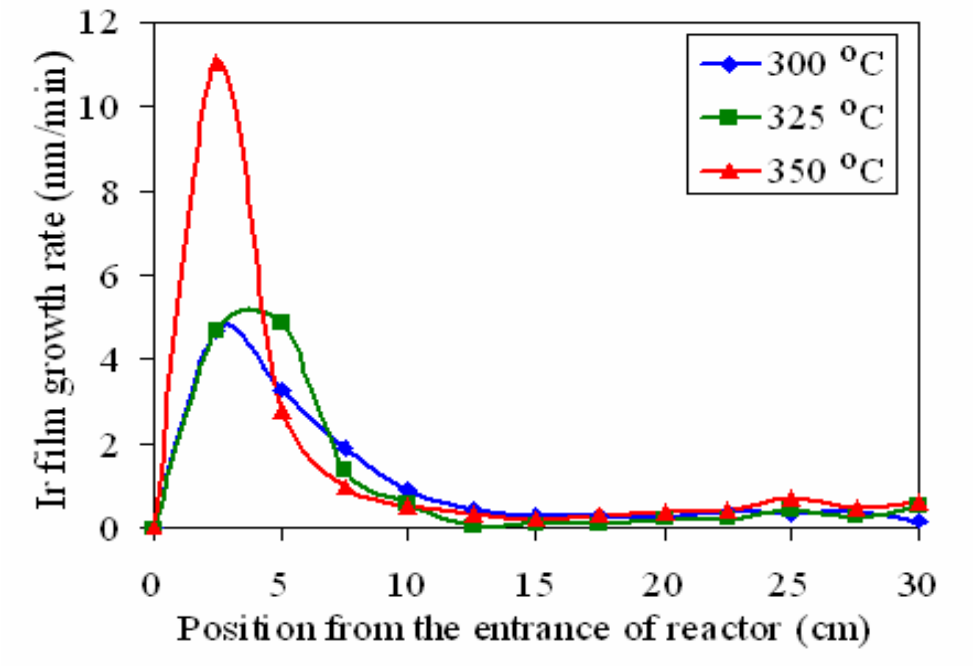

Figure 4-9 Effect of deposition temperature on Ir film growth rate at 12 Torr and O_2/(MeCp)Ir(COD) molar ratio of 1500

The effect of oxygen content in feed vapor mixture on deposition area was represented in Figure 4-10. At O_2/(MeCp)Ir(COD) molar ratio of 1545 (No. 41), (MeCp)Ir(COD) was completely decomposed and the yield of the Ir deposited film in the reactor was nearly 100%. However, the Ir film was deposited only at the entrance of the reactor and the gradient growth rate was observed because the system was very high reactivity when oxygen content was too high and the precursor consumed immediately. In contrast to low O_2/(MeCp)Ir(COD) molar ratio of 125 (No. 48), the reactivity of the system was decreased by reducing O_2/(MeCp)Ir(COD) molar ratio. In this case, the Ir film deposited uniformly over several centimeters distance through the reactor. It was confirmed by Figure 4-11, the growth rate increased to the maximum film growth rate at around 10 cm from the entrance before decreased rapidly downstream

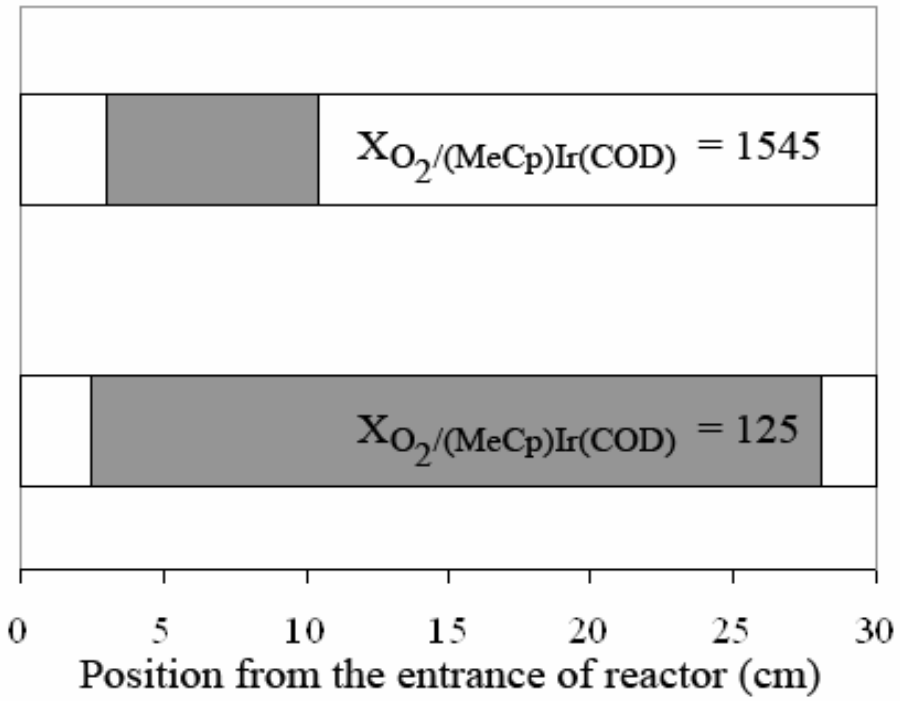

.

Figure 4-10 Effect of oxygen content in feed gas mixture on deposition area of Ir film at 300 ºC and 12 Torr, (□) deposition area

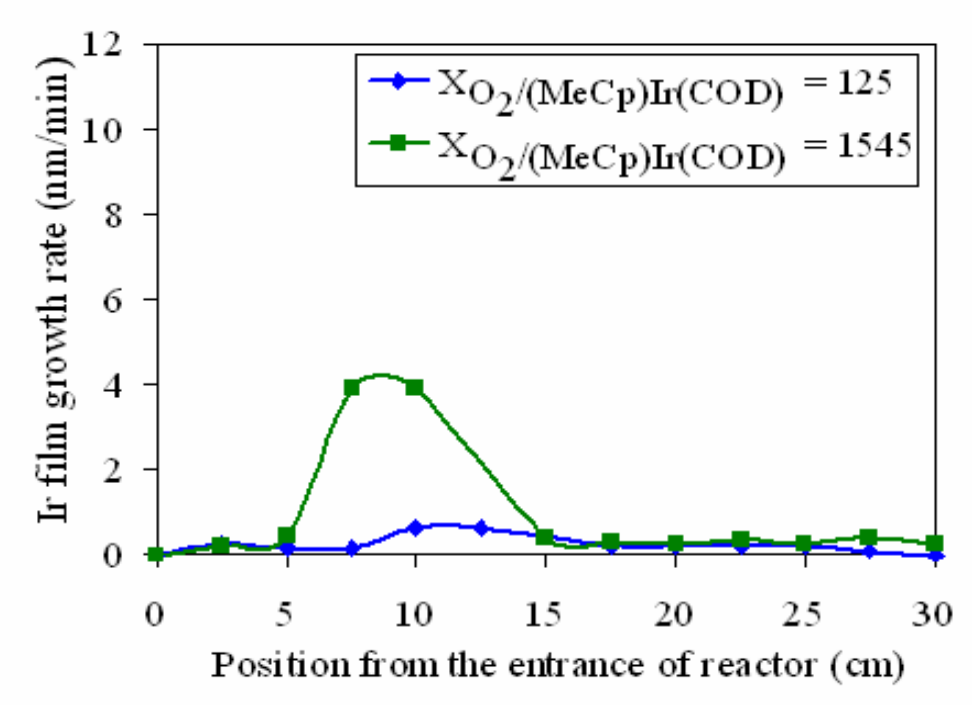

Figure 4-11 Effect of oxygen molar ratio on Ir film growth rate at 300 ºC and 12 Torr

Figure 4-12 represents the SEM images of Ir film on Si wafer and hot-HCl treated Ti substrate. The micrographs present the very smooth, homogeneous and good coverage deposition of Ir film. The Ir deposition also has very high purity. It could be confirmed by the XRD spectra in Figure 4-13. From these results, we could say that the deposited Ir film is very good to be used as the protective layer for SnO_2 specific electrode.

From these results it could be concluded that the Ir film was deposited at 300 ºC, total pressure of 12 Torr and O_2/(MeCp)Ir(COD) molar ratio of 125 is suitable to be used as the protective layer for specific electrode.

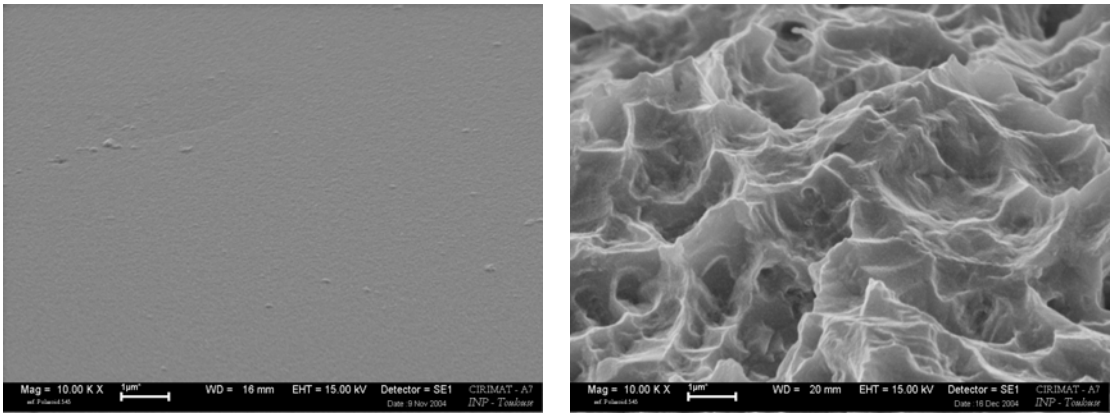

a) **b)**

Figure 4-12 Scanning electron micrographs of Ir film a) Ir film over Si wafer and b) Ir film over 1 hr hot-HCl treated Ti substrate

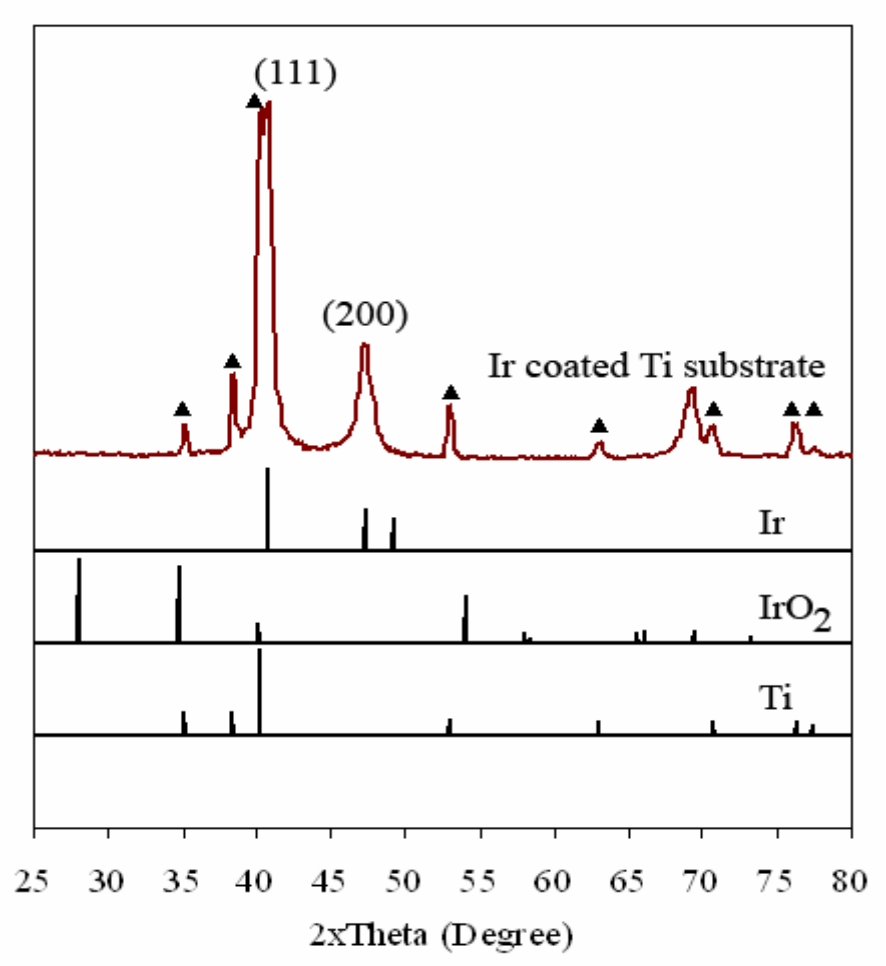

Figure 4-13 X-Ray diffraction of Ir coated Ti substrate (▲) substrate

4.3 Electrocatalytic layer deposition

4.3.1 Deposition of TiO_2 by spray coating

The deposition of TiO_2 by spray coating produced the uniform and good coverage TiO_2 coating over SUS 316L substrate. However, the TiO_2 stripping was observed in a few minutes when it was used as anode in an electrochemical oxidation of wastewater (Chulalongkorn University effluent). It may be because that the TiO_2 layer had high porosity and low adhesion. The oxidation of SUS 316L substrate was occurred due to the attack of wastewater at high potential.

Because of a very short service life of TiO_2/SUS 316L and low adhesion of TiO_2 layer, the TiO_2/SUS 316L was unsuitable to use as electrode for wastewater treatment by electrochemical oxidation.

4.3.2 Deposition of SnO_2 by spray pyrolysis

The deposition of SnO_2 by spray pyrolysis was investigated at 500 ^oC in ambient atmosphere. Due to the uncontrolled drop size of precursor solution sprayed by simple atomizer, the SnO_2 film is resulted in inhomogeneous coating. The unregulated surface temperature made some precursor incompletely reacted with oxygen. Some precursor was observed on the substrate surface.

Due to its inhomogeneous coating of SnO_2 film by spray pyrolysis, it could be mentioned that the spray pyrolysis technique was inappropriate to use as the method for production of SnO_2 specific electrode.

4.3.3 Deposition of SnO_2 by MOCVD

Figure 4-14 presents the effect of feed vapor composition on the SnO_2 deposition, it was found that the increasing O_2/TET molar ratio from 300 (No. 16) to 1,200 (No. 15), the both growth rates of SnO_2 film were quite similar in first 10 cm from the entrance of the reactor. However, in isothermal zone (after first 10 cm), the O_2/TET molar ratio of 300 represented the higher growth rate of SnO_2 film. It may caused by the first 10 cm, the system temperature was still low and the internal energy of TET precursor was not enough to react with mixed oxygen. However, after system reached to the isothermal zone (after first 10 cm), the effect of TET precursor in feed vapor was outstanding. The growth rate of SnO_2 film was a function of TET concentration in feed gas composition. Similar result was found in deposition of Ir film by MOCVD in previous reports [35]. The comparison of SnO_2 film thickness at each point in the reactor was presented in Figure 4-15.

The effect of deposition temperature on the SnO_2 deposition was not investigated in this work due to it was presented elsewhere that the good deposition temperature was 380 °C [41].

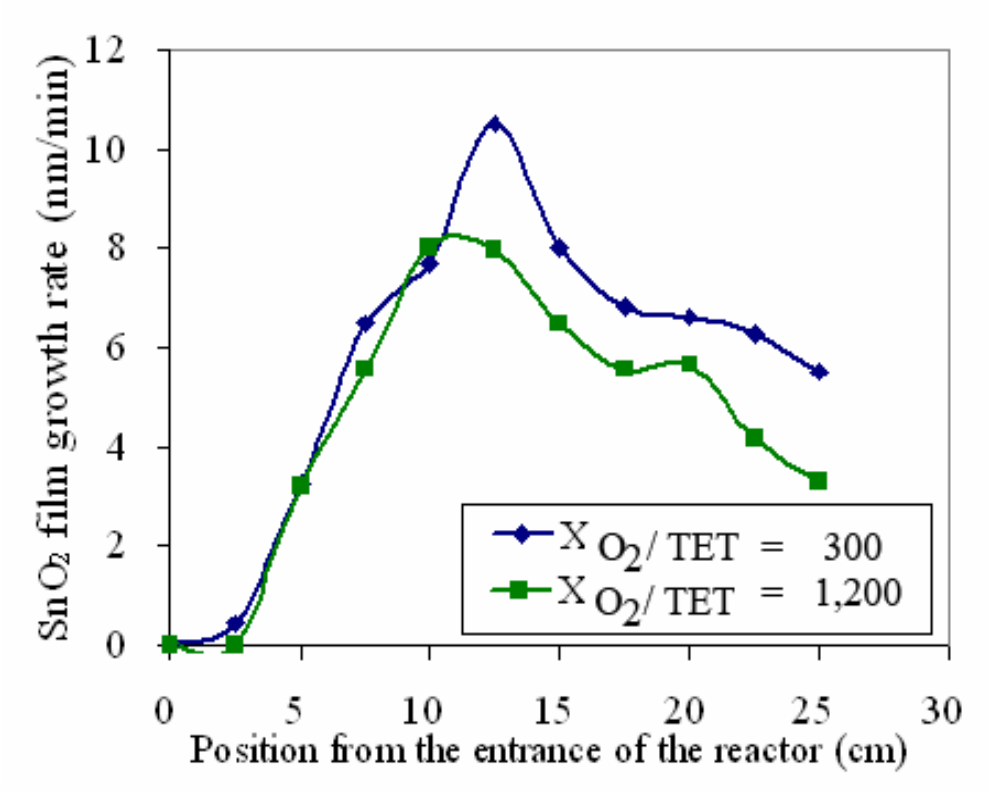

Figure 4-14 Effect of feed gas composition on SnO_2 film growth rate at 380 ºC and 15 Torr

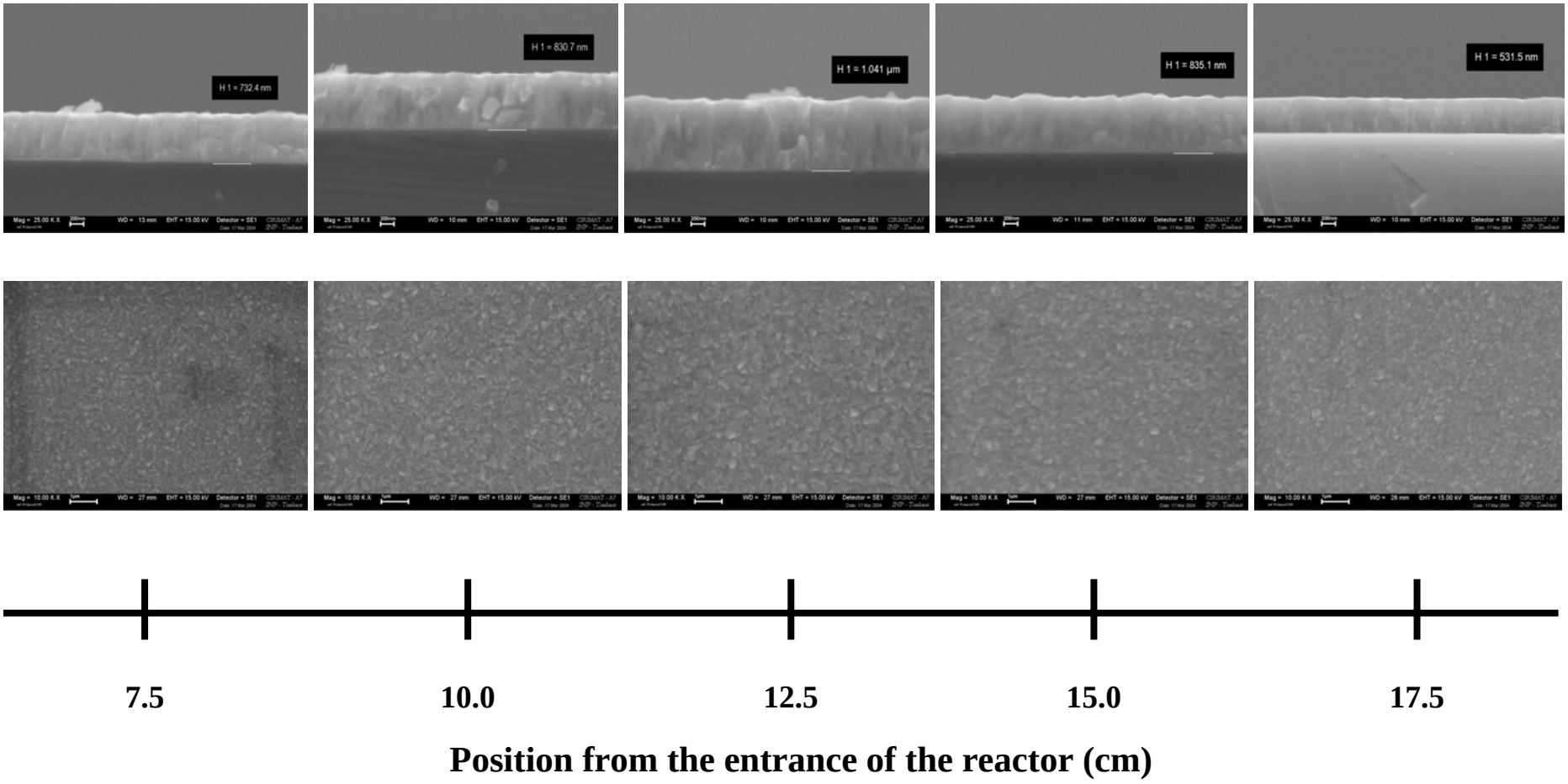

Figure 4-15 Comparison of SnO_2 film thickness at each point in the reactor, when deposition temperature of 380 °C, deposition pressure of 15 Torr and O_2/TET molar ratio of 1,200

The XRD spectra in Figure 4-16 presents that the increasing TET concentration in feed gas mixture has no influence on the microstructure of SnO_2 film. The SnO_2 film has nearly similar XRD spectra in both 300 and 1,200.

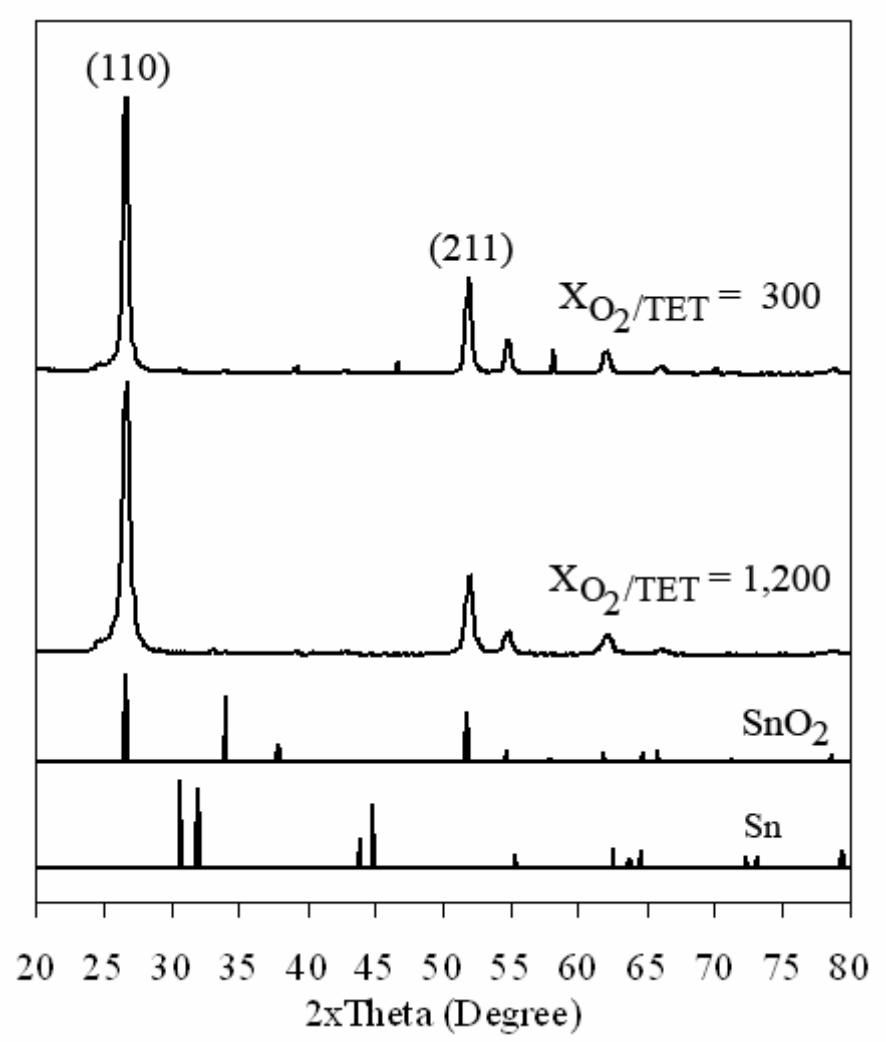

Figure 4-16 X-Ray diffraction of SnO_2 film over Si wafer at 380 ºC and 15 Torr

Figure 4-17 shows the more uniformly deposition of SnO_2 with decreasing total pressure when the TET precursor passed through the reactor faster and had shorter time to react with mixed oxygen. However, the SnO_2 growth rate and deposition yield were decreased with decreasing total pressure.

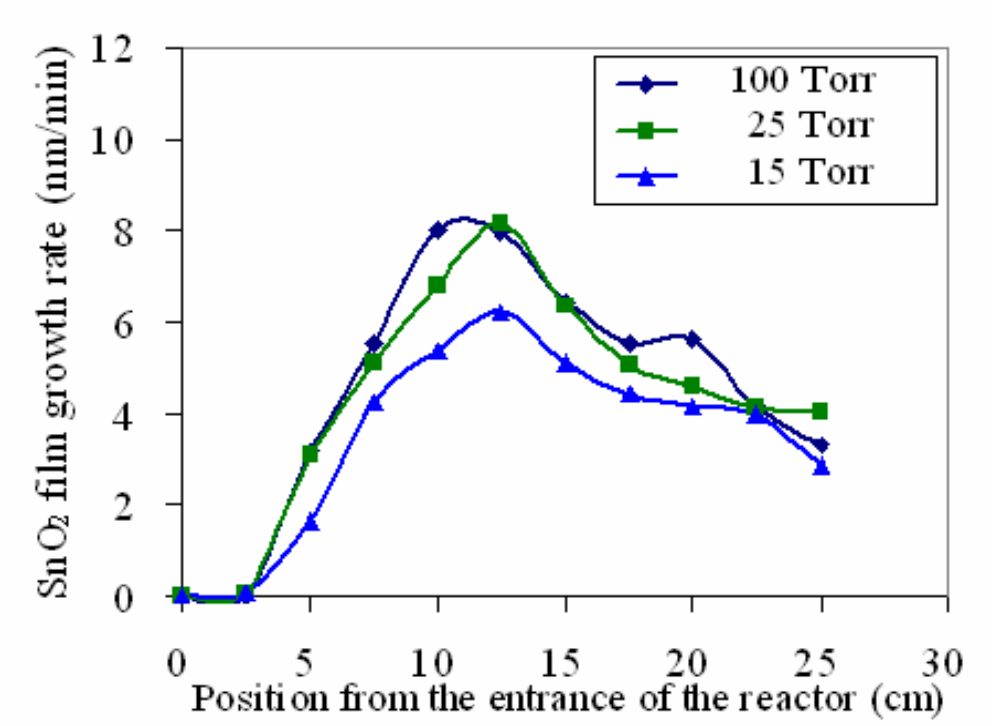

Figure 4-17 Effect of total pressure on SnO_2 film growth rate at 380 ºC

From the calibration of the system by deposited SnO_2 on Si wafer, it was found that the growth rate of SnO_2 film was smooth and uniform between 17.5-22.5 cm from the entrance of the reactor. So, in the preparation of useful electrode, the substrate was placed between 17.5-20.5 cm from the entrance and the dashed line in Figure 4-18 is represented the placement area of substrate in SnO_2 film deposition. To

measure the growth rate profile and to be sure that the system was similar to the calibration, the Si wafers still placed on the other point in the reactor as in calibration.

The effect of substrate on SnO_2 film growth rate was presented in Figure 4-18. In placement area of actual substrates, the growth rate of SnO_2 film was increased when substituted Si wafer with 1 min and 1 hr HF treated tantalum and it was suddenly increased after substituted by 1 hr HCl-treated titanium and Ir coated Ti substrate. The deposition rate was affected from the substrates substitution. However, after considered with the roughness of substrate as represented in Figure 4-4, it was found that the increasing SnO_2 growth rate was affected by the specific area of substrate which increased from the substrate treatment.

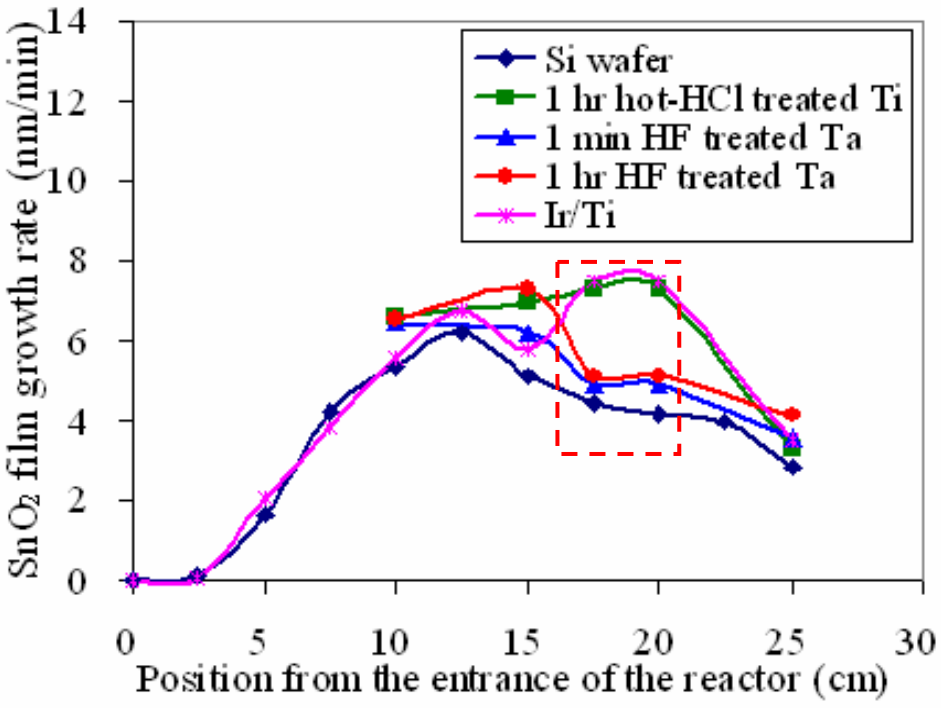

.

Figure 4-18 Effect of substrate on SnO_2 film growth rate at 380 ºC and 15 Torr

Figure 4-19 represents the surface and cross-sectional morphology of SnO_2 film on Si wafer and Ir coated Ti substrate. The deposited SnO_2 film over Si wafer was dense, smooth and homogeneous microstructure. In case of Ir coated Ti substrate, the microstructure of SnO_2 film was still dense and homogeneous. Furthermore, it also presents the good coverage deposition on the high surface roughness of Ir coated Ti substrate.

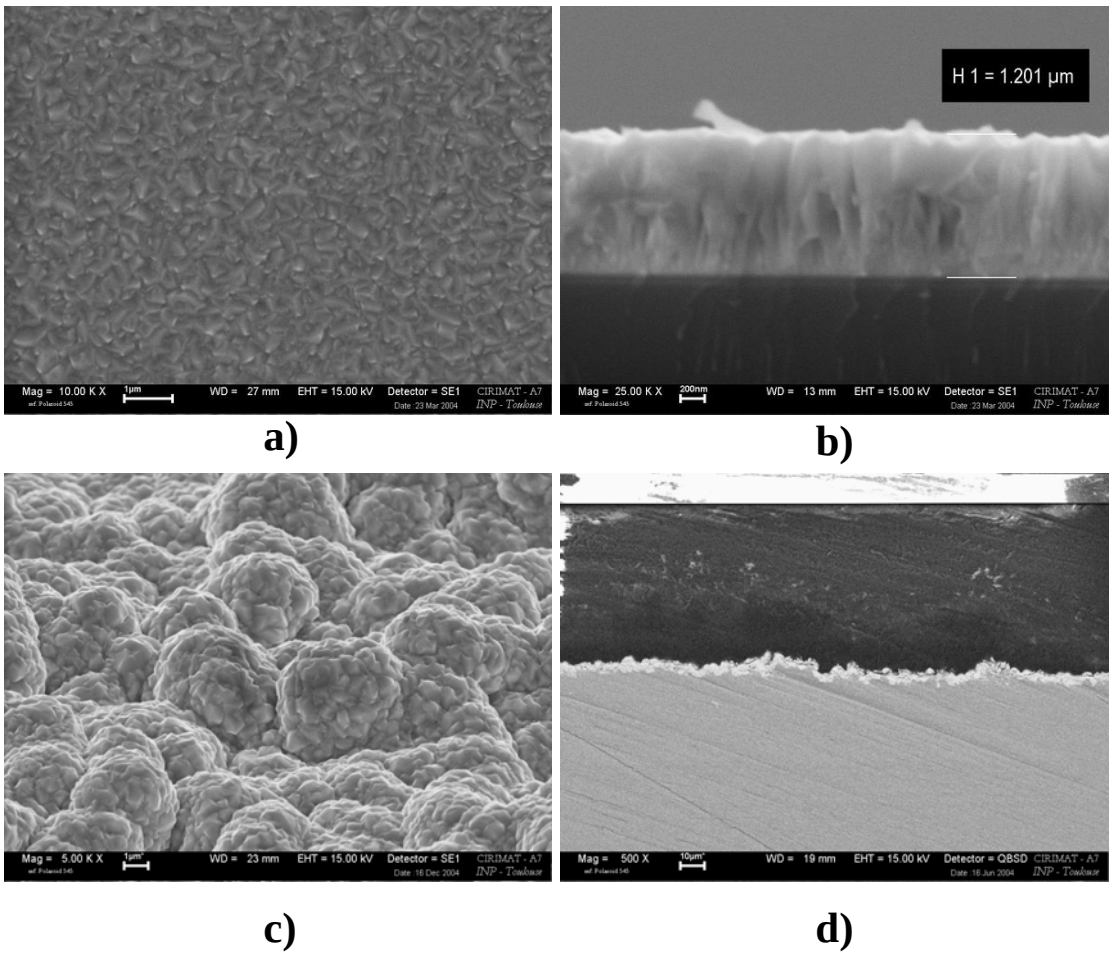

Figure 4-19 Surface and cross-sectional microstructure of SnO_2 film over various substrates a-b) Si wafer and c-d) Ir/Ti

From the results, it could be concluded that the suitable SnO_2 active coating for using as anode organic pollutant degradation was deposited at 380 ºC, 15 Torr of total pressure and 1,200 of O_2/TET molar ratio.

4.4 Simulation of Ir deposition using FLUENT®

In this part, the results dealing with velocity and temperature profile are presented before showing species concentration distributions and a comparison between experimental data and simulated deposition rate. For this work, only 3 operating conditions have been checked corresponding to experiment no. 39, 40 and 41.

4.4.1 Reaction mechanism

As the goal of this part is not to develop a new reaction mechanism of Ir deposition using (MeCp)Ir(COD) as precursor, the values and conclusions from Maury et al.[4] were taken for developing the simulation. In absence of O_2, Maury et al. [4] had shown that (MeCp)Ir(COD) decomposes at temperature higher than 760 K to produce MeCpH and COD [73-74]. When O_2 was used as co-reactive gas, it oxidized the organic ligands producing CO, CO_2 and H_2O. Furthermore, the presence of O_2 decreased the decomposition temperature to 465 K [74]. In addition to the by-products of this reaction, Maury et al. [4] have analyzed by using a cold trap at the outlet of the reactor with the presence of acetone and furan. It was concluded that the mechanism was complicated and in their work dealing with macroscopic modelling they have only considered the overall reaction as:

$$(MeCp)Ir(COD) + O_2 \rightarrow Ir + X \quad (4\text{-}1)$$

Where X represents of all organic by-products occurring in decomposition of (MeCp)Ir(COD) with presence of O_2.

The deposition rate increased with the partial pressure of both the Ir source and the oxygen. It was reported that the growth rate was approximately first-order in O_2 partial pressure at 550 K [74]. Consequently, Maury et al. [4] assumed the growth rate of the overall CVD reaction is:

$$G = k\mathrm{p}[(MeCp)Ir(COD)]\mathrm{p}[O_2] \quad (4\text{-}2)$$

Where k is the rate constant ($k = k_0 \exp(-E_a/RT)$). An activation energy E_a = 98 kJ/mol and a pre-exponential factor $k_0 = 5.8\times10^{14}$ were determined. In this case, E_a is approximately 30% higher than the value reported for a cold-wall reactor [73]. It was assumed that in the hot-wall CVD reactor there was more significant contribution of gas phase reactions, which elevated the apparent activation energy. These values were taken as initialisation values for the first simulation. These values have been converted to be use in the unit system of FLUENT® and have also been adjusted to have a better fit between experimental data and simulation results. The final values that were retained are:

E_a = 140 kJ/mol

$k_0 = 1\times10^{18}\ m^4/(kg\text{-}s)$

4.4.2 Velocity and pressure profiles

Figures 4-20, 4-21, 4-22, 4-23 and 4-24 present respectively the contour of the velocity magnitude for the horizontal plane, the vertical plane corresponding to x = 0, enlargement of the velocity vector for the vertical plane corresponding to x = 0 around the third silicon substrate, the velocity path lined for the vertical plane corresponding to x = 0 around the third silicon substrate and the velocity path lined for the vertical plane corresponding to x = 0 around substrate and substrate holder.

From these figures, it appears that the velocity increased for area close to the substrates due to the decrease of the cross sectional area. It could also be seen that in free substrate zones, the velocity has a parabolic distribution indicating a laminar flow in agreement with the Reynolds number, N_{Re}. In this case N_{Re} = 33, therefore the flow is fully laminar.

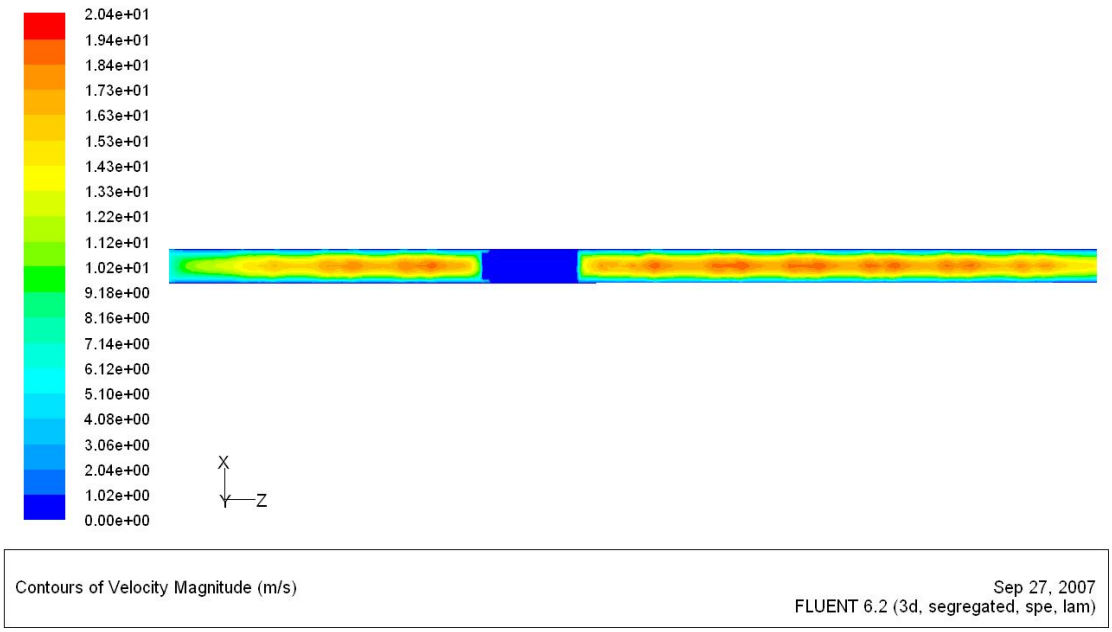

Figure 4-20 Contour of the velocity magnitude for the horizontal plane at y = 0 (Condition from electrode No. 40)

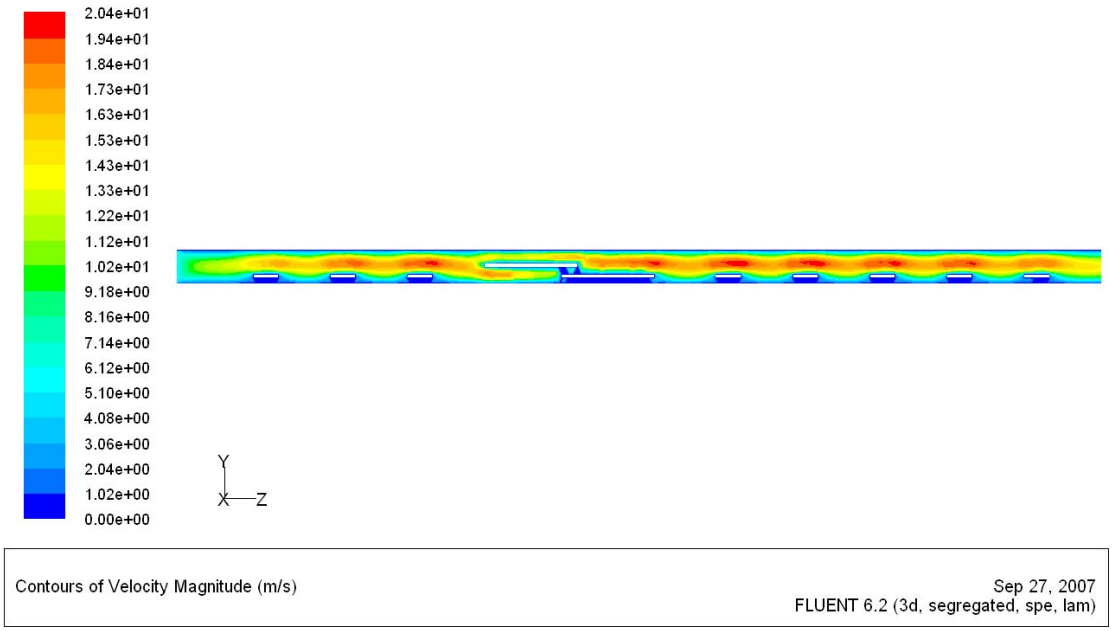

Figure 4-21 Contour of the velocity magnitude for the vertical plane corresponding at x = 0 (Condition from electrode No. 40)

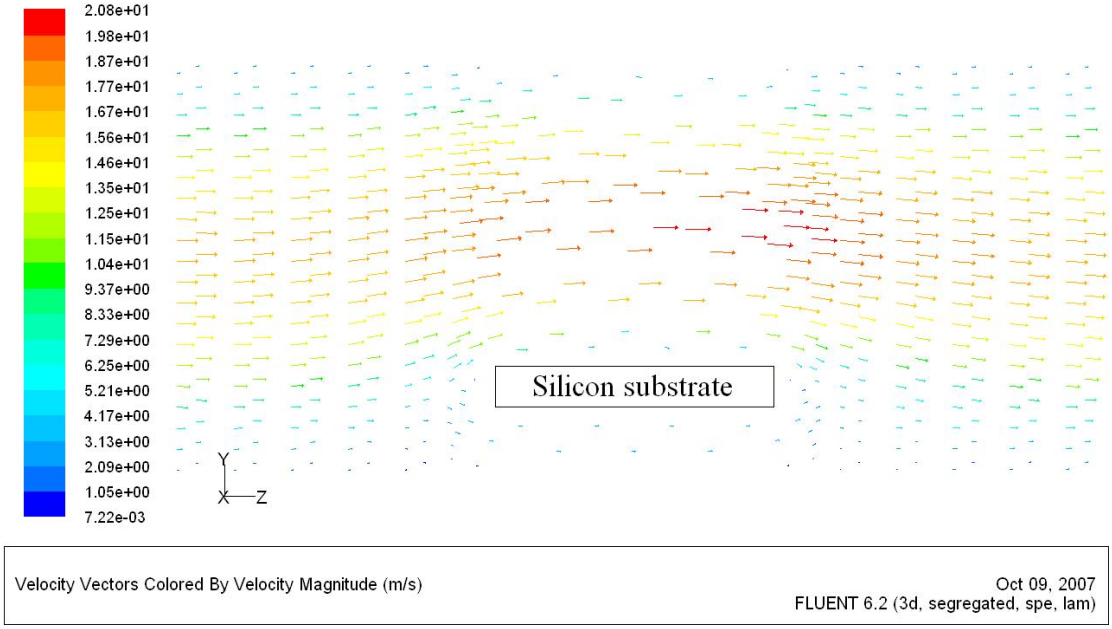

Figure 4-22 Velocity vector for the vertical plane corresponding to x = 0 around the third silicon substrate (Condition from electrode No. 40)

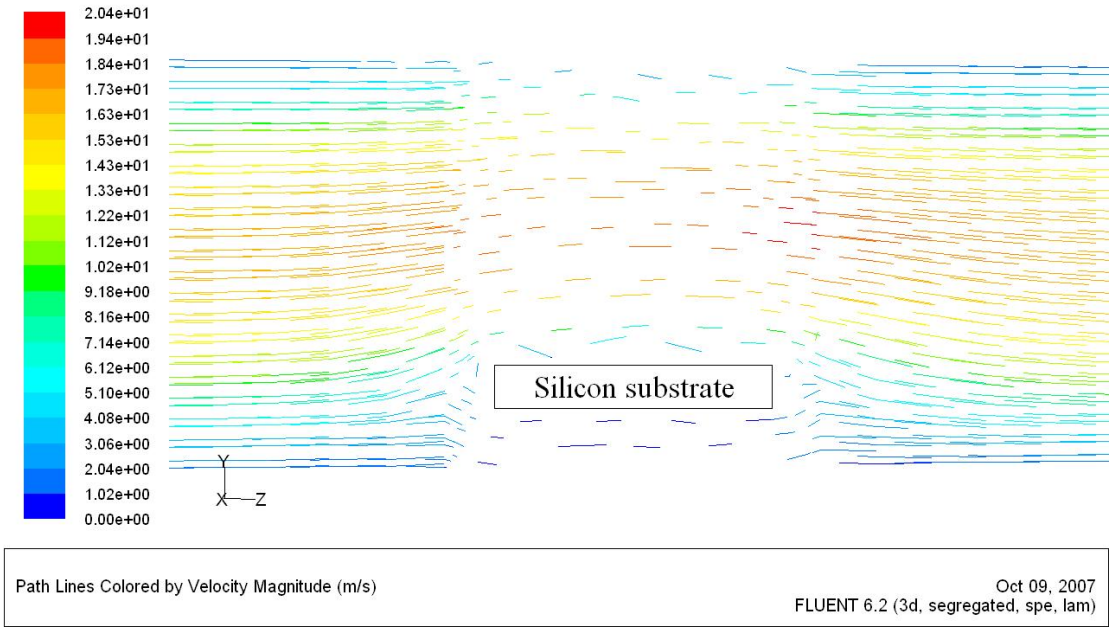

Figure 4-23 Velocity path line for the vertical plane corresponding to x = 0 around the third silicon substrate (Condition from electrode No. 40)

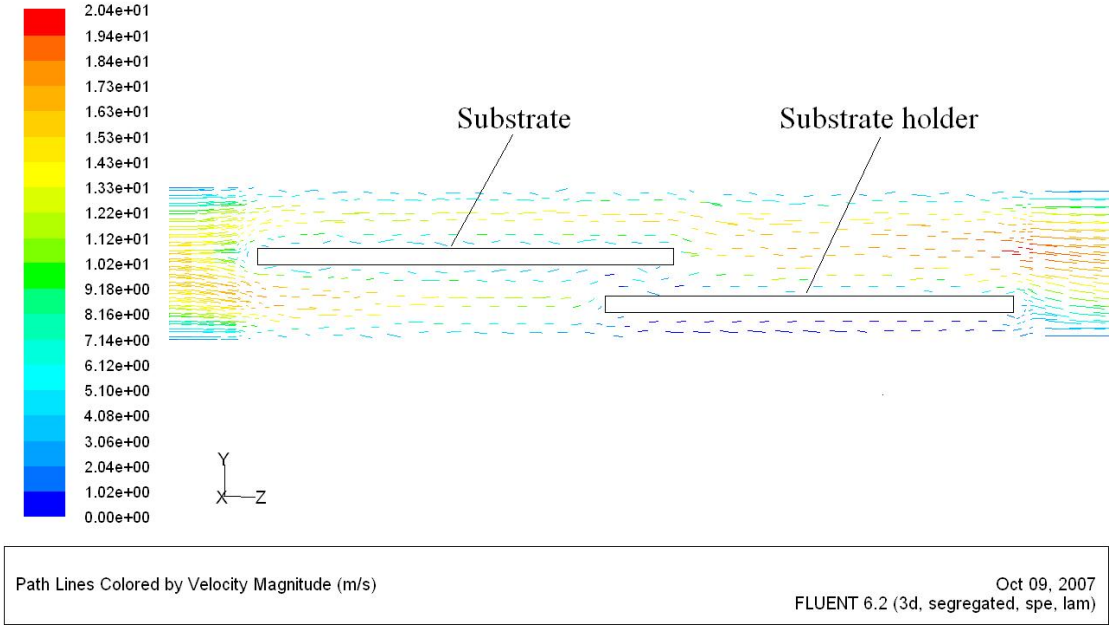

Figure 4-24 Velocity path line for the vertical plane corresponding to x = 0 around the real substrate and substrate holder (Condition from electrode No. 40)

Figure 4-25 depicts the distribution of the total pressure in the reactor. It is obviously to see that the pressure decrease from the inlet to the outlet of the reactor and the pressure drop through the reactor is very low, less than 0.2 torr. The low pressure drop was attributed to the low flow rate and to the nature of the fluid that it is a gas at low pressure.

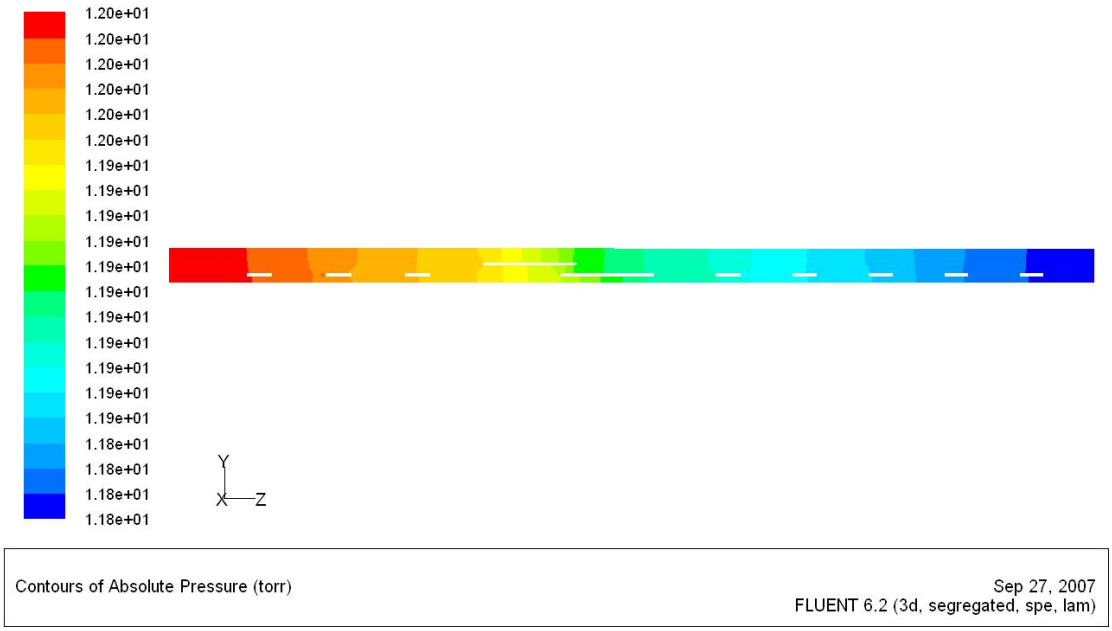

Figure 4-25 Contour of absolute pressure (Condition from electrode No. 40)

4.4.3 Temperature and gas density distribution

Figure 4-26 presents the evolution of the contour of gas temperature in the reactor. This profile has a parabolic form. This shape is due to the fact that gas was heated principally by the reactor wall and also to a more important residence time linked with a lower velocity near the reactor wall.

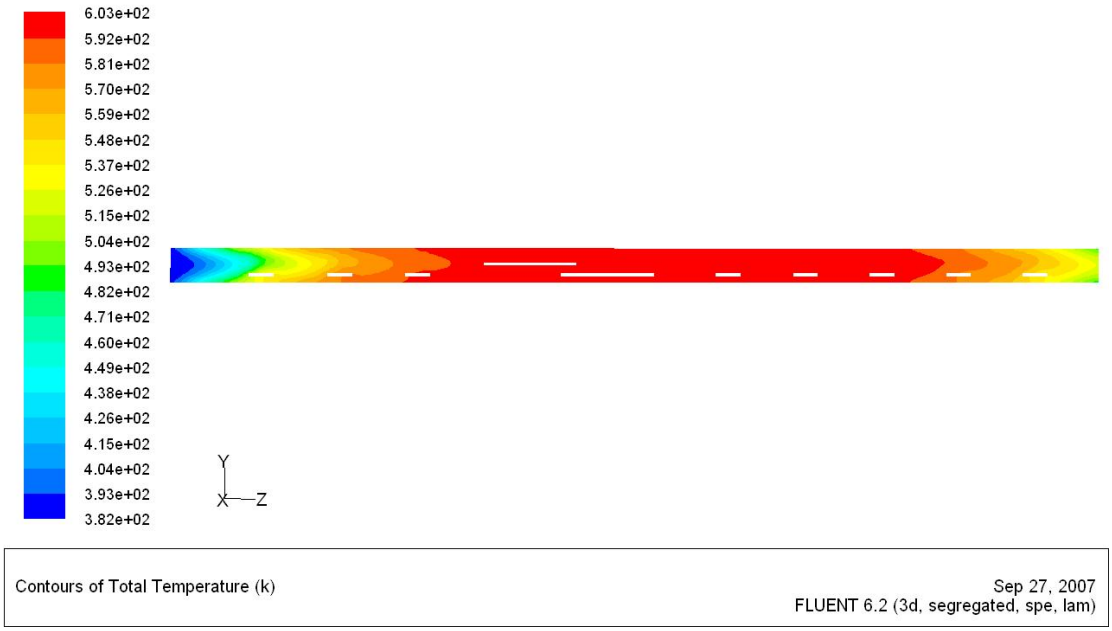

Figure 4-26 Contour of gas temperature (Condition from electrode No. 40)

Figure 4-27 presents the comparison of the experimental thermal profile to the calculated profile using FLUENT® software. For the calculated profile, it represents the temperature taken at the axis of the reactor.

In Figure 4-27, it presents obviously that the simulated temperature on the axis of the reactor is always belatedly when compare with the experimental values mainly at the entrance and at the exhaust of the reactor. It may caused by the velocity was a parabolic distribution that the gas velocity at the axis of the reactor was higher than that nearby the reactor wall. Therefore the gas temperature at the axis was lower by the lower residence time for heating. Nevertheless, these zones were less interesting for this work and the simulation was performed in heterogeneous reaction therefore it was not necessary to work on these zones of reactor.

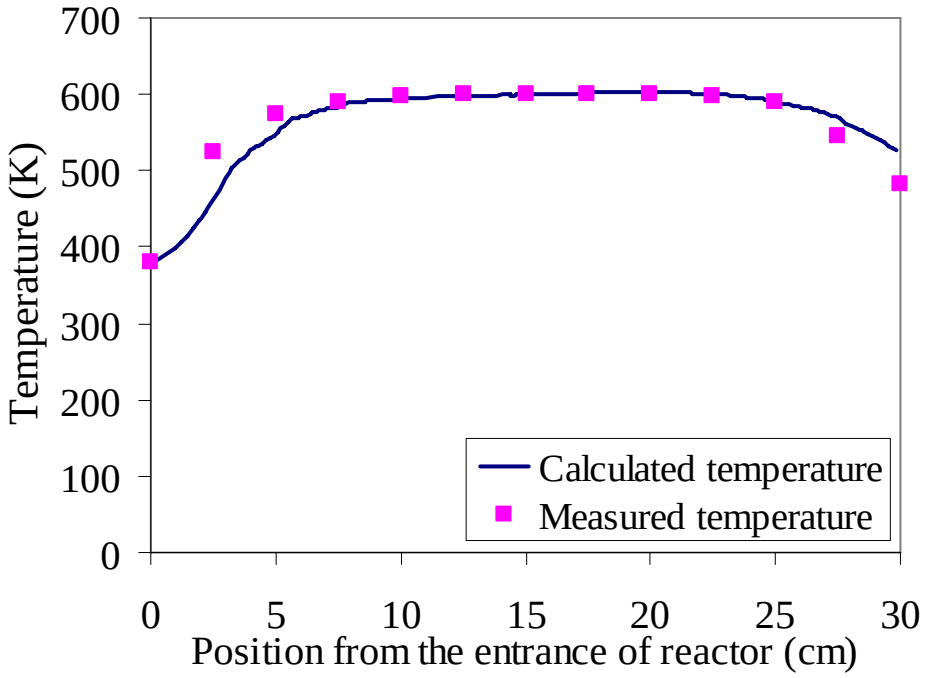

Figure 4-27 Comparison of the experimental and simulated temperature profile (Condition from electrode No. 40)

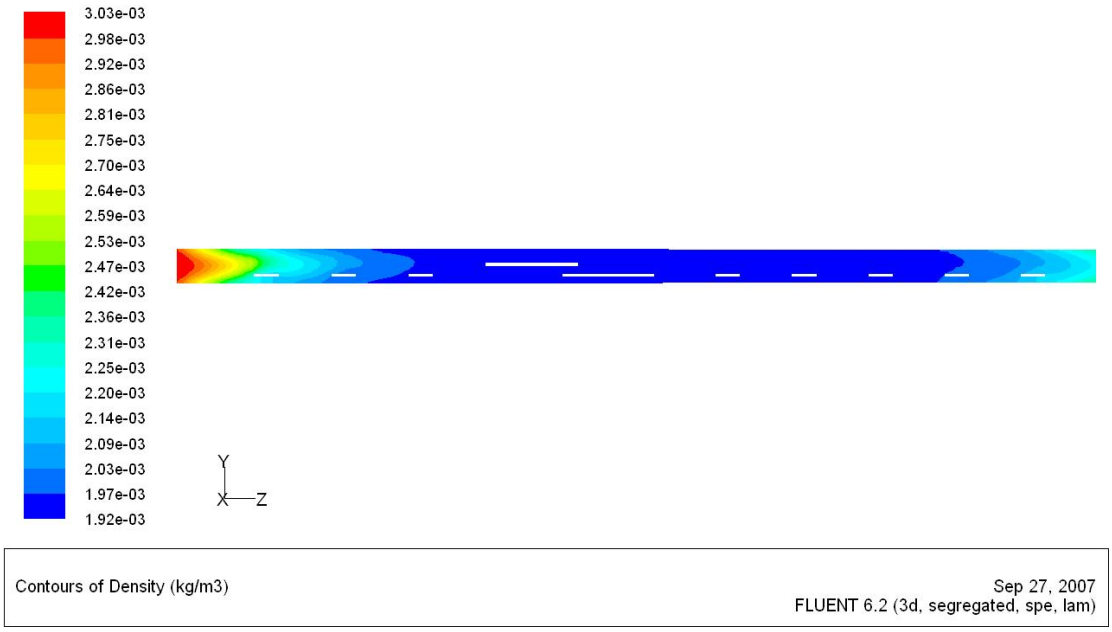

Figure 4-28 Contour of gas density (Condition from electrode No. 40)

Figure 4-28 indicates the evolution of the density of the gas. As the simulation assumption that the gas followed the law of ideal gas and low conversion rate in the reactor, the density profile is the contrary of the temperature profile. Therefore the gas density was decrease with the increase of the local temperature.

4.4.4 Species and growth rate distribution

Figures 4-29, 4-30 and 4-31 represent respectively of the contour of mass fraction for oxygen, iridium precursor and by product. For operating conditions utilized in the simulation, the iridium precursor is quickly consumed and after less than 6 cm its mass fraction reached nearly 0. While the inverse phenomenon was observed for the by product, it was reached quickly to its final value. Subsequently, the mass fraction was constant seem like the iridium precursor should not be converted. For oxygen, it was highly concentrated and excess feed when compared with the stoichiometric ratio of oxygen to iridium precursor. The oxygen mass fraction was petite changed from the entrance along through the reactor.

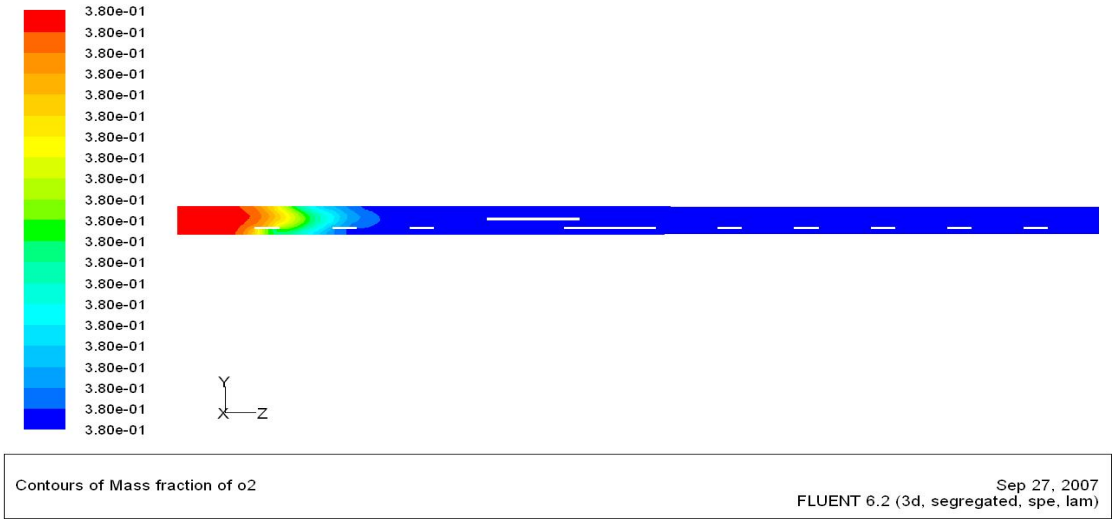

Figure 4-29 Contour of oxygen mass fraction (Condition from electrode No. 40)

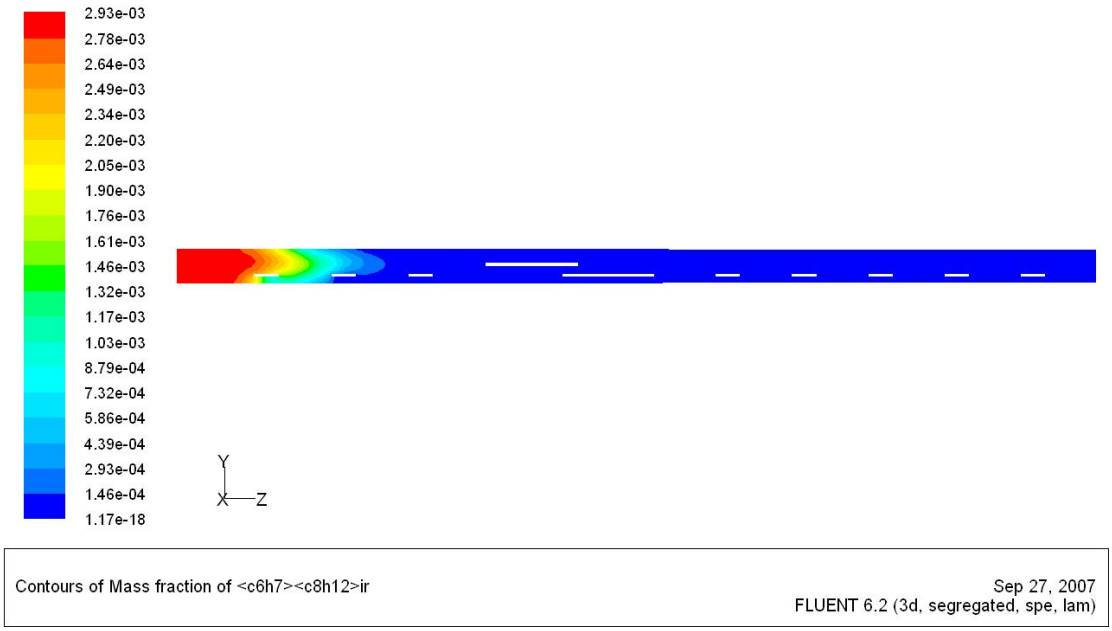

Figure 4-30 Contour of (MeCp)Ir(COD) mass fraction (Condition from electrode No. 40)

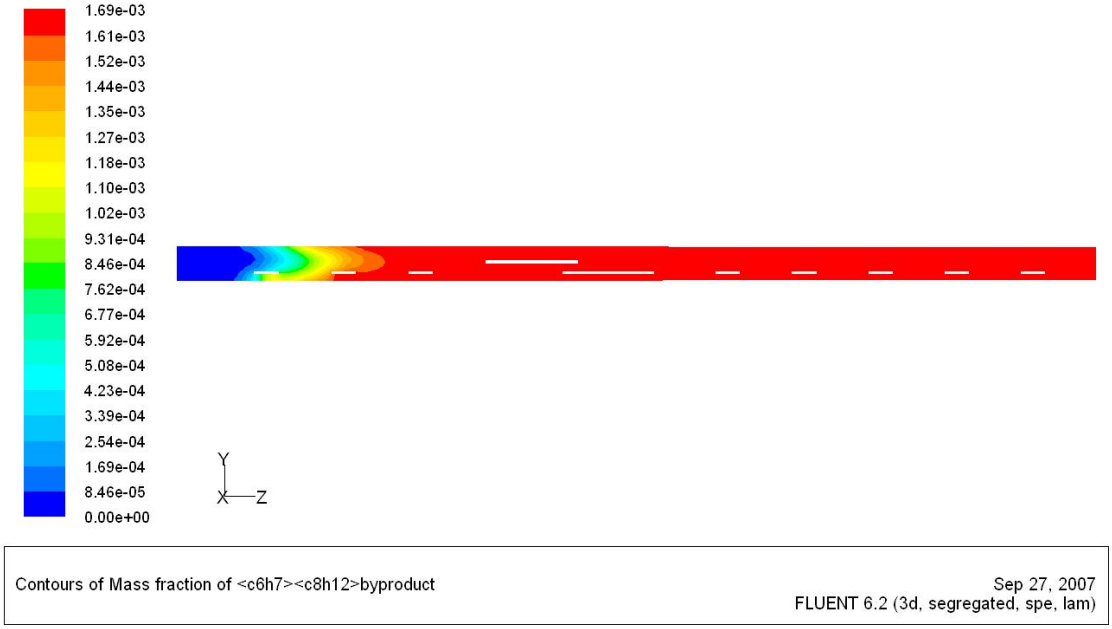

Figure 4-31 Contour of by product mass fraction (Condition from electrode No. 40)

One picture that should be shown in this section dealing with the simulation results would be the comparison of the experimental growth rate and the growth rate from the simulation. Nevertheless, before showing the comparison, it should present the distribution of growth rate on a substrate. Figure 4-32 (a) and (b) present instance of the distribution of the growth rate on the first control silicon wafer.

From Figure 4-32, it could be deduced that it would not be correct to assume a constant deposition growth rate for the substrate. Consequently, it has been decided to integrate the growth rate around the substrate and to divide this value by the area of the substrate to perform an average value for each position. Therefore, all results dealing on growth rate are reported as average values.

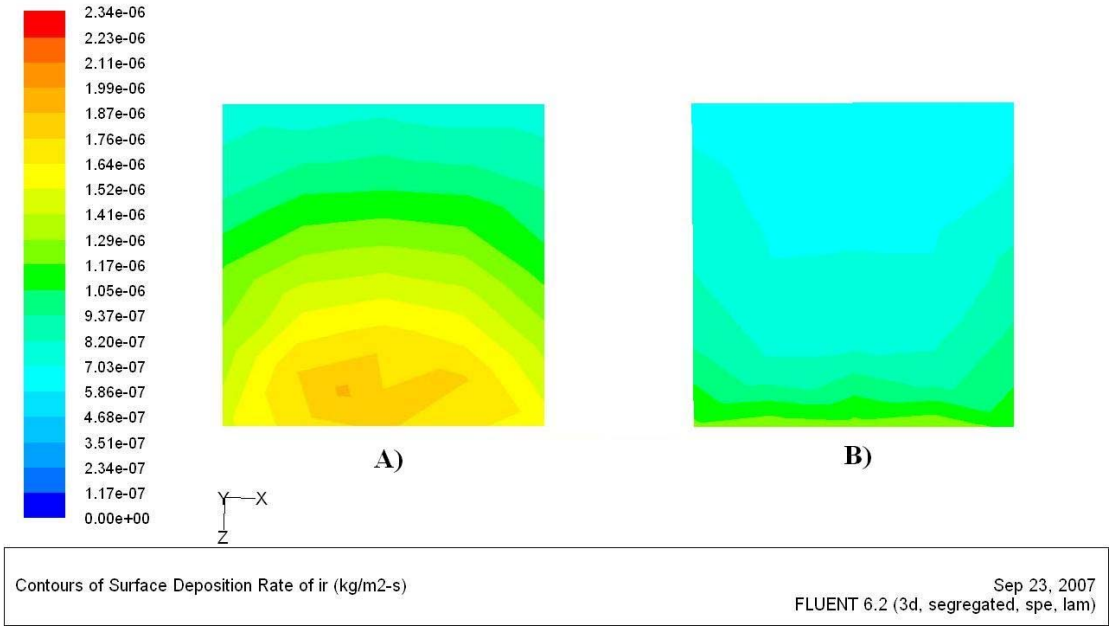

Figure 4-32 Contours of surface deposition rate; A) Top of the first silicon substrate and B) Bottom of the first silicon substrate (Condition from electrode No. 40)

4.4.5 Comparison of experimental data and simulation results

In this last part devoted to the study of the results from simulation, it will be reported on the comparison of the averaged simulated values against experimental values for three different operating conditions. These data were only ones that could permit us to determine the accuracy of our model to represent phenomena undergoing in the reactor.

Figures 4-33, 4-34 and 4-35 depict the comparison of the averaged simulated values and experimental values. It could be deduced that the results of the model were good agreement with the experimental data.

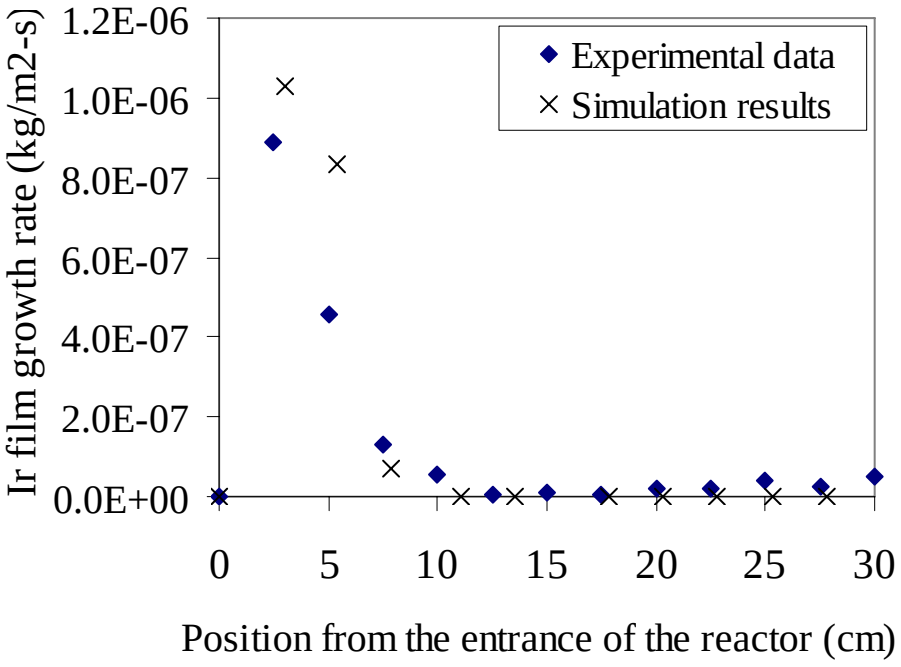

Figure 4-33 Comparison of experimental data and simulation results on Ir growth rates of electrode No. 40

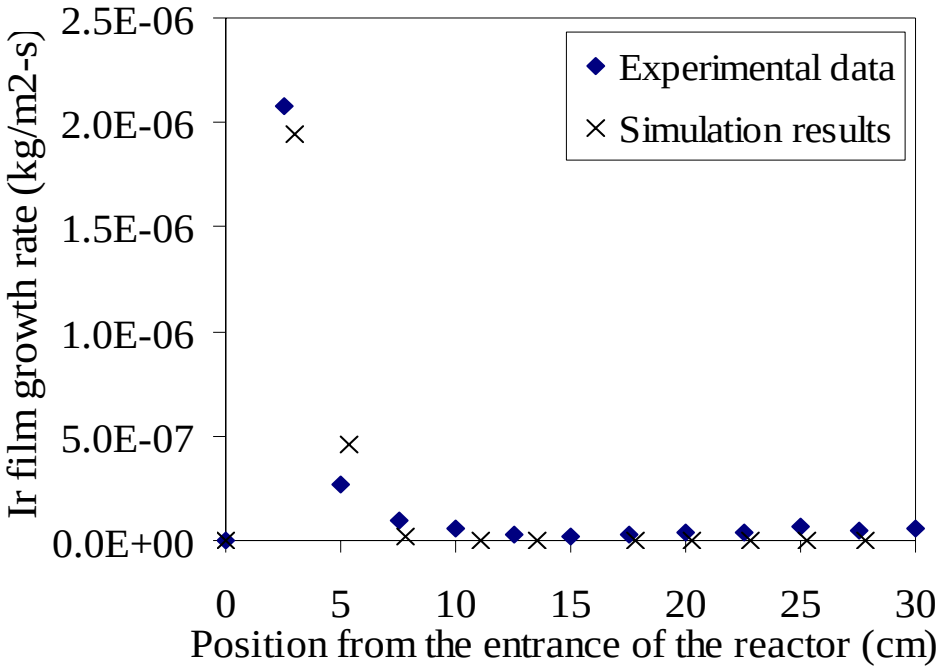

Figure 4-34 Comparison of experimental data and simulation results on Ir growth rates of electrode No. 39

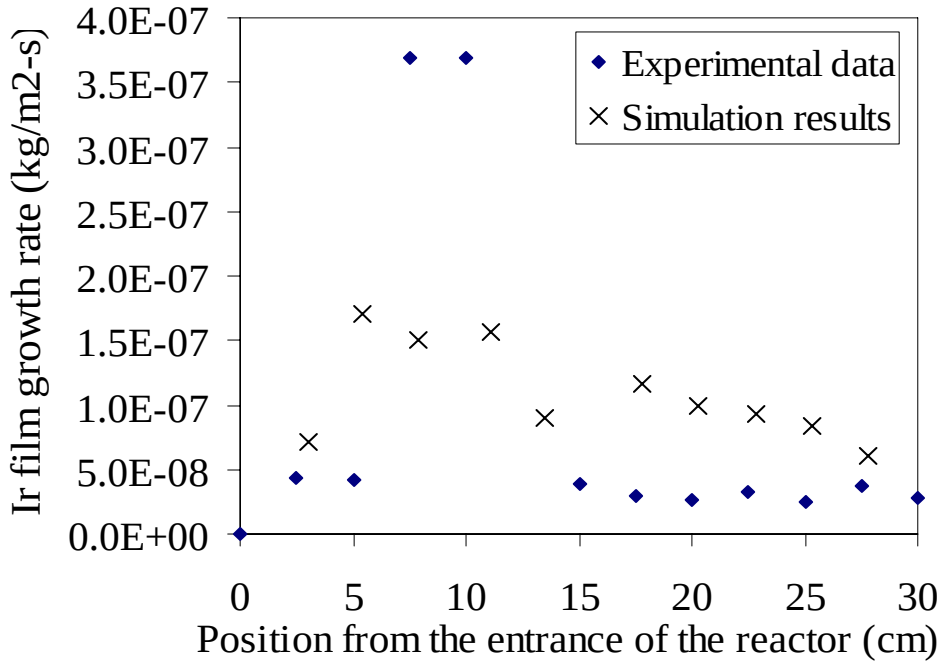

Figure 4-35 Comparison of experimental data and simulation results on Ir growth rates of electrode No. 41

From Figures 4-33, 4-34 and 4-35, two main facts could be concluded. In conditions of temperature higher that 300°C, the results of the simulations were well fit to the experimental data. While at condition of temperature of 300 °C, it appears that this agreement is less convergence. Nevertheless, when consider results, it appeared two phenomena. The first one was that for silicon substrates, the simulation results were higher that those experimentally measured. While for substrate and substrate holder, the experimental data was higher than the simulation results. It could be concluded that the nature of the substrate has an important effect for the iridium deposition. However, the substrate effect or surface chemistry of each material using as substrate have not been added into the simulation. Actually, it could be attributed to an increase of the reactivity of the (MeCp)Ir(COD) with titanium substrate or to an increase of the real surface area due to its higher surface roughness. This fact was not observed for previous results due to the operating conditions investigated, the (MeCp)Ir(COD) was fully consumed before reaching titanium substrate. It should be concluded that the model has been performed is useful for deposition simulation on silicon substrate. While, for titanium or stainless steel substrate the conclusion must be improved and further experiments must be performed to conclude of the accuracy of the model.

Nevertheless, it appears that the CFD modelling could be a convenient tool to better understand phenomena in CVD reactor. It could also be used to optimize easily operating conditions and be powerful tool for the design of new reactor or scale up operation.

4.5 Conclusions

The O_2/Ir(acac)$_3$ molar ratio was affected on the micro structure of IrO_2. The microstructure changed from dense film to columnar orientated film when the O_2/Ir(acac)$_3$ molar ratio increased from 11,000 to 17,000. While the deposition temperature and O_2/(MeCp)Ir(COD) molar ratio strongly affected on the deposition of Ir film. At high deposition temperature and high O_2/(MeCp)Ir(COD) molar ratio, (MeCp)Ir(COD) was consumed immediately. The Ir film growed more homogeneously at 300 °C and O_2/(MeCp)Ir(COD) of 125. While the SnO_2 film was grown uniformly at 380 °C, 15 Torr and O_2/TET of 1,200. In addition, the FLUENT® simulation results were agreed with the experimental data for Ir coating simulation.

Chapter 5

Electrochemical Oxidation

This chapter will be focused on the activation process needed before using the new electrodes. The results of electrochemical oxidation and discussion about the effect of the operating conditions on the performance of this process are presented. Finally, the cost analysis for restaurant wastewater treatment is presented.

5.1 Activation of new electrodes

In theoretical assumption, the stoichiometric ratio between tin and oxygen is 1:2 in SnO_2. However, the non-stoichiometry of SnO_2 is presented in as prepared SnO_2 film. This initial involves a larger concentration of catalytically actives sites. The reaction takes place with the formation of adsorbed hydroxyl radicals ($^{\bullet}OH$) as presented in equation (5-1).

$$SnO_{(2-X)} + H_2O \rightarrow SnO_{(2-X)}(^{\bullet}OH) + H^+ + e^- \quad (5\text{-}1)$$

A further oxidation may take place with an increase in oxygen stoichiometry. However, at this stage the oxygen stoichiometry is still below 2, as presented in equation (5-2)

$$SnO_{(2-X)}(^{\bullet}OH)_Y \rightarrow SnO_{(2-X+Y)} + yH^+ + ye^- \quad (5\text{-}2)$$

From the decomposition of the species $SnO_{(2-x+y)}$, oxygen can be evolved with the regeneration of $SnO_{(2-x)}$ as presented in equation (5-3).

$$SnO_{(2-X+Y)} \rightarrow SnO_{(2-X)} + \frac{1}{2}yO_2 \quad (5\text{-}3)$$

Under anodic polarization between hydrogen and oxygen evolution reaction, reconstruction of the film surface occurs with loss of defectivity. The oxygen evolution reaction could be presented in equation (5-4)

$$SnO_2(^{\bullet}OH) \xrightarrow{k_o} SnO_2 + \frac{1}{2}O_2 + H^+ + e^- \quad (5\text{-}4)$$

The anodic precondition could play the role of the progressive of the y value towards x.

Figure 5-1 represents the activation of SnO_2/Ir/Ti electrode with the applied current of 38.4 mA (current density 10 mA/cm^2). The potential was increased with the activation time of 0-430 min to the maximum potential due to the oxygen transfer from adsorbed hydroxyl to lattice for improving oxygen stoichiometry as equation (5-2). After the activation completed, the electrode was ready to work at the constant potential.

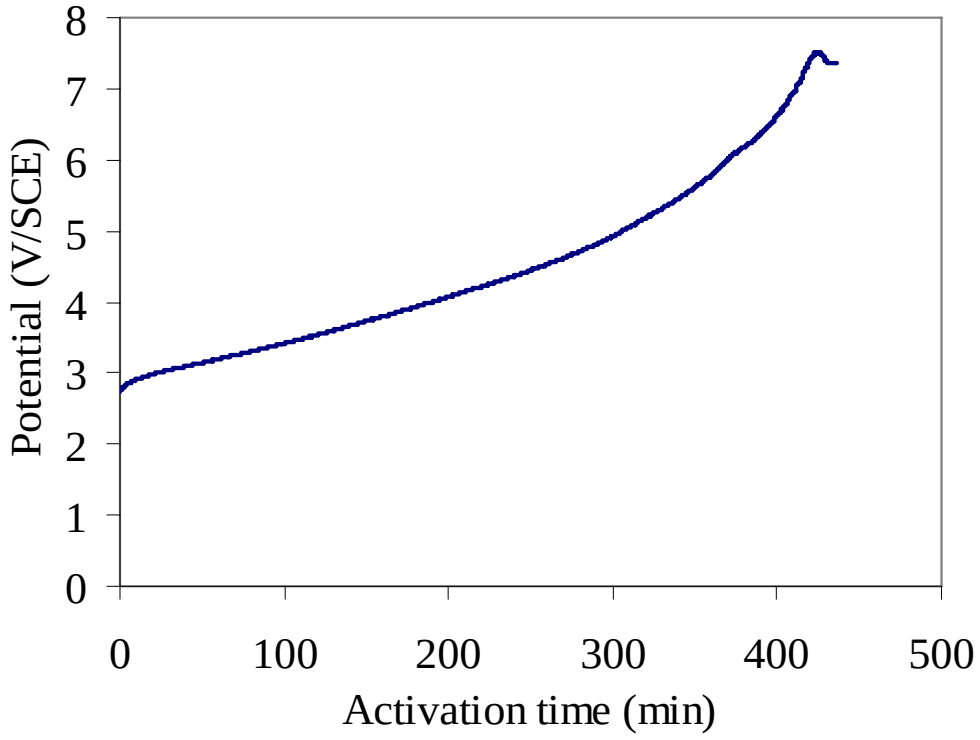

Figure 5-1 Activation of SnO_2/Ir/Ti electrode, current density of 10 mA/cm^2 (Electrode No. 44)

Figure 5-2 represents the evolution of the potential of the anode during the activation of SnO_2/TaC/Ta. The potential oscillations were observed. That could be explained by the modification of electrode surface during the transfer of oxygen to the lattice increased the internal stress of oxidized layer. Furthermore, the adhesion between SnO_2 layer and TaC was damaged by the free carbon that remained on TaC surface. Figure 5-3 presents the SnO_2/TaC/Ta after activation, the passivating SnO_2 layer was observed.

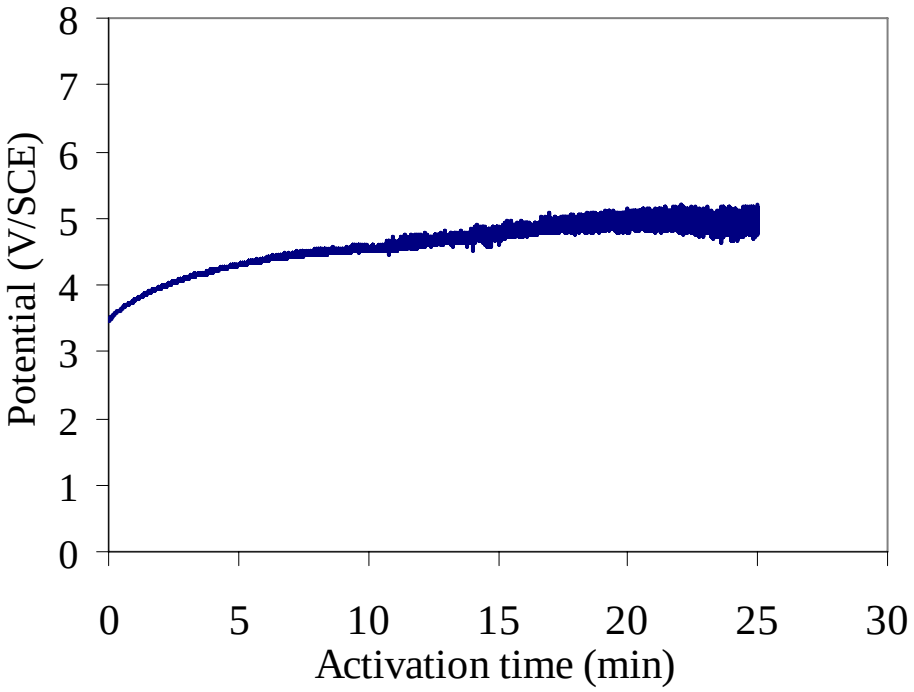

Figure 5-2 Activation of SnO_2/TaC/Ta electrode at current density of 10 mA/cm^2 (Electrode No. 30)

Figure 5-3 SnO_2/TaC/Ta after chronopotentiometrical activation at current density of 10 mA/cm^2 (Electrode No. 30)

5.2 Application of SnO_2/Ir/Ti specific electrodes in batch process with model solution

It is well known that SnO_2 electrode is powerful for organic pollutant destruction by anodic oxidation [3, 15-17, 41]. Figure 5-4 represents the destruction of oxalic acid by specific SnO_2/Ir/Ti electrode with 2 different SnO_2 film thicknesses.

The two regions of organic pollutant degradation can be defined. In first region ($t \leq 2$ hr), the TOC of model solution decreased immediately, but in the second region ($t > 2$ hr), the TOC of model solution decreased slightly. It could be explained that the reaction mechanism was changed after the first 2 hr due to the decreasing TOC concentration in model solution. The detail of reaction mechanism will be explained in the section of kinetic investigation.

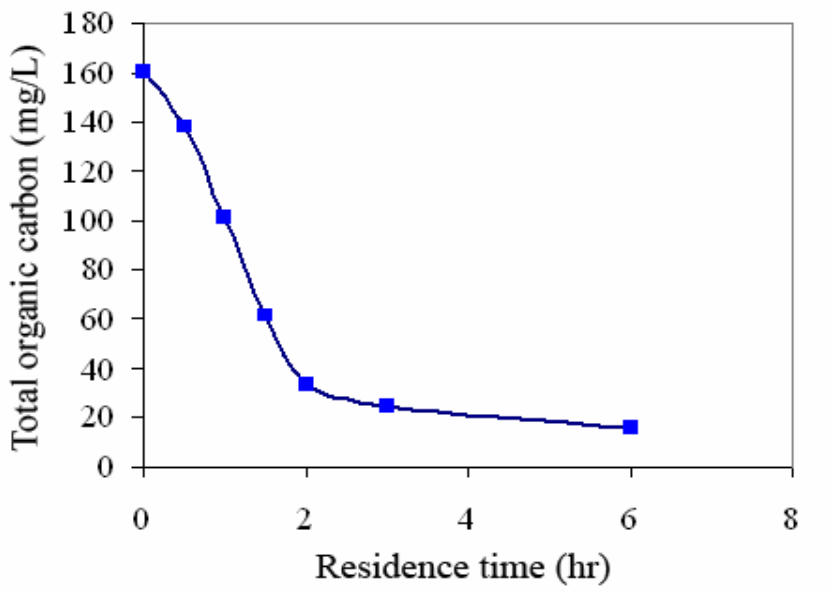

Figure 5-4 Evolution of the TOC concentration of an oxalic acid model solution obtained for electrode No. 52; electrode surface area of 3.2 cm^2 and current density of 5 mA/cm^2

5.2.1 Influence of SnO_2 active film thickness

Figures 5-5 and 5-6 represent the effect of SnO_2 film thickness on the pollutant degradation performance. The results presented that the SnO_2 thickness does not have the great effect on the oxalic acid destruction. It may be caused by the production of adsorbed hydroxyl radicals which was occurred only at the surface of electrode. Nevertheless, at more than 2 hr, the thickness 1.8 micron presented the slight higher removal efficiency. It should be explained that thickness of 3.6 micron has bigger grain size and lead to a less surface area therefore the reaction kinetic was slightly decreased. However, Duverneuil et al. [41] proposed that the optimum SnO_2 thickness is 2-5 micron because microcracks have been observed for thicker SnO_2 film thickness due to the thermal stress in SnO_2 film during the deposition process.

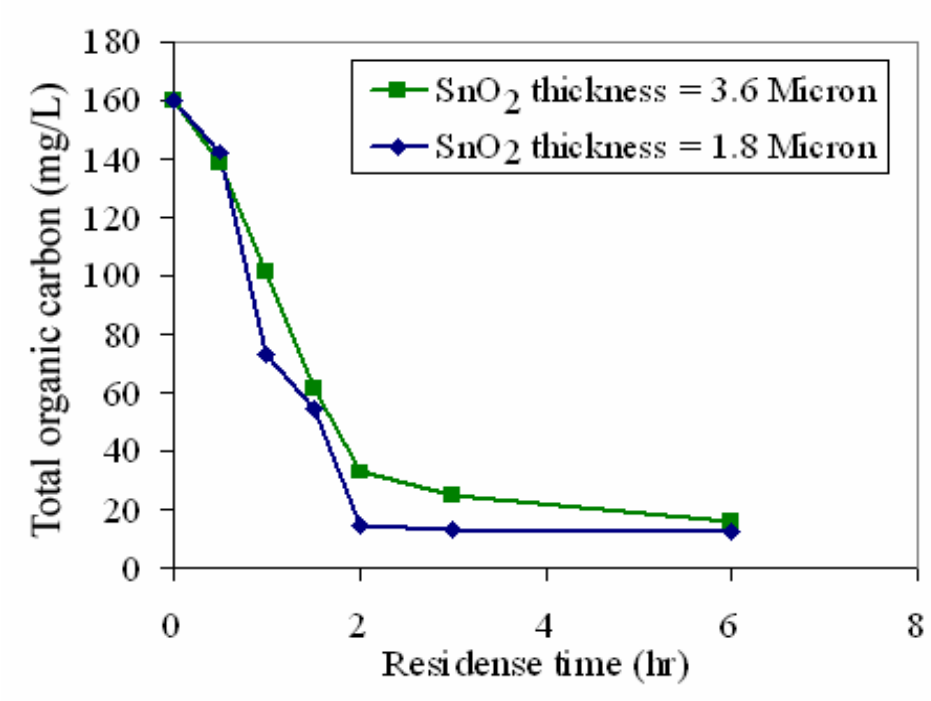

Figure 5-5 Effect of SnO_2 layer thickness on TOC removal by using of SnO_2/Ir/Ti, electrode surface area of 3.2 cm^2 and current density of 5 mA/cm^2 obtained on electrode No. 52 (3.6 micron) and electrode No. 59 (1.8 micron)

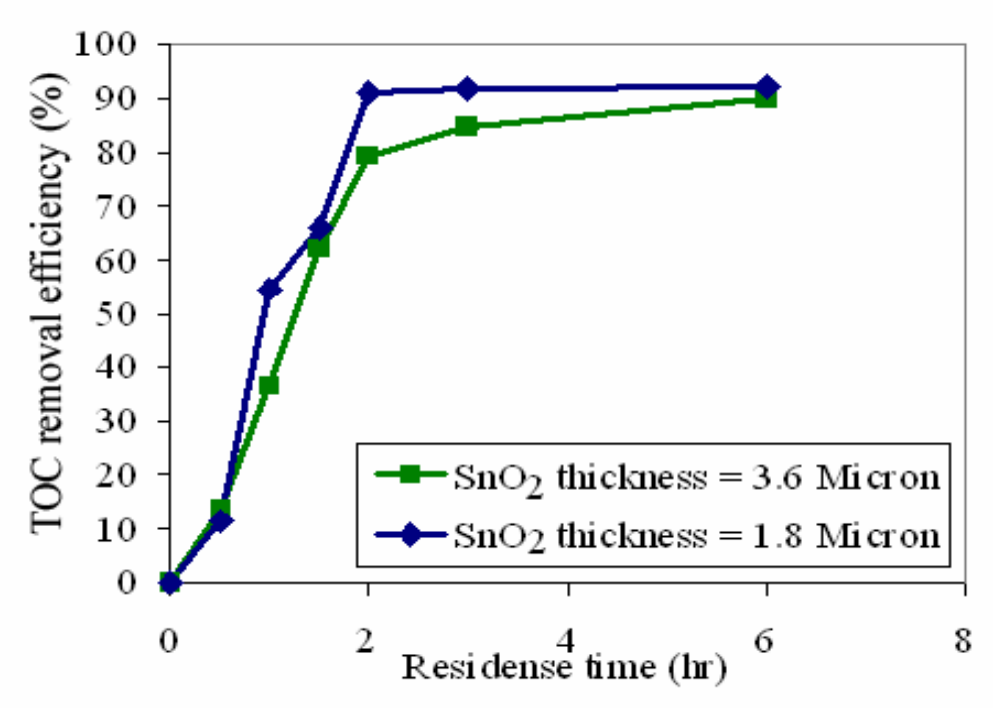

Figure 5-6 Effect of SnO_2 layer thickness on TOC removal efficiency by using of SnO_2/Ir/Ti, electrode surface area of 3.2 cm^2 and current density of 5 mA/cm^2

5.2.2 Kinetic investigation

Regarding the kinetics of TOC degradation by using oxalic acid as model solution with 160.4 mg/L initial TOC concentration, it was found that the kinetic of TOC degradation occurs as a two-kinetic process. Firstly, when the solution contains the high TOC concentration, the kinetic was the zero-order with respect to TOC of the model solution with kinetic limitation. The other one, at low TOC concentration, the kinetic was the first-order with respect to TOC concentration in the model solution with the mass transfer limitation.

At t ≤ 2 hr, the kinetics of TOC degradation was the zero-order reaction. The TOC concentration profile of the model solution was presented in Figure 5-7 and expressed by

$$TOC_t = TOC_i - k_O t \quad (5\text{-}1)$$

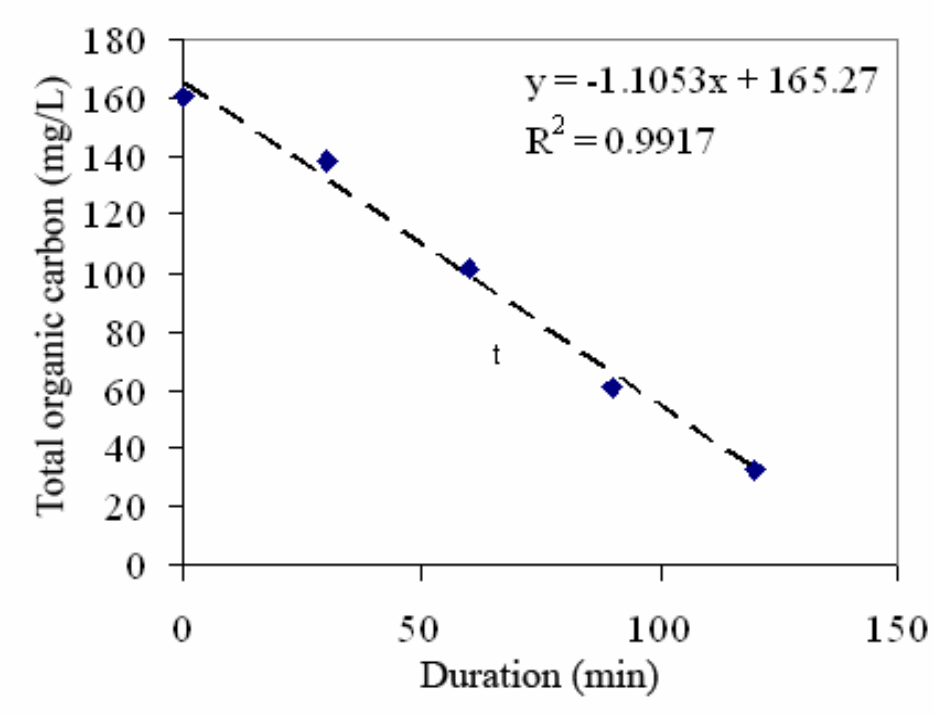

Figure 5-7 TOC concentration profile of model solution when t ≤ 2 hr by using of SnO_2/Ir/Ti, SnO_2 thickness of 1.8 micron, electrode surface area of 3.2 cm^2 and current density of 5 mA/cm^2

At t > 2 hr, the kinetics of TOC degradation was the first-order reaction. The TOC concentration profile of the model solution was presented in Figure 5-8 and expressed by

$$TOC_t = TOC_{t^*} \exp\left[-k_1(t - t^*)\right] \quad (5\text{-}2)$$

Where

TOC_i	initial TOC concentration of model solution (mg/L)
TOC_t	TOC concentration of model solution at time t (mg/L)
TOC_{t^*}	TOC concentration of model solution at transitional time t* (mg/L)
t	residence time (min)
t^*	transitional time (min), in this case was 120 min
k_0	rate constant for the zero-order reaction (mg/L·min)
k_1	rate constant for first-order reaction (min^{-1})

In this case, we found that the average k_0 = 1.1855 mg/(L·min) and k_1 = 0.0017 min^{-1}.

Figure 5-9 presents the comparison of experimental data and developed kinetic model. The developed kinetic model shows the good fit with the experimental data.

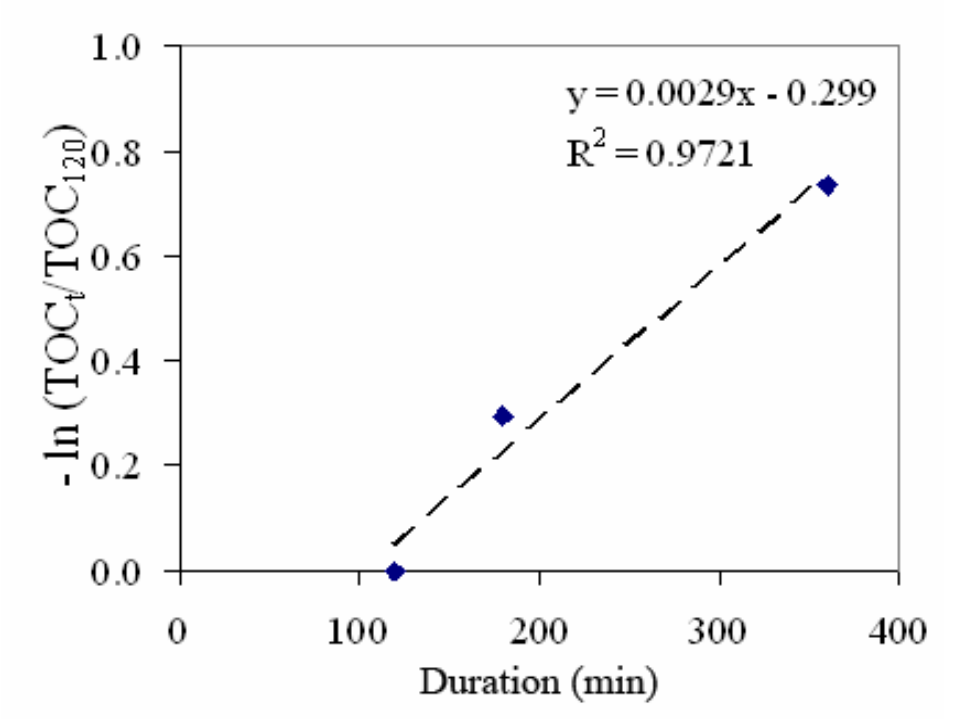

Figure 5-8 TOC concentration profile of model solution when t > 2 hr by using of SnO_2/Ir/Ti, SnO_2 thickness of 1.8 micron, electrode surface area of 3.2 cm^2 and current density of 5 mA/cm^2

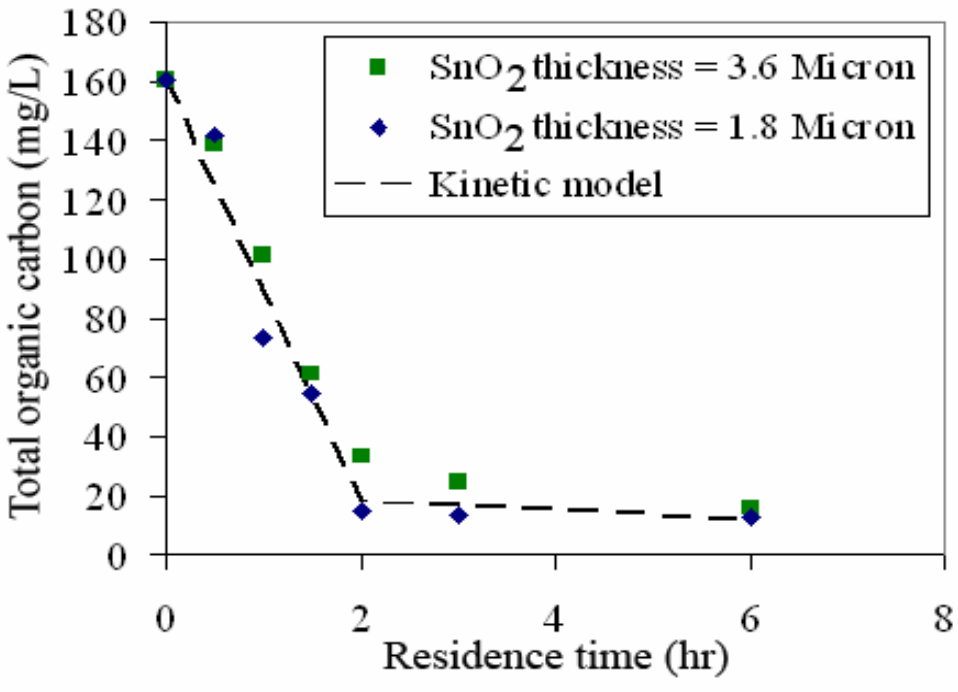

Figure 5-9 Comparison of experimental data and kinetic model (data from Figure 5-5)

5.2.3 Influence of current density

Figure 5-10 shows the influence of current density. Increasing current density from 5 to 10 mA/cm^2, leads to less degradation rate of oxalic acid by electrochemical oxidation. When the effect of charge loading to the system was considered in Figure 5-11, the system of 10 mA/cm^2 presented the higher charge required for destruction the same amount of oxalic acid.

In such system, the increasing of current density does not increase the pollutant removal efficiency at the electrode, but increases the side reaction of oxygen evolution at the anode. The oxygen bubbles perturb the discharge of the hydroxyl radicals and the pollutant removal at the electrode. As the life time of hydroxyl radicals is very short, it depart out in very thin diffusion layer to react with the organic pollutant.

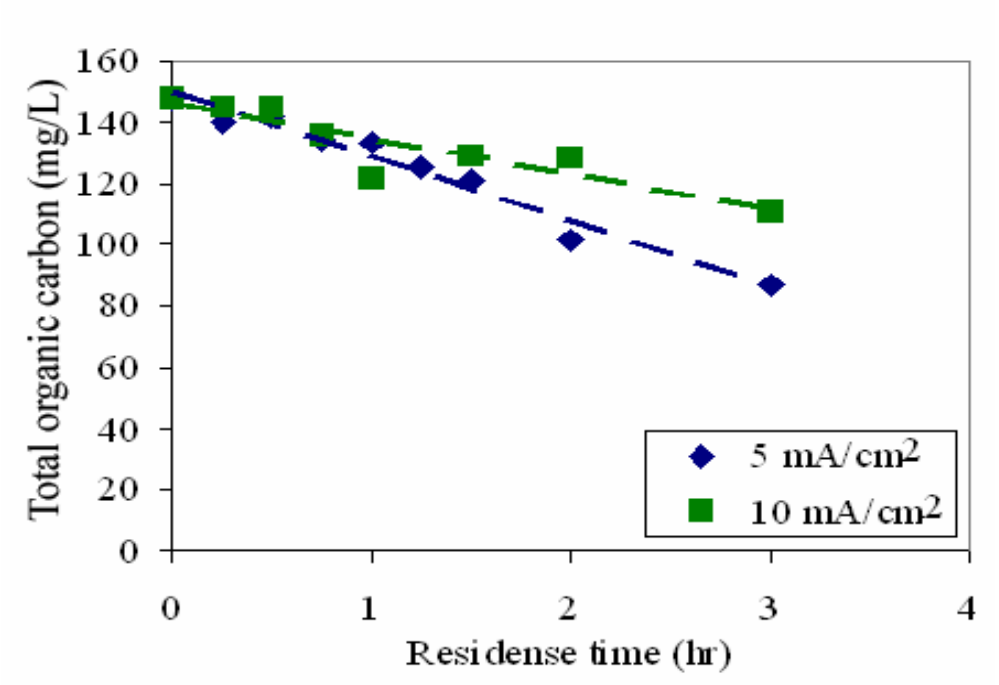

Figure 5-10 Effect of current density on TOC removal by using of SnO_2/Ir/Ti, SnO_2 thickness of 2.9 micron and electrode surface area of 3.2 cm^2 obtained by electrode No. 55

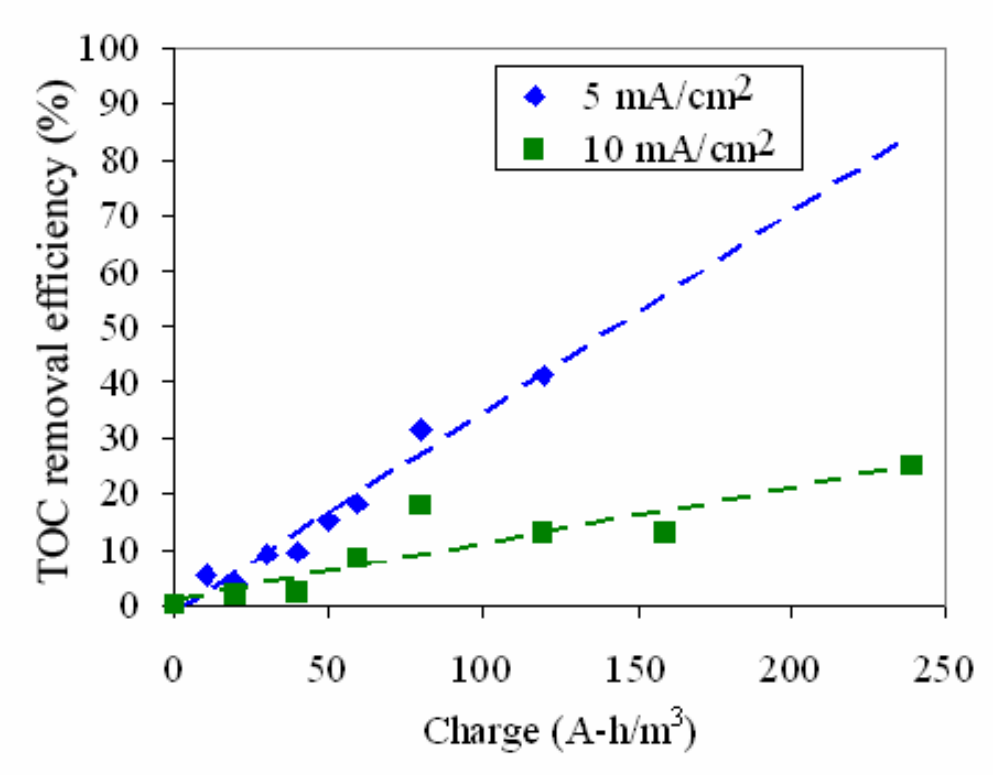

Figure 5-11 Effect of charge loading to the system on TOC removal by using of SnO_2/Ir/Ti, SnO_2 thickness of 2.9 micron and electrode surface area of 3.2 cm^2 obtained by electrode No. 55

Although, Ta and TaC/Ta substrates have some attractive properties to be used as substrate for specific SnO_2 electrode, but Ta substrate was brittle and lose some physical properties after etched by HF. In case of SnO_2/TaC/Ta, the passivation of SnO_2 film was observed after a few minutes in electrochemical characterization that affected by some free carbon between SnO_2 film and TaC surface.

5.3 Application of SnO_2/Ir/Ti specific electrodes for actual restaurant wastewater

The experiments in a continuous mixed flow reactor were carried out for the determination of the effects of the current density, residence time and SnO_2 film thickness on organic pollutant degradation. Due to the very small electrode area and easy to observe the change of TOC, the wastewater, which feed to the system, was diluted to around 140 mg TOC/L. The investigated current densities were 5 and 10 mA/cm^2 and residence times were 2 and 3 hr.

5.3.1 Influence of current density

The influence of current density in continuous mixed flow experiments is presented in Figure 5-12. The electrochemical degradation of organic pollutants presented in actual restaurant wastewater takes place slowly and its TOC removal efficiency presented in Figure 5-13 is higher at lower current density. The gain in efficiency being overwhelmed by the lower current values applied. This result may not be surprising on the basis of the previously discussed influence of current density in batch experiments, which indicated to a weak behavior for the characteristic of diffusion-controlled processes. Increase in current density cannot increase the organic removal efficiency at the electrode, but only favours the anodic side reaction which decreased the organic pollutant removal efficiency. It agrees with Figures 5-14 and 5-15 that the destruction of organic pollutants in term of COD was decreased with increasing of the current density from 5 to 10 mA/cm^2.

The equilibrium efficiencies of both TOC and COD removal were 62% when current density was 5 mA/cm^2. While their removal efficiencies were 47% when the current density was 10 mA/cm^2.

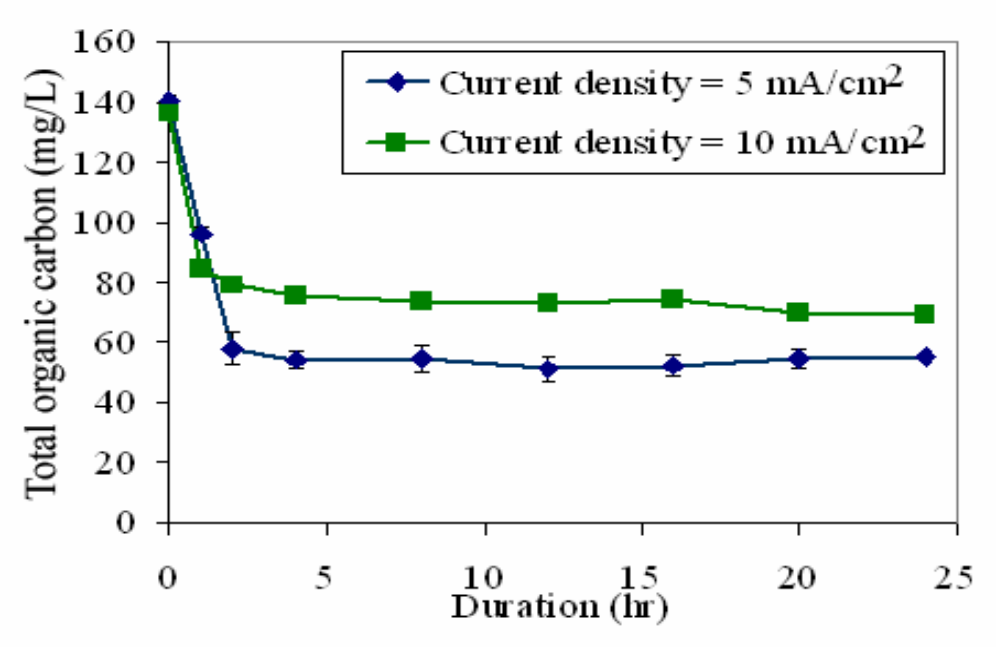

Figure 5-12 Effect of current density on TOC removal in continuous restaurant wastewater treatment by using of SnO_2/Ir/Ti, SnO_2 thickness of 1.8 micron (Electrode No. 59)

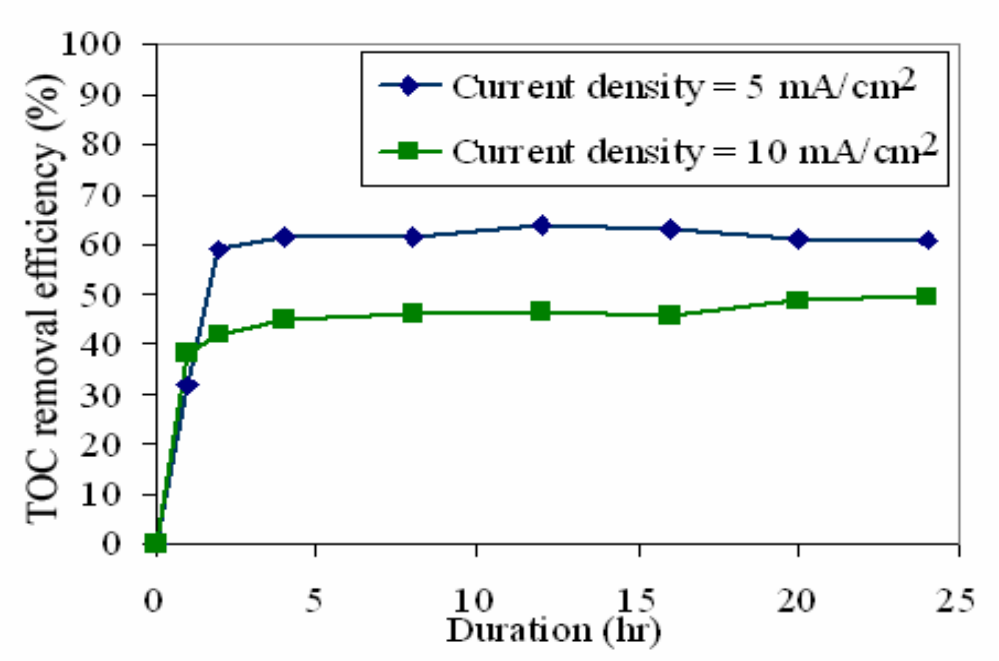

Figure 5-13 Effect of current density on TOC removal efficiency in continuous restaurant wastewater treatment by using of SnO_2/Ir/Ti, SnO_2 thickness of 1.8 micron (Electrode No. 59)

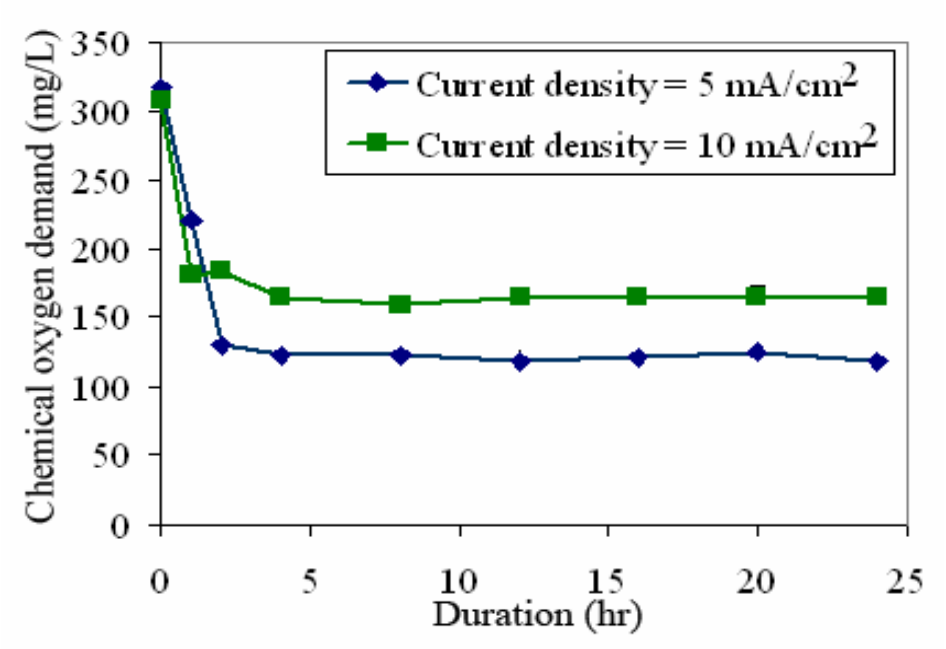

Figure 5-14 Effect of current density on COD removal in continuous restaurant wastewater treatment by using of SnO_2/Ir/Ti, SnO_2 thickness of 1.8 micron (Electrode No. 59)

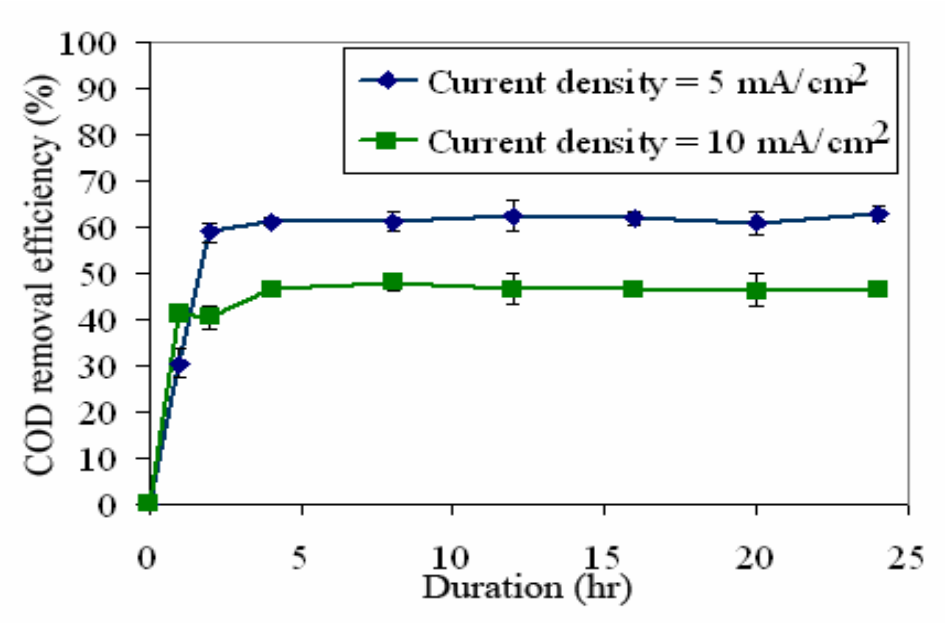

Figure 5-15 Effect of current density on COD removal efficiency in continuous restaurant wastewater treatment by using of SnO_2/Ir/Ti, SnO_2 thickness of 1.8 micron (Electrode No. 59)

5.3.2 Influence of residence time

Although the results in batch experiments represented that the increasing of residence time after first 2 hr was not greatly affect on the organic pollutant degradation efficiency due to the change reaction order from zero-order to first-order reaction with reduction of TOC. However, it would be practical interest to test how much an increase or decrease in the wastewater flow rate affects the TOC removal of the restaurant wastewater. This is demonstrated in Figures 5-16 to 5-19. Because of fixed total volume of the continuous mixed flow reactor at 18 ml, an increase in the wastewater flow rate from 0.10 to 0.15 ml/min translates to a proportional decrease in the wastewater hydraulic residence time from 3 to 2 hr.

Normally, a reduction in residence time would expectedly lead to a decrease in the wastewater TOC removal. But, in this case, increasing of residence time does not proportionally increase TOC removal. As seen in Figures 5-16 and 5-17, the TOC removal increases from around 55 to 62 % with the increase in the residence time from 2 to 3 hr. These results were also observed in the removal of COD and represented in Figures 5-18 and 5-19. The COD removal increased from around 54 to 62 % with the increase in residence time from 2 to 3 hr.

It could be explained by the increasing of residence time from 2 to 3 hr has not strongly affected on the TOC and COD removal due to the fast reaction with zero-order reaction occurred in the first 2 hr. Then, the reaction was changed to the slower step with the first-order reaction as we found in the batch experiments.

Hence, it would be more economical to operate the electrochemical treatment at a lower residence time as long as the pollutant concentration of the treated wastewater meets the safe discharge requirement.

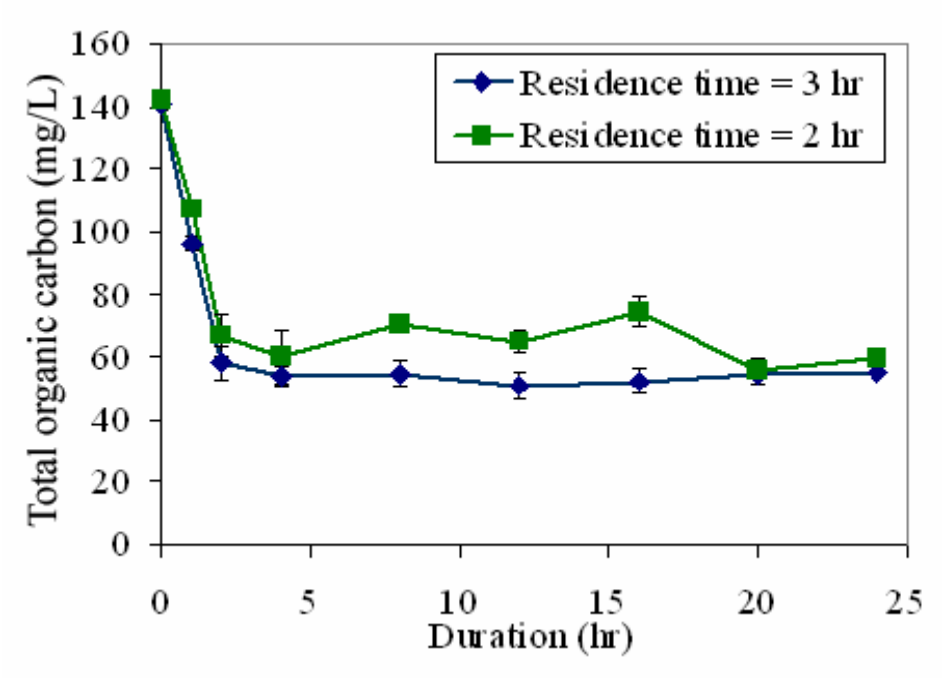

Figure 5-16 Effect of residence time on TOC removal in continuous restaurant wastewater treatment by using of SnO_2/Ir/Ti, SnO_2 thickness of 1.8 micron and current density 5 mA/cm^2 (Electrode No. 59)

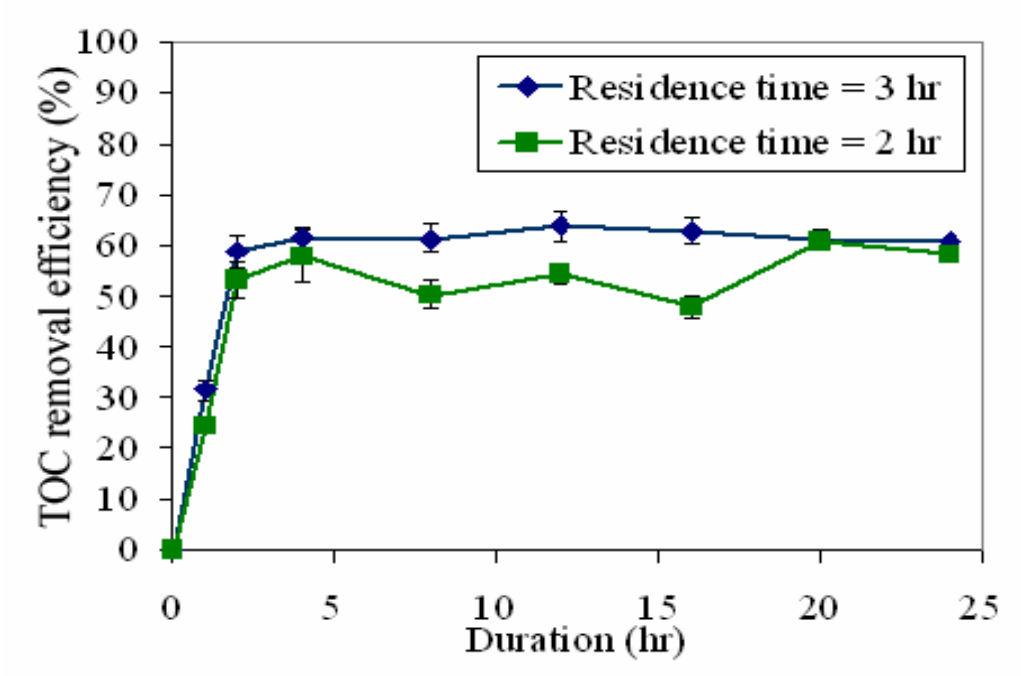

Figure 5-17 Effect of residence time on TOC removal efficiency in continuous restaurant wastewater treatment by using of SnO_2/Ir/Ti, SnO_2 thickness of 1.8 micron and current density 5 mA/cm^2 (Electrode No. 59)

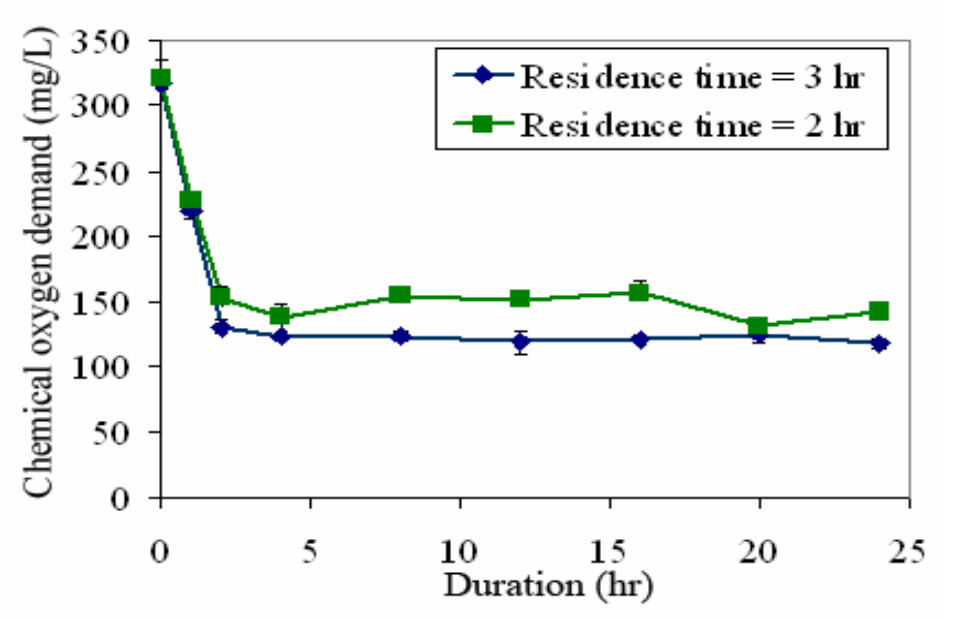

Figure 5-18 Effect of residence time on COD removal in continuous restaurant wastewater treatment by using of SnO_2/Ir/Ti, SnO_2 thickness of 1.8 micron, current density of 5 mA/cm^2 (Electrode No. 59)

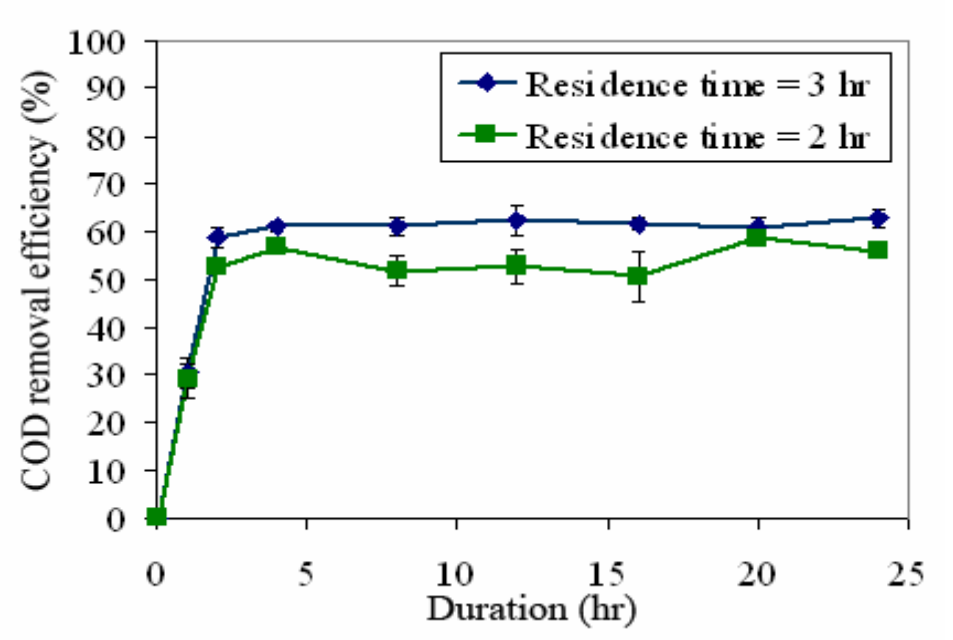

Figure 5-19 Effect of residence time on COD removal efficiency in continuous restaurant wastewater treatment by using of SnO_2/Ir/Ti, SnO_2 thickness of 1.8 micron and current density of 5 mA/cm^2 (Electrode No. 59)

5.3.3 Influence of SnO_2 active layer thickness

Figures 5-20 and 5-21 represent the effect of SnO_2 film thickness on the TOC degradation performance in continuous electrochemical oxidation. Similar to the pollutant degradation of organic pollutant in batch experiment, it shows that the SnO_2 active layer thickness was not a great influence on the TOC removal efficiency because the adsorbed hydroxyl radicals for organic pollutant degradation were produced only at the surface of electrode. However, the TOC removal efficiency was around 62% with the 1.8 micron of SnO_2 active layer while the efficiency was reduced to 51% with the SnO_2 active layer thickness of 3.6 micron. It agrees with the removal of COD from restaurant wastewater as presented in Figures 5-22 and 5-23. The COD removal efficiency was 62% when the thickness of SnO_2 active layer was 1.8 micron. However, the efficiency was decreased to 50% when the thickness of SnO_2 active layer was 3.6 micron. It should be explained that thickness of 3.6 micron has bigger grain size that leads to a less surface area; therefore, the reaction kinetic was decreased as found previously in the batch experiment.

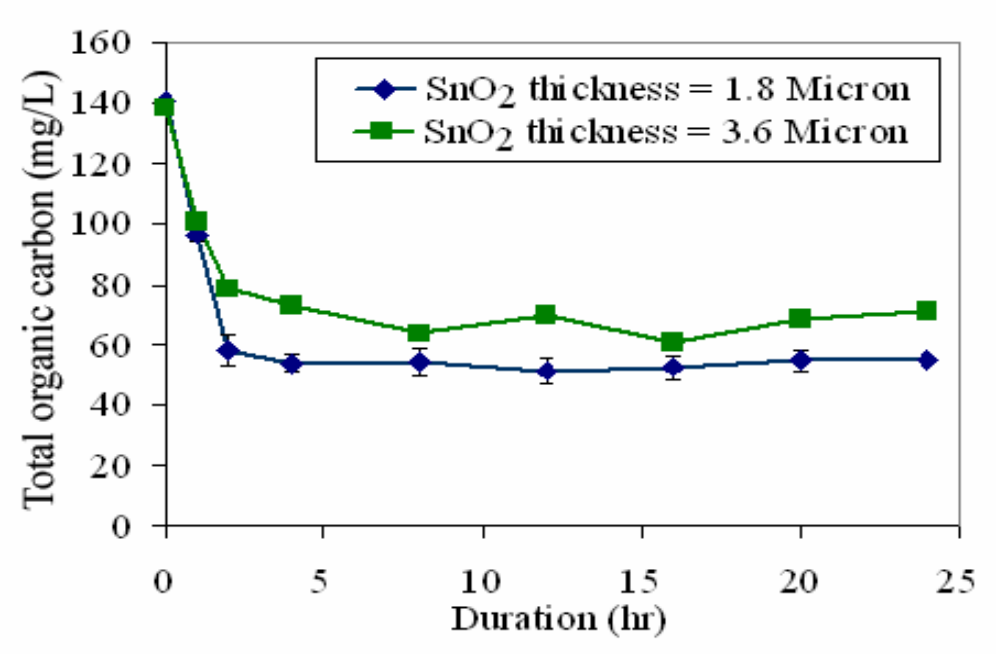

Figure 5-20 Effect of SnO_2 layer thickness on TOC removal in continuous restaurant wastewater treatment by using of SnO_2/Ir/Ti and current density of 5 mA/cm^2

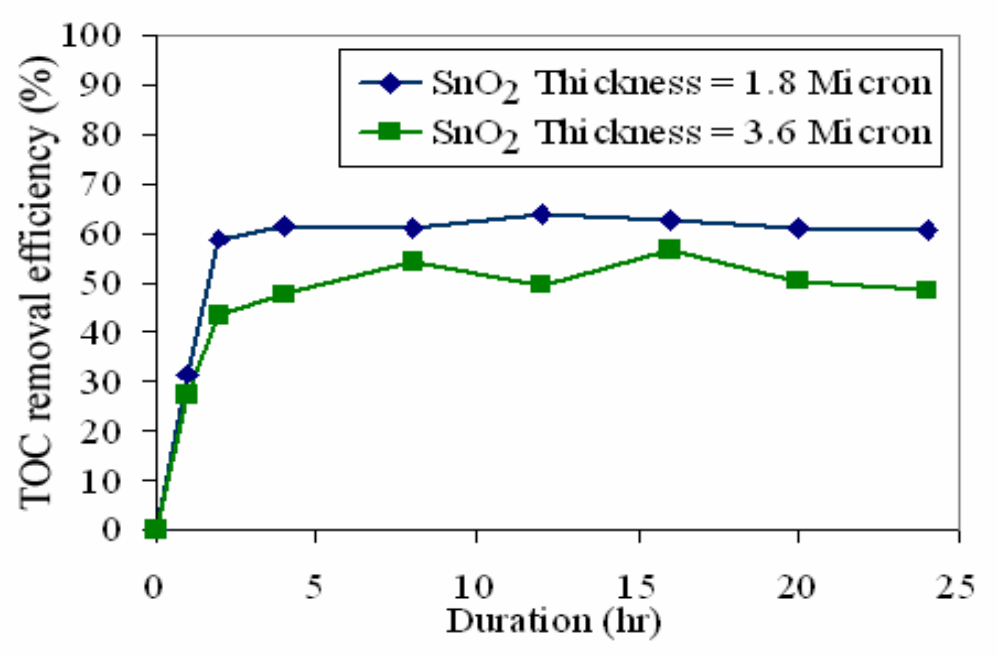

Figure 5-21 Effect of SnO_2 layer thickness on TOC removal efficiency in continuous restaurant wastewater treatment by using of SnO_2/Ir/Ti and current density of 5 mA/cm^2

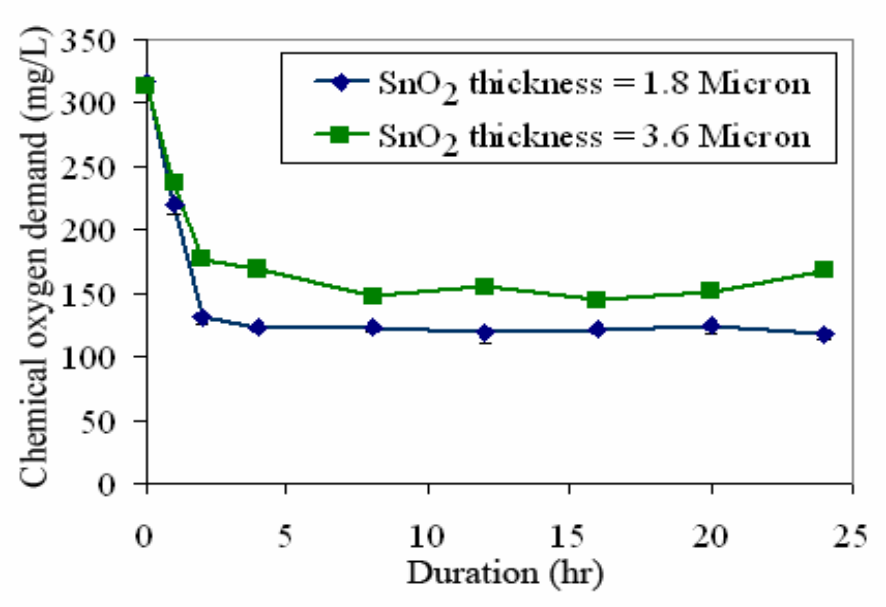

Figure 5-22 Effect of SnO_2 layer thickness on COD removal in continuous restaurant wastewater treatment by using of SnO_2/Ir/Ti and current density 5 mA/cm^2

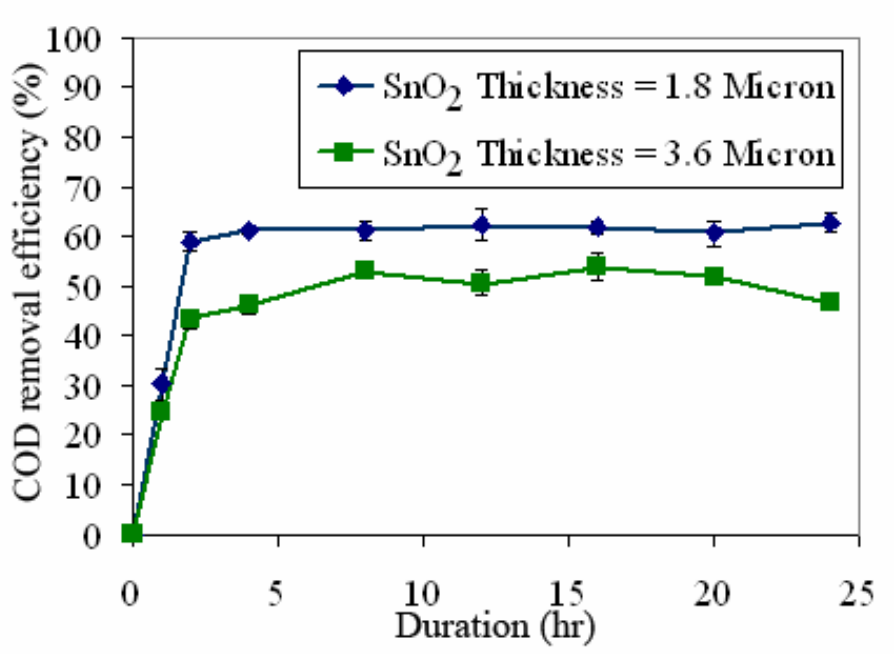

Figure 5-23 Effect of SnO_2 layer thickness on COD removal efficiency in continuous restaurant wastewater treatment by using of SnO_2/Ir/Ti and current density of 5 mA/cm^2

5.4 Treatment cost analysis of restaurant wastewater treatment by electrochemical oxidation

The cost analysis of restaurant wastewater treatment by electrochemical oxidation is presented in Tables 5-1, 5-2 and 5-3. The operating cost was calculated and based on the adjustment of operating parameters.

Table 5-1 represents the cost comparison of restaurant wastewater treatment with two current densities that were applied to wastewater treatment system. It was found that increasing current density from 5 to 10 mA/cm^3 decreases TOC and COD removal efficiency of the system because the increase of cell voltage which causes the anodic side reaction. Furthermore, the increase of cell voltage leads to the power requirement of the system. Consequently, the operating costs of restaurant wastewater treatment are 109 and 303 $baht/m^3$ when the current densities are 5 and 10 mA/cm^3, respectively.

Table 5-2 presents the operating cost with a variation of residence time. The TOC and COD removal efficiency with the residence time of 3 hr was 62% and the efficiency was 55% with residence time of 2 hr. However, the operating costs were 66 and 109 $baht/m^3$ when the residence times were 2 and 3 hr, respectively.

Table 5-3 presents the effect of the thickness of SnO_2 active layer on operating cost. It shows that the thickness of SnO_2 active layer has no effect on the operating cost. However, increasing twice SnO_2 thickness may increase the investment cost of electrode.

This study was based on a small reactor of 18 ml. and dilution of wastewater by deionized water causing the higher cell voltage and higher

electrical power consumption. With the small laboratory scale and dilution therefore the treatment cost per unit volume of solution may be excessively high. The actual cost of treatment in the large-sized system should be reasonably reduced per unit volume.

5.5 Conclusions

From the study of organic pollutant destruction by electrochemical oxidation in both batch and continuous processes, it should be concluded that the SnO_2 film thickness slightly affected on the organic pollutant removal efficiency. While the increase of current density had favored the side reaction that resulted on decrease of the pollutant removal efficiency. Finally, the increase of residence time leads to the increase of treatment efficiency.

Table 5-1 Effect of current density on restaurant wastewater treatment cost by electrochemical oxidation

SnO_2 Thickness (Micron)	Current density (mA/cm^2)	Applied current (A)	Cell voltage (V)	Flow rate (ml/min)	Residence time (hr)	Power required (kW-hr/m^3)	Operating cost (Baht/m^3)	TOC removal efficiency (%)	COD removal efficiency (%)
1.8	5	0.016	16.3	0.10	3	43.5	109	62	62
1.8	10	0.032	22.7	0.10	3	121.1	303	47	47

Table 5-2 Effect of residence time on restaurant wastewater treatment cost by electrochemical oxidation

SnO_2 Thickness (Micron)	Current density (mA/cm^2)	Applied current (A)	Cell voltage (V)	Flow rate (ml/min)	Residence time (hr)	Power required (kW-hr/m^3)	Operating cost (Baht/m^3)	TOC removal efficiency (%)	COD removal efficiency (%)
1.8	5	0.016	14.9	0.15	2	26.5	66	55	54
1.8	5	0.016	16.3	0.10	3	43.5	109	62	62

Table 5-3 Effect of SnO_2 thickness on restaurant wastewater treatment cost by electrochemical oxidation

SnO_2 Thickness (Micron)	Current density (mA/cm^2)	Applied current (A)	Cell voltage (V)	Flow rate (ml/min)	Residence time (hr)	Power required ($kW\text{-}hr/m^3$)	Operating cost ($Baht/m^3$)	TOC removal efficiency (%)	COD removal efficiency (%)
1.8	5	0.016	16.3	0.10	3	43.5	109	62	62
3.6	5	0.016	16.8	0.10	3	44.8	112	51	50

Chapter 6

General Conclusion

6.1 Electrodes elaboration

6.1.1 Protective underlayers elaboration

It was found that the IrO_2 film growth rate was affected by the $O_2/Ir(acac)_3$ molar ratio. With the increasing of $O_2/Ir(acac)_3$ molar ratio from 11,000 to 17,000, the maximum IrO_2 growth rate was decreased from 2.9 to 1.9 nm/min due to the higher Ir precursor concentration in feed vapor. Furthermore, the $O_2/Ir(acac)_3$ molar ratio affected on the microstructure of IrO_2 film. The SEM and X-ray diffraction of IrO_2 film indicated that the columnar growth of IrO_2 with (101) orientation was observed at $O_2/Ir(acac)_3$ molar ratio of 17,000, while the dense IrO_2 film with (110) orientation was observed at the molar ratio of 11,000. The IrO_2 film had homogeneous microstructure and good coverage on Si wafer. However, the gradient deposition of IrO_2 film on Ti substrate was observed because $Ir(acac)_3$ had low volatility and difficultly controlled mass transfer and also the delayed of research plan for finding the convenient operating condition for protective layer. Therefore the research was focused on the protection of substrate by the other material. From the previous results, it concludes that the IrO_2 film from $Ir(acac)_3$ is not suitable for using as protective layer for SnO_2 specific electrode.

Deposition of Ir film by using (MeCp)Ir(COD) as precursor with the presence of O_2 was investigated. It was found that the deposition of Ir film was strongly affected by deposition temperature and oxygen content in feed vapor mixture. The increasing of deposition temperature from 300 to 325 and 350 ºC has significantly affected on the Ir deposition area. The deposition area was decreased from 13 to 11 and 9.75 cm from the entrance of the reactor, respectively. The growth rate of Ir film was very high at a few centimeters nearby the entrance of the reactor, but rapidly decreased downstream because the system was very active at high deposition temperature and the (MeCp)Ir(COD) was consumed immediately in a few centimeters from the entrance. When the O_2/(MeCp)Ir(COD) molar ratio was 1545, the precursor was totally decomposed near the entrance of the reactor resulting the abrupt gradient film thickness. The maximum growth rate was approximately 4 nm/min at 10 cm from the entrance and fell down to nearly zero after a few centimeters. While the Ir film deposited uniformly over several centimeters long through the reactor when O_2/(MeCp)Ir(COD) molar ratio was 125 due to the reactivity of the system was reduced by decreasing of O_2/(MeCp)Ir(COD) molar ratio. The conditions for the suitable Ir film to be used as the protective layer for specific electrode was at 300 ºC, total pressure of 12 Torr and O_2/(MeCp)Ir(COD) molar ratio of 125.

6.1.2 Electrocatalytic layer deposition

The SnO_2 coatings were uniform and exhibited good conformal coverage. The increasing O_2/TET molar ratio from 300 to 1,200 was not greatly influence on the growth rate of SnO_2 in the first 10 cm of the reactor. However, the O_2/TET molar ratio at 300 presented the higher

growth rate of SnO_2 film after 10 cm from the entrance of the reacotr. The growth rate of SnO_2 film is a function of TET concentration in feed gas composition. The increasing of TET concentration in feed gas mixture has no influence on the microstructure of SnO_2 film. The substrate materials have not affected on SnO_2 film growth rate. However, the SnO_2 film growth rate could be improved by the substrate with high surface roughness due to its higher specific area. The SEM images show that the SnO_2 film was dense, smooth, homogeneous microstructure and uniform coverage of deposition on the high surface roughness substrate. The suitable SnO_2 active coating for using as anode organic pollutant degradation was deposited at 380 ºC, 15 Torr of total pressure and O_2/TET molar ratio of 1,200.

6.1.3 Simulation of Ir deposition using FLUENT®

The comparison of Ir deposition rate between the experimental data and the simulation results from FLUENT®. The simulation results were agreed with the experimental data at the position that was placed by Si wafer. While the difference on surface chemistry and in the high genuine surface area of Ti substrate by treating with HCl acid led to the higher Ir deposition rate in experimental data with the same geometrical dimension. However, the FLUENT® simulation is a powerful tool for the optimization of suitable operating conditions and the scaling up of the reactor.

6.2 Electrochemical oxidation

6.2.1 Application of specific electrodes in batch process with model solution

From the application of SnO_2/Ir/Ti specific electrode for oxalic acid destruction, it was found that the SnO_2 thickness does not have the great influence. It may be caused by the production of adsorbed hydroxyl radicals that was occurred only at the surface of electrode. While increasing the current density from 5 to 10 mA/cm^2 leads to less degradation rate of oxalic acid by electrochemical oxidation due to the characteristic of diffusion-controlled processes. In such system, increasing current density cannot increase the organic removal efficiency, but only favors the anodic side reaction. In case of SnO_2/Ta and SnO_2/TaC/Ta electrodes, Ta substrate was brittle and lose some physical properties after being etched by HF. While the passivation of SnO_2 layer was observed in the electrochemical activation of SnO_2/TaC/Ta due to the low cohesion between SnO_2 film and TaC surface.

6.2.2 Kinetic investigation for batch process with model solution

The kinetics of TOC degradation on SnO_2/Ir/Ti occur as a two-mechanism process. Firstly, when the solution contains the high TOC concentration, the reaction kinetic was the zero-order with respect to TOC, and the pollutant decomposition rate was controlled by the kinetic of the reaction.

$$TOC_t = TOC_i - k_O t$$

Secondly, at low TOC concentration, the kinetic was the first-order with respect to TOC concentration, and the pollutant decomposition rate was controlled by the mass transfer of pollutant to the electrode.

$$TOC_t = TOC_{t^*} \exp\left[-k_1(t - t^*)\right]$$

When transitional time, t^* = 120 min., k_0 = 1.1855 mg/L-min and k_1 = 0.0017 min^{-1}.

6.2.3 Application of specific electrodes for actual restaurant wastewater

Similar to the degradation of organic pollutants in batch process, TOC removal efficiency on SnO_2/Ir/Ti is high at 5 mA/cm^2, then decreased when increased current density to 10 mA/cm^2, which indicated the characteristic of diffusion-controlled processes. Increasing of residence time is not proportion to increase of TOC and COD removal. Around 55 to 62 % increase for TOC and 54 to 62 % increase for COD with an increase in the residence time from 2 to 3 hr due to the fast step of reaction with zero-order reaction within 2 hr. Then, the reaction was changed to the slower step with first-order reaction based on TOC concentration in wastewater. Similar to the degradation of organic pollutant in the batch experiments, it shows that the SnO_2 active layer thickness was not a great influence on the TOC removal efficiency due to the adsorbed hydroxyl radicals for organic pollutant degradation were produced only at the surface of electrode.

From these results, it should be concluded that the specific SnO_2/Ir/Ti prepared by metal-organic chemical vapor deposition can be

used for the degradation of organic pollutants presented in wastewater by electrochemical oxidation.

References

[1.] Chen, X., Chen, G. and Yue, P.L. Separation of pollutants from restaurant astewater by lectrocoagulation. Separation and Purification Technology Vol. 19 (2000): 65-76.

[2.] Grimm, J. et al. Sol-gel film preparation electrodes for the electrocatalytic oxidation of organic pollutants in water. Desalination Vol. 115 (1998): 295-302.

[3.] Comninellis, C. Electrocatalysis in the electrochemical conversion/ combustion of organic pollutants for waste water treatment. Electrochimica Acta Vol. 39 (1994): 1857-862.

[4.] Maury, F. and Senocq, F. Irirdium coatings grown by metal-organic chemical vapor deposition in a hot-wall CVD reactor. Surface & Coatings Technology Vol. 163-164 (2003): 208-213.

[5.] http://www.environmental-center.com/articles/article1149/ article1149.htm

[6.] http:www.barnstablecountryhelath.org/AlternativeWebpage/Grease/ Grease.htm

[7.] Hanze, M., Harremës, P., Jansen, J. C. and Arvin, E. Wastewater Treatment: Biological and Chemical Processes. New York: Springer, 1995.

[8.] Chen, G. Electrochemical technologies in wastewater treatment. Separation and Purification Technology Vol. 38 (2004): 11–41.

[9.] Den, W. and Huang, C. Electrocoagulation for removal of silica nano-particles from chemical–mechanical-planarization wastewater. Colloids and Surfaces A: Physicochemical Engineering Aspects Vol. 254 (2005): 81–89.

[10.] Hosny, A. Y. Separating oil from oil-water emulsions by electroflotation Technique. Separation Technology Vol. 6 (1996): 9-17.

[11.] Kuhn, A. T., Electrolytic decomposition of cyanides, phenols and thiocyanates in effluents streams-a literature review. Journal of Chemical Technology and Biotechnology Vol. 21 (1971): 29–34.

[12.] Azzam, M.O., Tahboub, Y. and Al-Tarazi, M. Effect of counter electrode material on the anodic destruction of 4-Cl phenol solution, Transactions of the Institution of Chemical Engineers Vol. B 77 (1999): 219–226.

[13.] Rosenthal, K.I. and Veselovkii, V.I. Doklady Akademii Nauk SSR Vol. 111 (1956): 637.

[14.] Eley, D.D., Pines, H. and Weisz, P.B. Advance in Catalysis Vol. 38 (1992): 1.

[15.] Vercesi, G. et al. Characterization of DSA-type oxygen evolving electrodes. Choice of base metal. Thermochimica Acta Vol. 176 (1991): 31-47.

[16.] Comninellis, C. and Vercesi, G. P. Characterization of DSA®-type oxygen evolving electrodes. Choice of a Coating. Journal of Applied Electrochemistry Vol. 21(1991): 335-345.

[17.] Comninellis, C. and Nerini, A. Anodic oxidation of phenol in the presence of NaCl for wastewater treatment. Journal of Applied Electrochemistry Vol. 25 (1995): 23-28.

[18.] Diniz, A. V. et al. Efficiency study of perforated diamond electrodes for organic compounds oxidation process. Diamond and Related Materials Vol. 12 (2003): 577–582.

[19.] Panizza, M. and Cerisola, G. Application of diamond electrodes to electrochemical processes. Electrochimica Acta Vol. 51 (2005): 191–199.

[20.] Fernandes, A., et al. Electrochemical degradation of C. I. Acid Orange 7. Dyes and Pigments Vol. 61 (2004): 287–296.

[21.] Morão, A., Lopes, A. Pessoa de Amorimb, M. T. and Gonçalves, I. C. Degradation of mixtures of phenols using boron doped diamond electrodes for wastewater treatment. Electrochimica Acta Vol. 49 (2004): 1587–1595.

[22.] Lissens, G., et al. Electrochemical degradation of surfactants by intermediates of water discharge at carbon-based electrodes. Electrochimica Acta Vol. 48 (2003): 1655-1663.

[23.] Stucki, S., Kötz, R., Carcer, B. and Suter, W. Electrochemical waste water treatment using high overvoltage anodes Part II: Anode performance and applications. Journal of Applied Electrochemistry Vol. 21(1991): 99-104.

[24.] Cañizares, P. et al. Electrochemical treatment of 2,4-dinitrophenol aqueous wastes using boron-doped diamond anodes: Part II. Influence of waste characteristics and operating conditions. Electrochimica Acta Vol. 49 (2004): 4641-4650.

[25.] Couper, A.M., Pletcher, D. and Walsh, F. C. Electrode materials for electrosynthesis. Chemical Reviews Vol. 90 (1990): 837-865.

[26.] Makgae, M. E. et al. Preparation and surface characterization of Ti/SnO_2–RuO_2–IrO_2 thin films as electrode material for the oxidation of phenol. Material Chemistry and Physics Vol. 92 (2005): 559-564.

[27.] Kötz, R., Stucki, S. and Capcer, B. Electrochemical Waste Water Treatment Using High Overvoltage Anodes. Part I: Physical and Electrochemical Properties of SnO_2 Anodes. Journal of Applied Electrochemistry Vol. 21 (1991): 14-20.

[28.] Pierson, H. O. Handbook of chemical vapor deposition (CVD): principles technology and applications. New Jersey, USA: Noyes Publications, 1992.

[29.] Rantala, T. T., Rantala, T. S., and Lantto, V. Electronic structure of SnO_2 (110) surface. Materials Science in Semiconductor Processing Vol. 3 (2000): 103-107.

[30.] Ruske, M., et al. Properties of SnO_2 films prepared by DC and MF reactive sputtering. Thin Solid Films Vol. 351 (1999): 146-150.

[31.] Vergnes, H. INPT-ENSIACET, Private contact.

[32.] Liu, Y., Li, Z. and Li, J. IrO_2/SnO_2 electrodes: prepared by sol–gel process and their electrocatalytic for pyrocatechol. Acta Materialia Vol. 52 (2004): 721-727.

[33.] Patil, P. S. Versatility of chemical spray pyrolysis. Material Chemistry and Physics Vol. 59 (1999): 185-198.

[34.] Lampkin, C. M. Aerodynamics of nozzles used in spray pyrolysis. Progress in Crystal Growth and Characterization Vol. 1 (1979): 405-416.

[35.] Ohring, M. The materials science of thin films: deposition and structure. California, U.S.A: Academic Press, 2002.

[36.] Stringfellow, G. B. Fundamental aspects of organometallic vapor phase epitaxy. Materials Science and Engineering: B Vol. 87 (2001): 97-116.

[37.] Manasevit, H. M. and Simpson, W. I. Single-Crystal Silicon on a Sapphire Substrate. Journal of Applied Physics Vol. 35 (1964): 1349-1351.

[38.] Schuegraf, K. K. Handbook of thin-film deposition processes and techniques: principles, methods equipment and applications. New Jersey, USA: Noyes Publications, 1988.

[39.] Ghandhi, S. K. and Bhat, I. B. Organometallic Vapor Phase Epitaxy: Features, Problems, New Approaches. MRS Bulletins Vol. 13 (1988): 37-43.

[40.] Amjoud, M'B., Maury, F., Soukane, S. and Duverneuil, P. Making of Specific Electrodes by CVD. Surface and Coatings Technology Vol. 100-101 (1998): 169-172.

[41.] Duverneuil, P. et al. Chemical vapor deposition of SnO_2 coatings on Ti plates for the preparation of electrocatalytic anodes. Surface and Coatings Technology Vol. 151-152 (2002): 9-13.

[42.] Kaminori, T. and Mizuhashi, M. CVD of SnO_2 films from organotin compounds. Proceedings of the 8th International Conference on Chemical Vapor Deposition. 1981, Gouvieux-Chantilly, France.

[43.] Amjoud, M., Maury, F. and Elaatmani, M. Metalorganic chemical vapor deposition of SnO_2 thin films using tetraethyltin: Growth and characterization. Annales de Chimie Science des Matériaux Vol. 23 (1998) : 355-358.

[44.] Bertrand, N. Elaboration d'électrodes volumiques par dépôt CVD de dioxyde d'étain. Thèse de doctorat. Génie des procédés et de l'environnement. Institut National Polytechnique de Toulouse, Toulouse, France, 2001.

[45.] Chi, Y. et al., Volatile noble metal organometallic complexes. U.S. Patent No. 20050033075A1, 2005.

[46.] Dey, S. K. et al. Preparation of iridium films by liquid source metalorganic chemical vapor deposition. Japanese Journal of Applied Physics Vol. 38 (1999): L1052-L1054.

[47.] Chen, Y. L., Deposition of iridium thin films using new Ir^{I} CVD precursors. Chemical Vapor Deposition Vol. 8 (2002): 17-20.

[48.] Sun, Y. M. Precursor chemistry and film growth with (methylcyclopentadienyl) (1,5-cyclooctadiene) iridium. Journal of Vacuum Science & Technology: A Vol. 18 (2000): 10-16.

[49.] Chen, R. S., Growth control and characterization of vertically aligned IrO_2 nanorods. Journal of Materials Chemistry Vol. 13 (2003): 2525-2529.

[50.] Chen, R. S., Growth of IrO_2 films and nanorods by means of CVD: An example of compositional and morphological control of nanostructures. Chemical Vapor Deposition Vol. 9 (2003): 301-305.

[51.] Sun, Y. M., Iridium film growth with iridium tris-acetylacetonate: Oxygen and substrate effects. Thin Solid Films Vol. 346 (1999): 100-107.

[52.] Hoke, J. B., Stern, E. W. and Murray, H. H., Low-temperature vapour deposition of high-purity iridium coatings from cyclooctadiene complexes of iridium. Synthesis of a novel liquid iridium chemical vapour deposition precursor. Journal of Materials Chemistry Vol. 1 (1991): 551-554.

[53.] Xu, C., Baum, T. H. and Rheingold, A. L. New Precursors for Chemical Vapor Deposition of Iridium. Chemistry of Materials Vol. 10 (1998): 2329–2331.

[54.] Norton, T. and Sun, D. W. Computational fluid dynamics (CFD)-an effective and efficient design and analysis tool for the food industry: A review. Trend in Food Science & Technology Vol. 17 (2006): 600-620.

[55.] Richardson, L. F. The approximate arithmetical solution by finite differences of physical problems involving differential equations, with an application to the stresses in a masonry dam. Philosophical Transactions of the Royal Society of London, Series A Vol. 210 (1910): 307–357.

[56.] Courant, R., Friedrichs, K. and Lewy, H. Die partiellen differenzengleichungen der mathematischen Physik. Mathematische Annalen Vol. 100 (1928): 32–74.

[57.] Shang, J. S. Three decades of accomplishments in computational fluid dynamics. Progress in Aerospace Sciences Vol. 40 (2004):173–197.

[58.] Xia, B. and Sun, D. W. Applications of computational fluid dynamics (CFD) in the food industry: a review. Computers and Electronics in Agriculture Vol. 34 (2002): 5–24.

[59.] Abdul Ghani, A. G., Farid, M. M., Chen, X. D. and Richards, P. Numerical simulation of natural convection heating of canned food by computational fluid dynamics. Journal of Food Engineering Vol. 41 (1999): 55–64.

[60.] Ferziger, H. and Peric, M. Computational methods for fluid dynamics. Berlin/Heidelberg, Germany: Springer-Verlag, 2002.

[61.] Foster, A. M., Barrett, R., James, S. J. and Swain, M. J. Measurement and prediction of air movement through doorways in refrigerated rooms. International Journal of Refrigeration Vol. 25 (2002): 1102–1109.

[62.] Versteeg, H. K. and Malalsekeera, W. An introduction to computational fluid dynamics. Harlow, UK: Longman Group Ltd, 1995.

[63.] Patankar, S.V. and Spalding, D.B. A calculation procedure for heat, mass and momentum transfer in three-dimensional parabolic flows. International Journal for Heat and Mass Transfer Vol. 15 (1972): 1787–1806.

[64.] Ferry, M. New features of the MIGAL solver. In Proceedings of the 9th PHOENICS user conference. Moscow, Russia: Moscow Power Engineering Institute, 2002: 1–23.

[65.] Foster, A. M., Madge, M. and Evans, J. A. The use of CFD to improve the performance of a chilled multi-deck retail display cabinet. International Journal of Refrigeration Vol. 28 (2005): 698–705.

[66.] Kopyt, P. and Gwarek, W. A comparison of commercial CFD software capable of coupling to external electromagnetic software for modeling of microwave heating process. In Proceedings of the 6th seminar in computer modeling and microwave power engineering, Austin, Texas, USA: Worcester Polytechnic Institute, Worcester, 2004: 33–39.

[67.] Fluent Inc. FLUENT® 6.0 User's Guide. New Hamshire, USA: 2001.

[68.] Fluent Inc. CVD Reactor Design [Online].2007 Available from http://www.fluent.com/solutions/examples/x64.htm [2007, Sep 24]

[69.] Bryne, J. A. et al. Immobilisation of TiO_2 Powder for the Treatment of Polluted Water. Applied Catalysis B: Environmental Vol. 17 (1998): 25-36.

[70.] Kesselman, J.M. et al. Electrochemical production of hydroxyl radical at polycrytalline Nb-doped TiO_2 electrode and estimation of the partitioning between hydroxyl radical and direct hole oxidation pathways. Journal of Physical Chemistry: B Vol. 101 (1997): 2637-2643.

[71.] Fluent Inc. Modeling Surface Chemistry. In FLUENT® 6.2 Tutorial. New Hamshire, USA: 2005.

[72.] Greenberg, A. E., Clesceri, L.S. and Eaton, A. D. Standard methods for the examination of water and wastewater. Washington, D.C., USA: American Public Health Association, 1992.

[73.] Sun, Y. M. et al. Precursor chemistry and film growth with (methylcyclopentadienyl) (1,5-cyclooctadiene) iridium. Journal of Vacuum Science & Technology: A Vol. 18 (2000): 10-16.

[74.] Endle, J. P. et al. Iridium precursor pyrolysis and oxidation reactions and direct liquid injection chemical vapor deposition of iridium films. Thin Solid Films: Vol. 388 (2001): 126-133.

Appendices

Appendix A

Standard methods for the examination of water and wastewater [72]

1. Chemical oxygen demand (COD)

1.1 Introduction

The chemical oxygen demand (COD) is used as a measure of the oxygen equivalent of the organic matter content of a sample that is susceptible to oxidation by a strong chemical oxidant. For samples from a specific source, COD can be related empirically to BOD, organic carbon, or organic matter. The test is useful for monitoring and control after correlation has been established. The dichromate reflux method is preferred over procedures using other oxidants because of superior oxidizing ability, applicability to a wide variety of samples, and ease of manipulation. Oxidation of most organic compounds is 95 to 100% of the theoretical value. Pyridine and related compounds resist oxidation and volatile organic compounds are oxidized only to the extent that they remain in contact with the oxidant. Ammonia, present either in the waste or liberated from nitrogen-containing organic matter, is not oxidized in the absence of significant concentration of free chloride ions.

1.2 Closed reflux with titrimetric method

1.2.1 Principle

Most types of organic matter are oxidized by a boiling mixture of chromic and sulfuric acids. A sample is refluxed in strongly acid solution with a known excess of potassium dichromate ($K_2Cr_2O_7$). After digestion, the remaining unreduced $K_2Cr_2O_7$ is titrated with ferrous ammonium sulfate to determine the amount of $K_2Cr_2O_7$ consumed and the oxidizable organic matter is calculated in terms of oxygen equivalent. Keep ratios of reagent weight, volumes, and strengths constant when sample volumes other than 50 ml are used. The standard 2 hr reflux time may be reduced if it has been shown that a shorter period yields the same results.

1.2.2 Interferences and limitations

Volatile organic compounds are more completely oxidized in the closed system because of longer contact with oxidant. Before each use inspect culture-tube caps for breaks in the TFE liner. Select culture-tube size for the degree of sensitivity desired. Use the 25 mm x 150 mm tube for samples with low COD content because a larger volume sample can be treated.

1.2.3 Apparatus

1. Digestion vessels preferably use borosilicate culture tubes, 16 mm x 100 mm, 20 mm x 150 mm, or 25 mm x 150 mm, with TFE-lined screw caps. Alternatively, use borosilicate ampules, 10 ml capacity, 19 to 20 mm diameter.
2. Heating block, cast aluminium, 45 to 50 mm deep, with holes sized for close fit of culture tubes or ampules.

3. Block heater or oven, to operate at 150 ± 2 °C. Severe damage of most culture tube closures from oven digestion introduces a potential source of contamination and increases the probability of leakage. Use an oven for culture-tube digestion only when it has been determined that 2 hr exposure at 150 °C will not damage the caps.
4. Ampule sealer: Use only a mechanical sealer to insure stronger, consistent seals.

1.2.4 Reagents

1. Standard potassium dichromate digestion solution, 0.0167M: Add to about 500 ml distilled water 4.913 g $K_2Cr_2O_7$, primary standard grade, previously dried at 103 °C for 2 hr, 167 ml concentrated H_2SO_4 and 33.3 g $HgSO_4$. Dissolve, cool to room temperature and dilute to 1000 ml.
2. Sulfuric acid reagent.
3. Ferroin indicator solution.
4. Standard ferrous ammonium sulfate titrant (FAS), approximately 0.10M: Dissolve 39.2 g $Fe(NH_4)_2(SO_4)_2.6H_2O$ in distilled water. Add 20 ml concentrated H_2SO_4, cool, and dilute to 1000 ml. Standardize solution daily against standard $K_2Cr_2O_7$ digestion solution.

$$Molarity of\ FAS\ solution = \frac{Volume\ 0.0167M\ K_2Cr_2O_7\ solution titrated, ml}{Volume FAS\ used\ in\ titration, ml} x\ 0.10 \quad \text{(A-1)}$$

5. Sulfamic acid.
6. Potassium hydrogen phthalate standard.

1.2.5 Procedure

Wash culture tubes and caps with 20% H_2SO_4 before first use to prevent contamination. Refer to Table A. 1 for proper sample and reagent volumes. Place sample in culture tube or ampule and add digestion solution. Carefully run sulfuric acid reagent down inside of vessel so an acid layer is formed under the sample digestion solution layer. Tightly cap tubes or seal ampules, and invert each several times to mix completely.

CAUTION: Wear face shield and protect hands from heat produced when contents of vessels are mixed. Mix thoroughly before applying heating heat to prevent local heating of vessel bottom and possible explosive reaction.

Place tubes or ampules in block digester or oven preheated to 150 °C and reflux for 2 hr. Cool to room temperature and place vessels in test tube rack. Remove culture tubes caps and add small TFE-covered magnetic stirring bar. If ampules are used, transfer contents to a larger container for titrating. Add 0.05 to 0.10 ml (1 to 2 drops) ferroin indicator and stir rapidly on magnetic stirrer while titrating with 1.10M FAS. The end point is a sharp color change from blue-green to reddish brown, although the blue-green may reappear within minutes. In the same manner reflux and titrate a blank containing the reagents and a volume of distilled water equal to that of the sample.

1.2.6 Calculation

$$COD\ as\ mg/L\ of\ O_2 \quad = \quad \frac{(A-B)\ x\ M\ \ x\ 8000}{ml\ sample} \qquad \text{(A-2)}$$

where:

A = Volume of FAS used for blank (ml),

B = Volume of FAS used for sample (ml), and

M = Molarity of FAS

Table A-1 Sample and reagent quantities for various digestion vessels

Digestion vessel	Sample (ml)	Digestion solution (ml)	Sulfuric acid reagent (ml)	Total final volume (ml)
Culture tubes;				
16 mm x 100 mm	2.5	1.5	3.5	7.5
20 mm x 150 mm	5.0	3.0	7.0	15.0
25 mm x 150 mm	10.0	6.0	14.0	30.0
Standard 10 ml ampules	2.5	1.5	3.5	7.5

1.2.7 Precision and Bias

Sixty synthetic samples containing potassium hydrogen phthalate and NaCl were tested by six laboratories. At an average COD of 195 mg O_2/L in the absence of chloride, the standard deviation was ± 11 mg O_2/L (coefficient of variation, 5.6%). At an average COD of 208 mg O_2/L and 100 mg Cl^-/L, the standard deviation was ± 10 mg O_2/L (coefficient of variation, 4.8 %).

2. Total organic carbon (TOC)

2.1 Introduction

The organic carbon in water and wastewater is composed of a variety of organic compounds in various oxidation states. Some of these carbon compounds can be oxidized further by biological or chemical processes, and the biochemical oxygen demand (BOD) and chemical oxygen demand (COD) may used to characterize these fractions. The presence of organic carbon that does not respond to either the BOD or COD test makes them unsuitable for the measurement of total organic carbon. Total organic carbon (TOC) is a more convenient and direct expression of total organic content than either BOD or COD, but does not provide the same kind of information. If a repeatable empirical relationship is established between TOC and BOD or COD, then TOC can be used to estimate the accompanying BOD or COD. This relationship must be established independently for each set of matrix conditions, such as various points in a treatment process. Unlike BOD or COD, TOC is independent of the oxidation state of the organic matter and

does not measure other organically bound elements such as nitrogen and hydrogen, and inorganics that can contribute to the oxygen demand measured by BOD and COD. TOC measurement does not replace BOD and COD testing.

To determine the quantity of organically bound carbon, the organic molecules must be broken down to single carbon units and converted to a single molecular form that can be measured quantitatively. TOC methods utilize heat and oxygen, ultraviolet irradiation, chemical oxidants, or combinations of these oxidants to convert organic carbon to carbon dioxide (CO_2). The CO_2 may be measured directly by a nondispersive infrared analyzer, it may be reduced to methane and measured with a flame ionization detector, or CO_2 may be titrated chemically.

2.2 Combustion-infrared Method

The combustion-infrared method has been used for a wide variety of samples, but its accuracy is dependent on particle size reduction because it uses small-orifice syringes.

2.2.1 Principle

The sample is homogenized and diluted as necessary and a microportion is infected into a heated reaction chamber packed with an oxidative catalyst such as cobalt oxide. The water is vaporized and the organic carbon is oxidized to CO_2 and H_2O. The CO_2 from oxidation of organic and inorganic carbon is transported in the carrier gas streams and is measured by means of a non-dispersive infrared analyzer.

Because total carbon is measured, IC must be measured separately and TOC obtained by difference.

Measure IC by injecting the sample into a separate reaction chamber packed with phosphoric acid coated quartz beads. Under the acidic conditions, all IC is converted to CO_2, which is measured. Under these conditions organic carbon is not oxidized and only IC is measured.

Alternatively, convert inorganic carbonates to CO_2 with acid and remove the CO_2 by purging before sample injection. The sample contains only the NPOC fraction of total carbon; a VOC determination also is necessary to measure true TOC.

2.2.2 Interference

Removal of carbonate and bicarbonate by acidification and purging with purified gas results in the loss of volatile organic substances. The volatiles also can be lost during sample blending, particularly if the temperature is allowed to rise. Another important loss can occur if large carbon-containing particles fail to enter the needle used for injection. Filtration, although necessary to eliminate particulate organic matter when only DOC is to be determined, can result in loss or gain of DOC, depending on the physical properties of the carbon-containing compounds and the adsorption of carbonaceous material on the filter, or its desorprtion from it. Check filters for their contribution to DOC by analyzing a filtered blank. Note that any contact with organic material may contaminate a sample. Avoid contaminated glassware, plastic containers, and rubber tubing. Analyze treatment, system, and reagent blanks.

2.2.3 Minimum detectable concentration

1 mg carbon/L this can be achieved with most combustion-infrared analyzers although instrument performance varies. The minimum

detectable concentration may be reduced by concentrating the sample, or by increasing the portion taken for analysis.

2.2.4 Sampling and storage

Collect and store samples in amber glass bottles with TFE-lined cap. Before use, wash bottles with acid, seal with aluminum foil, and bake at 400 °C for at least 1 h. Wash TFE septa with detergent, rinse repeatedly with organic-free water, wrap in aluminum foil, and bake at 100 °C for 1 h. Preferable use thick silicone rubber-backed TFE septa with open ring caps to produce a positive seal. Because the detection limit is relatively high, less rigorous cleaning may be acceptable; use bottle blanks with each set of samples. Use a Kemmerer or similar type sampler for collecting samples from a depth exceeding 2 m. Preserve samples that cannot be examined immediately by holding at 4 °C with minimal exposure to light and atmosphere. Acidification with phosphoric or sulfuric acid to a pH $\leq$ 2 at the time of collection is especially desirable for unstable samples, and may be used on all samples; acid preservation, however, requires that inorganic carbon subsequently is purged before analysis.

2.2.5 Apparatus

1. Total organic carbon analyzer, Shimadzu TOC-5050A.
2. Syrings: 0 to 50 μl, 0 to 200 μl, 0 to 500 μl, and 0 to 1 ml capacity.
3. Sample blender or homogenizer.
4. Magnetic stirrer and TFE-coated stirring bars.
5. Filtering apparatus and 0.45-μm-pore-diameter filters.

2.2.6 Reagents

1. Reagent water, prepare blanks and standard solutions from carbon-free water; preferable use carbon-filtered, redistilled water.
2. Concentrated phosphoric acid, H_3PO_4. Alternatively use sulfuric acid, H_2SO_4, but not hydrochloric acid.
3. Organic carbon stock solution: dissolve 2.1254 g anhydrous potassium biphthalate, $C_8H_5KO_4$, in carbon free water and dilute to 1000 ml; 1.00 ml = 1.00 mg carbon. Alternatively, use any other organic carbon-containing compound of adequate purity, stability, and water solubility. Preserve by acidifying with H_3PO_4 or H_2SO_4 to pH $\leq$ 2.
4. Inorganic carbon stock solution: dissolve 4.4122 g anhydrous sodium carbonate, Na_2CO_3, in water, add 3.497 g anhydrous sodium bicarbonate, $NaHCO_3$, and dilute to 1000 ml; 1.00 ml = 1.00 mg carbon. Alternatively, use any other inorganic carbonate compound of adequate purity, stability, and water solubility. Keep tightly stoppered.
5. Carrier gas: purified oxygen or air, CO_2-free and containing less than 1 ppm hydrocarbon (as methane).
6. Purging gas: Any gas free of CO_2 and hydrocarbons.

2.2.7 Procedure

1. Instrument operation: Follow manufacturer’s instructions for analyzer assembly, testing, calibration, and operation. Adjust to optimum combustion temperature (900 °C) before using instrument; monitor temperature to insure stability.
2. Sample treatment: If a sample contains gross solids or insoluble matter, homogenize until satisfactory replication is obtained.

Analyze a homogenizing blank consisting of reagent water carried through the homogenizing treatment.

If inorganic carbon must be removed before analysis, transfer a representative portion of 10 to 15 ml to a 30 ml beaker, add conc H_3PO_4 to reduce pH to 2 or less, and purge with gas for 10 min. Do not use plastic tubing. Inorganic carbon also may be removed by stirring the acidified sample in a beaker while directing a stream of purified gas into the beaker. Because volatile organic carbon will be lost during purging of the acidified solution, report organic carbon as total nonpurgeable organic carbon.

If the available instrument provides for a separate determination of inorganic carbon (carbonate, bicarbonate, free CO_2) and total carbon, omit decarbonation and proceed according to the manufacturer's directions to determine TOC by difference between TC and IC.

If dissolved organic carbon is to be determined, filter sample through 0.45-μm-pore-diameter filter with vacuum; analyze a filtering blank.

3. Sample injection: Withdraw a portion of prepared sample using a syringe fitted with a blunt-tipped needle. Select sample volume according to manufacturer's direction. Stir samples containing particulates with a magnetic stirrer. Select needle size consistent with sample particulate size. Inject samples and standards into analyzer according to manufacturer's directions and record response. Repeat injection until consecutive peaks are obtained that are reproducible to within ±10%.

4. Preparation of standard curve: Prepare standard organic and inorganic carbon series by diluting stock solutions to cover the expected range in samples, Inject and record peak height or area of these standards and a dilution water blank. Plot carbon concentration in milligrams per liter against corrected peak height or area on rectangular coordinate paper. This is unnecessary for instruments provided with a digital readout of concentration. If desirable, prepare a standard curve having concentrations of 1 to 10 mg/L by making appropriate dilutions of the standards.

With most TOC analyzers, it is not possible to determine separate blanks for reagent water, reagents and the entire system. In addition, some TOC analyzers produce a variable and erratic blank that cannot be corrected reliable. In many laboratories, reagent water is the major contributor to the blank value. Correcting only the peak heights of standards (which contain reagent water + reagents + system blank) crates a positive error, while also correcting samples (which contain only reagents and system blank contributions) for the reagent water blank creates a negative error. Minimize errors by using reagent water and reagents low in carbon.

Inject samples and procedural blanks (consisting of reagent water taken through any pre-analysis steps-values are typically higher than those for reagent water) and determine sample organic carbon concentrations by comparing corrected peak heights to the calibration curve.

2.2.8 Calculations

1. When reagent water is a major portion of the total blank:

- Calculate corrected peak height of standards by subtracting the reagent-water blank peak height from the standard peak heights

- Prepare a standard curve of corrected peak height vs. TOC concentration.

- Subtract the procedural blank from each sample peak height and compare to the standard curve to determine carbon content.

NOTE: There will be a positive error if the TOC of the reagent water is significant in comparison to the TOC of the sample. Make a special effort to obtain carbon-free reagent water.

- Apply the appropriate dilution factor when necessary.

- Subtract the inorganic carbon from the total carbon when TOC is determined by difference.

2. When reagent water is a minor portion of the total blank:

- Calculate corrected peak height of standards and samples by subtracting the reagent-water blank peak height from the standard and sample peak heights.

- Prepare a standard curve of corrected peak height vs. TOC concentration.

- Subtract the procedural blank from each sample peak height and compare to the standard curve to determine the carbon content. Values

will have a negative error equal to the blank contribution from the reagent water.

- Apply the appropriate dilution factor when necessary.

- Subtract the inorganic carbon from the total carbon when TOC is determined by difference.

NOTE: If the TOC analyzer design permits isolation of each of the contributions to the total blank, apply appropriate blank corrections to peak heights of standards (reagent blank, water blank, system blank) and sample (reagent blank and system blank).

Appendix B

Simulation steps of MOCVD using FLUENT®

In chemically reacting laminar flows, such as those encountered in chemical vapor deposition (CVD) applications, accurate modeling of time-dependent hydrodynamics, heat and mass transfer and chemical reactions is very important. The surface reactions are considered. Modeling the reactions taking place at gas-solid interfaces is complex and involves several elementary physico-chemical processes like adsorption of gas-phase species on the surface, chemical reactions occurring on the surface and desorption of gases from the surface back to the gas phase.

The steps of working with FLUENT® for simulation the growth of Ir film by MOCVD are listed:

Step 1: Geometry and grid generation

The geometry and grid of the hot-wall CVD used in Ir film deposition was generated by using GAMBIT.

Step 2: Start the FLUENT®

The FLUENT® was started with solver for 3D modeling.

Step 3: Import of grid

The geometry and grid of the reactor was imported by using command;

File → Read → Case…

Step 4: Check for the grid;

Grid → Check…

The grid check lists the minimum and maximum x, y and z values from the grid and reports on a number of other grid features that are checked. Any errors in the grid would be reported.

Step 5: Define the solver default:

Choose the basic equations to be solved: laminar or turbulent, chemical species or reaction, heat transfer models etc.

Define → Models → Solver…

Enable heat transfer by activating the energy equation;

Define → Models → Energy…

Enable chemical species transport and reaction;

Define → Models → Species → Transport & Reaction…

Step 6: Define the materials:

Define → Materials…

Create and specify the material properties of the gas-phase species, the site species and the solid species. Set up the mixture reaction and reaction mechanisms.

Step 7: Specify the operating conditions:

Define → Operating Conditions…

Step 8: Specify the boundary conditions:

Define → Boundary Conditions…

Step 9: Adjust the solution control parameters:

Solve → Controls → Solution…

Step 10: Initialize the flow field:

Initialize the flow field using the boundary conditions set at velocity-inlet;

Solve → Initialize…

Turn on residual plotting during the calculation:

Solve → Monitor → Residual…

Step 11: Calculate for a solution:

Start the calculation by requesting the number of iterations;

Solve → Iterate…

Step 12: Examine the results:

The simulation results should be displayed in various formats such as contour, vector and XY plot, etc.

Appendix C

Sample of calculations

1. Chemical oxygen demand (COD)

$$COD\ as\ mg/L\ of\ O_2 \quad = \quad \frac{(A-B)\ x\ M\ \ x\ 8000}{ml\ sample}$$

Given

Volume of FAS used for blank (A)	3.25 ml
B = Volume of FAS used for sample (B)	0.30 ml
Molarity of FAS (M)	0.043 M
Volume of sample	0.50 ml

$$COD\ as\ mg/L\ of\ O_2 \quad = \quad \frac{(3.25-0.30)\ x\ 0.043\ x\ 8000}{0.50}$$

$$= \quad 2{,}029.6\ mg/L$$

2. COD removal efficiency

$$COD\,removal\,efficiency \;=\; \frac{COD_i - COD_t}{COD_i} x100$$

Given

Initial COD of solution (COD_i)	314 mg/L
COD at 24 hr (COD_{24})	121 mg/L

$$COD\,removal\;\;efficiency \;=\; \frac{314-121}{314} x100$$

$$=\; 61.5\ \%$$

3. TOC removal efficiency

$$TOC\,removal\,efficiency \;=\; \frac{TOC_i - TOC_t}{TOC_i} x100$$

Given

Initial TOC of solution (TOC_i)	314 mg/L
TOC at 24 hr (TOC_{24})	121 mg/L

$$TOC\,removal\;\;efficiency \;=\; \frac{142-56}{142} x100$$

$$=\; 60.6\ \%$$

4. IrO_2 film thickness

$$IrO_2\ film\ \ thickness\ \ =\ \ \frac{Wt.\ of\ IrO_2\ coated\ Si\ wafer - Wt.\ of\ Si\ wafer}{Si\ wafer\ surface\ area\ x\ IrO_2\ density} x\, 10{,}000$$

Given

Width of Si wafer	0.873 cm
Length if Si wafer	0.987 cm
Density of IrO_2	11.7 g/cm^3
Weight of Si wafer	0.11920 g
Weight of IrO_2-coated Si wafer	0.11934 g

$$IrO_2\ film\ thickness\ \ =\ \ \frac{0.11934 - 0.11920}{0.873 x\, 0.987 x\, 11.7} x\, 10{,}000$$

$$= 0.139 \text{ micron}$$

5. IrO_2 film growth rate

$$IrO_2\ film\ growth\ rate\ \ =\ \ \frac{IrO_2\ film\ thickness}{Deposition\ time} x\, 1{,}000$$

Given

IrO_2 film thickness	0.139 micron
Deposition time	300 min

$$IrO_2 \ film \ growth \ rate = \frac{0.139}{300} x 1{,}000$$

$$= 0.46 \text{ nm/min}$$

6. Ir film thickness

$$Ir \ film \ thickness = \frac{Wt. of \ Ir \ coated \ Si \ wafer - Wt. of \ Si \ wafer}{Si \ wafer surface \ area \ x \ Ir \ density} x 10{,}000$$

Given

Width of Si wafer	0.819 cm
Length if Si wafer	0.878 cm
Density of Ir	22.65 g/cm^3
Weight of Si wafer	0.10177 g
Weight of Ir-coated Si wafer	0.10185 g

$$Ir \ film \ thickness = \frac{0.10185 - 0.10177}{0.819 x 0.878 x 22.65} x 10{,}000$$

$$= 0.049 \text{ micron}$$

7. Ir film growth rate

$$Ir\ film\ growth\ rate\ =\ \frac{Ir\ film\ thickness}{Deposition\ time} x\,1{,}000$$

Given

Ir film thickness	0.049 micron
Deposition time	270 min

$$Ir\ film\ growth\ rate\ =\ \frac{0.049}{270} x\,1{,}000$$

$$=\ 0.18\ \text{nm/min}$$

8. SnO_2 film thickness

$$SnO_2\ film\ \ thickness\ =\ \frac{Wt.\ of\ SnO_2\ coated\ Si\ wafer - Wt.\ of\ Si\ wafer}{Si\ wafer\ surface\ area\ x\ SnO_2\ density} x\,10{,}000$$

Given

Width of Si wafer	0.690 cm
Length if Si wafer	0.755 cm
Density of SnO_2	7 g/cm^3
Weight of Si wafer	0.07444 g
Weight of SnO_2-coated Si wafer	0.07536 g

$$SnO_2\ film\ thickness = \frac{0.07536 - 0.07444}{0.690\,x\,0.755\,x\,7} x\,10{,}000$$

$$= 2.52 \text{ micron}$$

9. SnO_2 film growth rate

$$SnO_2\ film\ growth\ rate = \frac{SnO_2\ film\ thickness}{Deposition\ time} x\,1{,}000$$

Given

SnO_2 film thickness	2.52 micron
Deposition time	120 min

$$SnO_2\ film\ growth\ rate = \frac{2.52}{120} x\,1{,}000$$

$$= 21 \text{ nm/min}$$

10. Power required

$$Power\ required = \frac{Applied\ current\ x\ Cell\ voltage}{Flow\ rate\ x\ 1{,}000}$$

Given

Applied current	0.016 A
Cell voltage	14.9 V
Flow rate	$9x10^{-6}$ m^3/hr

$$Power\ required = \frac{0.016\ x\ 14.9}{9x10^{-6}\ x\ 1{,}000}$$

$$= 26.5\ \text{kW-hr/m}^3$$

11. Treatment cost

$$Treatment\ cost = Power\ required\ x\ Electricity\ cost$$

Given

Power required	26.5 kW-hr/m^3
Electricity cost	2.5 Baht/kW-hr

$$Treatment\ cost = 26.5\ x\ 2.5$$

$$= 66.25\ \text{Baht/m}^3$$

Biography

Mr. Songsak Klamklang was born on March 12, 1975 in Chainat Province, Thailand. He got his Bachelor of Engineering in Chemical Engineering from Department of Chemical Engineering, Faculty of Engineering, Kasetsart University in 1998. He got his Master of Science in Chemical Technology from Department of Chemical Technology, Faculty of Science, Chulalongkorn University in 2000. Then, he had further persuade study and got his Doctor of Philosophy in Chemical Technology from Chulalongkorn University and Docteur de l'Institut National Polytechnique de Toulouse in Chemical Engineering from Institut National Polytechnique de Toulouse in 2007.